POLITECNICO DI MILANO

Master's Degree in Biomedical Engineering

Master's Degree Thesis

Effects of Structural Parameters on the Buckling and Post-buckling Behavior of Auxetic Cellular Plates and Cylinders

Supervisor
Prof. Pasquale Vena

Co-supervisors
Dr. Mohammad J. Mirzaali
Prof. Amir A. Zadpoor

Coaches
Dr. Mohammad KHoshgoftar
Dr. Mehdi Habibi

Candidates
Ali Abaeian - 894273

2020-2021

This page intentionally left blank

ABSTRACT

Cellular materials are those materials which is made by interconnection of solid beam, truss plates that form the edges of the unit cells. Cellular structures possess superior properties over their solid counterpart such as strength-to-weight ratio and surface area properties. Apart from the mentioned advantages, these structures due to their high performance, high strength-to-weight ratio, low heat conduction properties, superior energy absorption and excellent thermal and acoustic insulation have attracted much attention in the engineering industries especially medical field. Auxetic cellular material are a type of cellular materials which provide unique properties due to their negative Poisson's ratio. These sort of material expand laterally in the direction perpendicular to the stretching loading direction. On the other hand if they are compressed longitudinally they contract in transverse directions. One of the biggest weaknesses of all cellular structures including conventional and auxetic one is their buckling instability when they are under the action of compressive stress, which leads to premature collapse in cellular structures. The critical compressive stress required for the collapse of the cellular structure is far less than the critical compressive stress of the material that makes up the cellular structure. Structural parameters of cellular structures play an important role in the performance of these structures. They can help improve the static and dynamic properties of the structure or, conversely, their improper design can jeopardize the stability of the structure. As a result, determining the optimal cellular structure parameters is essential for a particular application.

In order to investigate more precisely the effect of structural parameters on the buckling and post-buckling behavior of cellular structures, two different geometry of plate and cylinder have been studied. 84 plate models and 45 cylindrical models have been designed by exploiting the re-entrant honeycomb model proposed by Gibson. While defining the structural parameters of the cellular structure, we will describe the models created by the variation of these parameters. All models were analyzed by finite element method and the accuracy of the results obtained from the numerical method has been investigated by fabricating reference models (three reference models for plate geometry and two reference models for cylindrical geometry). All five reference models are fabricated by additive manufacturing technology and buckling mechanical test have been conducted on them. The experimental

results for all reference models follow the simulation results so well, and there is a perfect agreement between the two results.

The results show that in the cellular plate structure, the stiffness-weight-normalized critical stress in cellular plates with different Poisson's ratio gains its maximum value generally in the auxetic region and close to Poisson's ratio equals to zero. On the other side, in a cylindrical structure, the normalized critical stress increases with increasing Poisson's ratio. It can also be interpreted that for sufficient slender cellular plates the post-buckling behavior of the cellular plate with a Poisson's ratio close to zero has the least dependence on the out-of-plane thickness of the plate and its dependence on the out-of-plane thickness increases by moving away from zero Poisson's ratio. On the other side, the results of the data of the cylindrical structure show that the post-buckling behavior of this structure for the maximum Poisson's ratio is the most affected by the change in membrane thickness. The structure also has a larger negative slope for the maximum Poisson's ratio. As a result, although the cellular cylinder with maximum Poisson's ratio has a higher buckling resistance, it is more unstable in the post-buckling regime. Moreover it seems that for plate models when the ratio of the in-plane thickness of the struts to the scaling parameter increases, the auxeticity has practically less effect on the post-buckling behavior of the structure. The results have also reveals the superiority of using a cellular plate with zero Poisson's ratio over a bulk plate with the same Poisson's ratio especially in smaller thicknesses. In general, all structural parameters including the Poisson's ratio (for both plate and cylindrical models), the out-of-plane thickness (for plate models), the membrane thickness (for cylindrical models), the in-plan thickness of the struts (for plate models), the width (for plate models), the scaling parameter of the unit cells (for both plate and cylinder models) and the height-to-width ratio of the unit cells (for both plate and cylinder models) have undeniable effects on the critical buckling load and post-buckling behavior of structures. In fact, by changing the geometric parameters, a wide range of post-buckling slopes of the structure can be achieved in both plate and cylindrical geometry and the post-buckling behavior of the structure can be tuned by designing geometric parameters.

Keywords: *Auxetic Materials, Additive Manufacturing, Buckling and Post-buckling Behavior, Cellular Structures, Finite Element Analysis, Structural Parameters*

ACKNOWLEDGEMENT

I want to express my deepest gratitude to my parents for all the constant emotional, financial and spiritual support they have given and give me throughout my studies and life. In fact, this work could not have been completed without them.

I would like to express the deepest appreciation to Professor Pasquale Vena who gave me the honor to carry out my master thesis under his name, guidance and support. I am also forever grateful to Prof. Amir Zadpoor and Dr. Mohammad Mirzaali who trusted and provided me with the opportunity to conduct this study and learn the skills necessary to succeed as a researcher and engineer under the supervision of their group in a fully professional atmosphere at Technical University of Delft. My deepest appreciation goes to Dr. Mohammad Khoshgoftar and Mehdi Habibi for their useful comments. I would also like to thank Dr. Shahram Janbaz, who has willingly and humbly shared his precious time wheneve I need his help and support. God bless him.

Once again, I have to thank my family, especially my parents, from the bottom of my heart. I am always indebted to the unconditional love and support of my parents and I will never forget it. I hope one day I would be able to repay a little of their love.

Last but not least, I am deeply grateful to the Polytechnic University of Milan for providing such an opportunity to peruse my carrier in Italy and be one step closer to my goals. Wishing all people around the world brighter days, especially the people of my forever homeland Iran.

TABLE OF CONTENTS

1.8 Buckling of a structure… 16
1.8.1 Load vs in-plane displacement… … … … … … … … … … … … … … … … 16
1.8.2 Load vs out-of-plane displacement… … … … … … … … … … … … … … 17
1.8.3 Buckling of cellular structures… … … … … … … … … … … … … … … ….18
1.9 Buckling of a rectangular auxetic plate… … … … … … … … … … … … … … …..20
1.10 Buckling of a cylindrical auxetic shell… … … … … … … … … … … … … … …..22
1.11 Research questions… … … … …..… … … … … … …. … … … … … … … … … ….23
1.12 Study outline… … …. … ….… 24

2 Material and experimental methods… … … … … … … … … … 25

2.1 Auxetic cellular plate… … … … … … … … … … … … … … … … … … … …

LIST OF FIGURES

LIST OF TABLES

Chapter 1

Introduction

In this chapter, we first define the Poisson ratio and its historical developments. The reader then becomes familiar with the definition of auxetic materials and its relevance to the Poisson's ratio. We will also review the history of auxetic materials. Thereafter we will get acquainted with natural auxetic materials as well as those auxetic materials that are made by humans. Auxetic cellular materials which are basis of our studies will be explained in more details. Then we review on the definition of buckling and post-buckling behavior of a structure. Finally, the classical relations governing both plate and cylindrical structures made of auxetic materials under compressive uniaxial stress will be expressed. Since our study is based on models built in these two structures (plate and cylinder), this introduction will help us to have a better understanding of how auxetic materials behave in the two aforementioned structures and make it more efficient and straightforward to compare our results with the classical behavior of these materials.

1.1 Poisson's ratio

Suppose there is a bar of a given material. Based on visual and empirical evidences it is quite clear that if the bar is stretched in longitudinal direction, it contracts in the transverse directions as presented in Figure 1.1.1 (top). As a consequence if the material is contracted rather than stretched, it is prone to expand perpendicularly to the direction of contraction which is shown in Figure 1.1.1 (bottom). Poisson's ratio in material science and solid mechanics has been defined as a ratio of transverse deformation to longitudinal deformation in the direction of applying force. It follows that Poisson's ration can be defined as:

$$\upsilon = -\frac{\varepsilon_p}{\varepsilon_l} \tag{1.1.1}$$

Where ε_l is the strain in the direction of applying load and ε_p is considered as the strain in the direction of perpendicular to the loading direction. As it mentioned above in most materials, contraction in one direction is a consequence of expansion in other directions and vice versa. Therefor in $Eq.(1.1.1)$ ε_p and ε_l possess opposite signs, i.e. When ε_l owns a positive sign the value of ε_p is negative and the ratio $\frac{\varepsilon_p}{\varepsilon_l}$ would be negative. As a result a minus sign has been added to $Eq.(1.1.1)$ to obtain a positive Poisson's ratio for the normal materials.

By knowing the value of Poisson's ratio and implementing mathematical rules, the relative change of volume $\frac{\Delta V}{V}$ of an isotropic solid for a very small strain can be obtained as:

$$\frac{\Delta V}{V} = (1 - 2\upsilon)\frac{\Delta l}{l} \tag{1.1.2}$$

Where, υ, l and Δl are respectively Poisson's ratio, initial length and length deformation in the direction of the applying load.

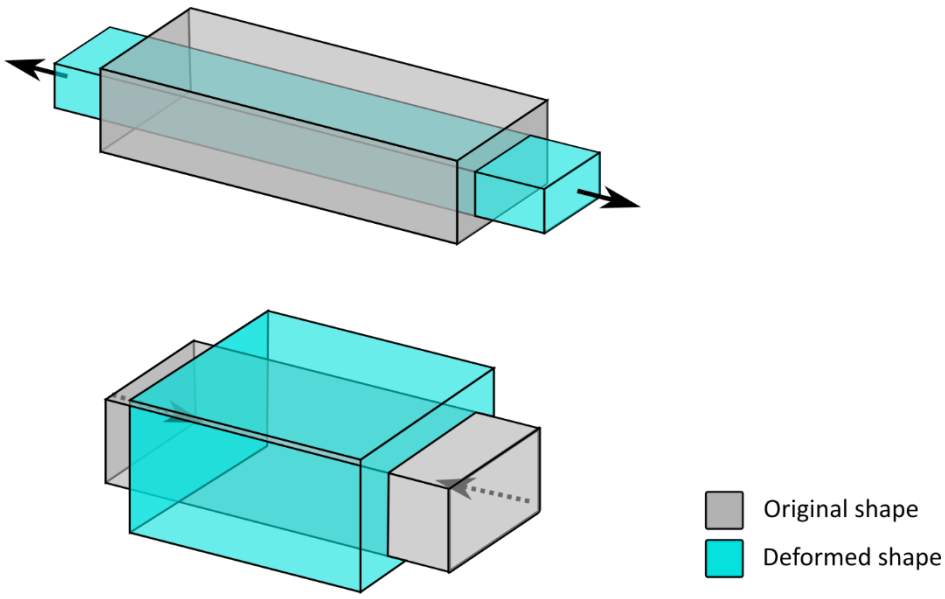

FIGURE 2.1.1 Three-dimensional schematic of how conventional materials with positive Poisson's ratio deform under uniaxial force

It is worth mentioning that for an isotropic material each elastic constant can be expressed as a function of two other elastic constants [1]. Elastic constants such as bulk modulus K, Young modulus E and shear modulus G possess same units. However the only elastic constant which is dimensionless is the Poisson's ratio. It follows that the ratio between each two elastic constants is unit less and can be represented by only Poisson's ratio. The following relations express some of these ratios:

$$\frac{E}{G} = 2(1+\upsilon) \tag{1.1.3}$$

$$\frac{E}{K} = 3(1-2\upsilon) \tag{1.1.4}$$

$$\frac{G}{K} = \frac{3(1-2\upsilon)}{2(1+\upsilon)} \tag{1.1.5}$$

1.2 History of Poisson's ratio

Young was the first one who observed the resulted transverse contraction due to applied stretching load [2]. Twenty years later Poisson could derive a constant value of $\upsilon = 0.25$ by implementing the theory of molecular interaction [1]. Later in 1859 Kirchhoff worked on several metals. He measured their Young and shear modulus and then by implementing $Eq.\,1.1.3$ he could obtain the Poisson's ratio of such metals [1]. The results of Kirchhoff's work as well as subsequent measurements of the Poisson's ratio revealed that the Poisson's ratio not only does not have a constant value but also varies in different materials.

1.3 Auxetic materials

In the previous section we mentioned that normal materials have positive Poisson's ratio. On the contrary, there are some solid materials which possess negative Poisson's ratio. Auxetic is the name which is given to these sort of materials. Unlike conventional materials with positive Poisson's ratio they stretched laterally in the direction perpendicular to the tensile loading direction. On the other hand if they are compressed longitudinally they contract in transverse directions. Deformation of auxetic materials under tension and compression loads are shown in Figure 1.3.1.

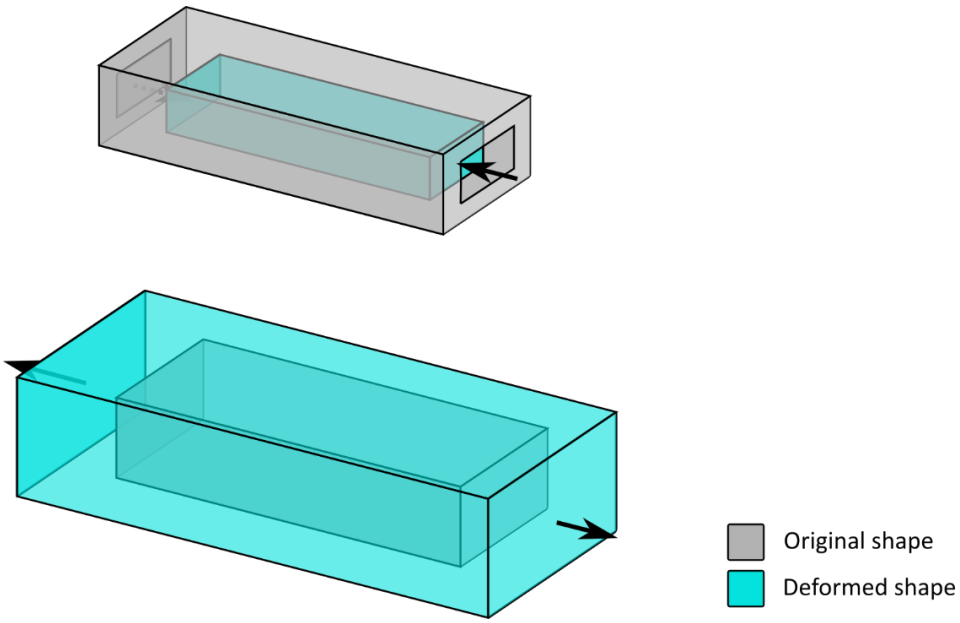

FIGURE 1.3.1 Three-dimensional schematic of how auxetic materials with negative Poisson's ratio deform under uniaxial force

Now it is turn to introduce five turning points of Poisson's ratio of solid isotropic materials. At each of these turning points one of the quality of the described material is preserved without any changes. In the case of Poisson's ratio equals to zero $(\upsilon = 0)$ cross section is Preserved.

According to the $Eq.(1.3.1)$ Young modulus and shear modulus possess the same value in the case of $\upsilon = -0.5$, therefor these two most common engineering moduli are preserved. When $\upsilon = -1$ caused lateral strains have equal value and sign as applied longitudinal strain. It follows that the material is deformed (expanded or compressed) in all direction equally. Therefore no changes in shape is observed and it will be preserved. In the two dimensional deformation, when a solid possess $\upsilon = 1$, it means that the strain in the direction of applying load has an equal but opposite sign of the strain in the perpendicular direction. For that reason this area is preserved. And the last turning point is for those materials which have Poisson's ratio of 0.5. Under this condition, substation of $\upsilon = 0.5$ in $Eq.(1.1.2)$ gives $\Delta V = 0$. It follows that the value of volume of the solid will not change due to deformation, and the material is considered incompressible [1]. The contents presented above are summarized in Table 1.2.1.

TABLE 1.3.1 Five turning points of isotropic solid materials and corresponding physical interpretation

Turning point	*Preserved quality*
υ = -1	Area
υ = -0.5	Young modulus and Shear modulus, E=G
$\upsilon = 0$	Cross section
$\upsilon = 0.5$	Volume
υ = -1	Shape

1.4 History of negative Poisson's ratio

In the year 1848 Saint-Venant was the first one who proposed negative value for Poisson's ratio of the anisotropic materials [1]. By expressing Cauchy relations in his words he also suggested that Poisson's ratio can be greater than 0.5 [1]. This property later in 1910 was identified and reported by Woldemar Voigt who was working on iron pyrite [3]. He suggested the crystals of iron pyrite expanded transversely when stretched longitudinally. Negative Poisson's ratio have also been reported for pyrites [4], single crystal [5], biological tissues [6], Alpha-quartz [7], re-enterant hexagonal honeycomb [8], shape-preserved three-dimensional isotropic structures build up rods, hinges and springs [9] and cellular materials [10].

Evans in 1991 used the word auxetic for the first time to refer to the negative Poisson's ratio materials [11]. The term auxetic has the same root as the word auxetikos which means "that which tends to increase".

1.5 Natural auxetic materials

Alpha-cristobalite, a silicon dioxide is the first naturally occurring material reported by Yegane-Haeri et al which presents negative Poisson's ratio [12]. They carried out a tonsorial analysis on Alpha-cristobalite and found that although the average Poisson's ratio for its single-phased aggregate was -0.16 but its Poisson's ration can reach to -0.5 in certain directions.

1.5.1 Auxetic biomaterials

Biomaterials that exhibit auxetic behaviors under certain conditions are called Auxetic biomaterials. These materials have been reported in some biological sources. For instance, Williams et al [13] during their investigation on tibia found negative Poisson's ratio properties for the spongy bone of the proximal tibial epiphysis. Studies on the cat skin by Veronda et al [14] have shown that it exhibits auxetic behavior under limited deformation. Also, uniaxial and biaxial experiments performed on the cow teat skin by Lis et al [15] demonstrated that at low strains it can give negative Poisson's ratio properties. It seems that fibrillar structures at the microstructural level cause such a property in these materials [16].

Auxetic behavior in biological materials has been observed also on the microscopic scale. According to Bogman [17], the membranes in the cytoskeleton of the red blood cells show auxetic properties. In another study, Wang [18] stated that the nucleus of embryonic stem cells (ESCs) of mouse exhibited auxetic behavior during the differentiation process.

1.6 Man-made auxetic materials

1.6.1 Auxetic foams

In spite of the fact that some materials are not naturally-occurring auxetic materials, they can exhibit negative Poisson's ratio if they are composed in some certain ways. As an example consider conventional foams which can give auxetic properties by bending the struts of each unit cells inward. The re-entrant structure has been firstly suggested by Lake [19]. A collapsed cubic re-entrant unit cell which exhibit negative Poisson's ratio is depicted in 1.6.1.

FIGURE 1.6.1 A cubic re-entrant unit cell based on collapse of polyhedron which exhibit negative Poisson's ratio [1]

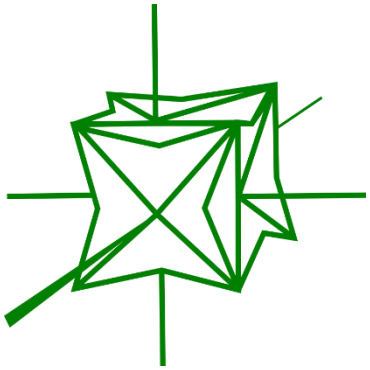

1.6.2 Auxetic liquid crystalline polymers (LCR)

Liquid crystalline polymers was firstly introduced by He et al [20] as the polymeric auxetic materials. By connecting molecular rods to the polymeric chain one can compose these type of auxetic materials. The molecular rods are originally oriented in the direction of the polymeric chain. As it shown in Figure 1.6.2 when the load is applied to the chain it stretches and molecular rods orient in the direction perpendicular to the chain to give the polymeric material negative Poisson's ratio.

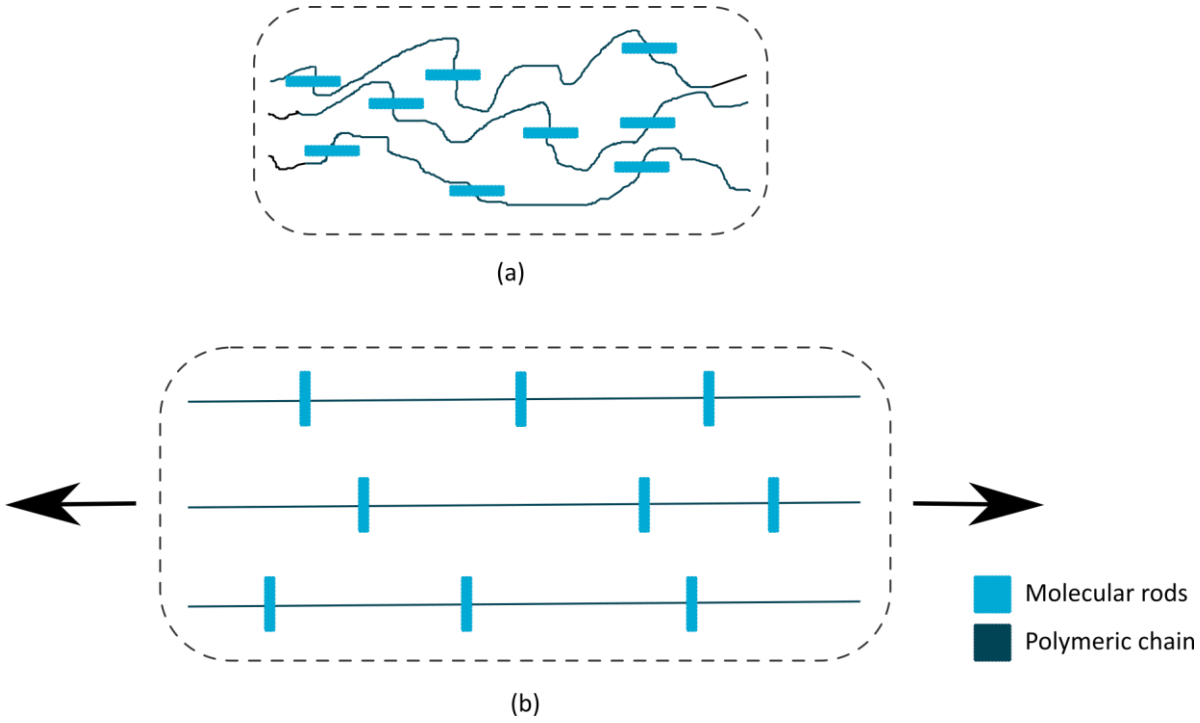

FIGURE 1.6.2 Concept of liquid crystalline polymers which gives auxetic properties [1]

1.6.3 Auxetic yarn and textile

In order to make an auxetic yarn two types of strings are needed. For this purpose first an inflexible string which has smaller diameter is twisted around an elastic string of larger diameter in a helical way as depicted in Figure 1.6.2 (a). When the yarn is longitudinally stretched, the inflexible string is no longer wrapped helically and becomes stiff. It follows that the originally straight elastic string starts to develop a new helical configuration as shown in Figure 1.6.2 (b). Although the elastic string due to its positive Poisson's ratio contracted transversely, the overall configuration of the yarn expands laterally to exhibit negative Poisson's ratio. Now if a number of such yarn are placed next to each other as depicted in Figure 1.6.2 (c), and stretched in the longitudinal direction, each single yarn develops a helical

shape and in meanwhile it pushes its adjacent yarn aside which leads the aligned group of yarns become thicker (Figureh 1.6.2 (d)). It is worth mentioning that each yarn must be placed symmetrically to its neighbor yarn to give more effective auxetic properties which leads to maximum dilating of the longitudinally stretched yarns. However if the yarns are all placed in a similar way rather than symmetrical as depicted in Figure 1.6.2 (e), it still gives negative Poisson's ratio. However it is very little in magnitude in comparison to the former configuration (see Figure 1.6.2 (f)).

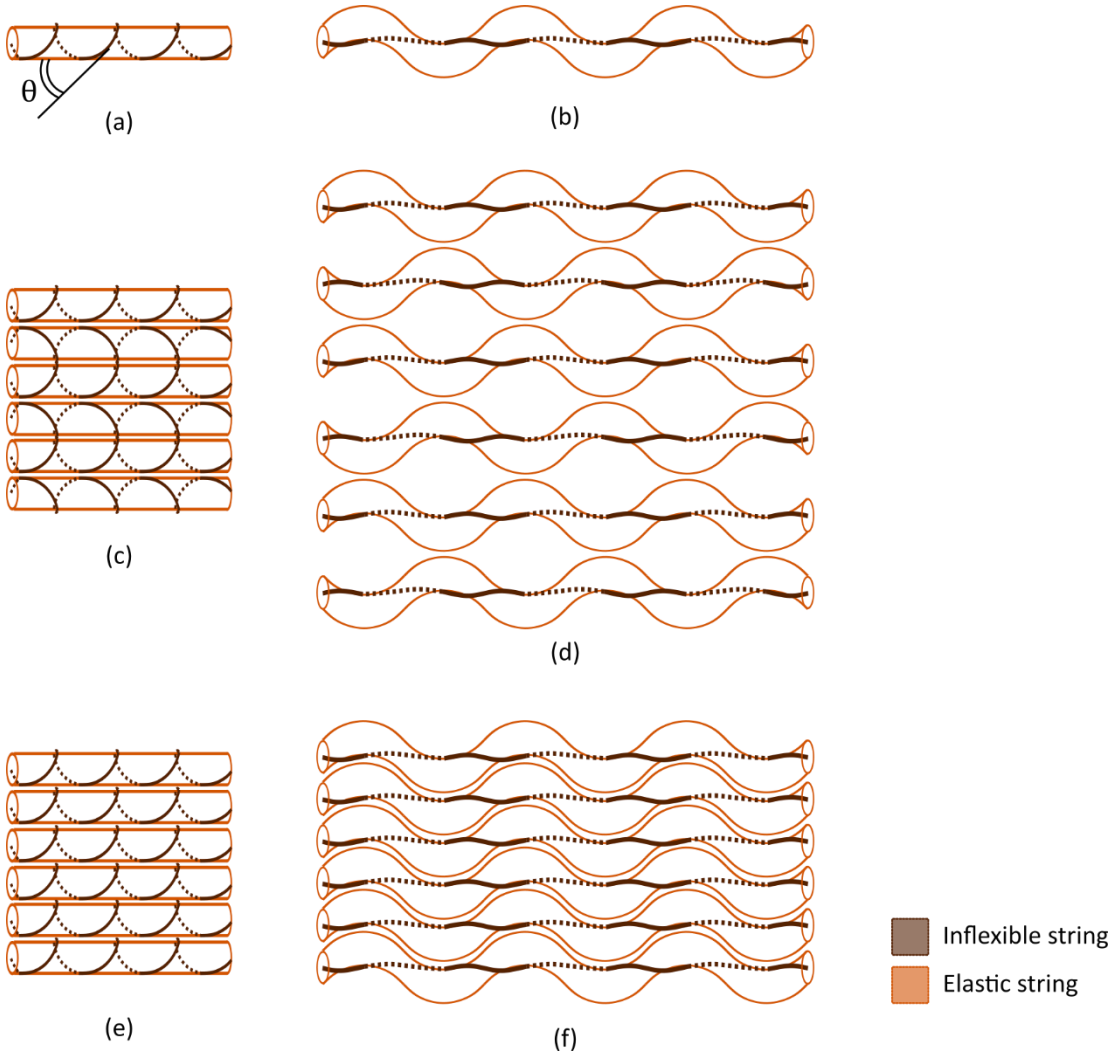

FIGURE 1.6.3 Schematic of auxetic yarn: (**a**) single yarn consists of inflexible and elastic strings, (**b**) stretched helical yarn which gives negative Poisson's ratio, **c** out of phase arrangement of yarns, (**d**) efficient auxetic property due to out of phase alignment of yarns, (**e**) in phase arrangement of yarn, (**f**) weak auxeticity due to in phase alignment of yarns [1]

Salon et al [21] performed a study of the yarn to investigate its auxetic behavior. They stated that the wrapping angle θ of the inflexible string has the most effect on auxetic behavior of

the yarn. They made a yarn from conventional available filaments with positive Poisson's ratio and observed that the minimum Poisson's ratio of such yarns is -2.7

1.6.4 Auxetic cellular materials

Cellular materials are those materials which is made by interconnection of solid beam, truss plates that form the edges of the unit cells. Various examples of such materials like wood, cork and bone can be found in nature [22]. Cellular structures possess superior properties over their solid counterpart such as strength-to-weight ratio and surface area properties [23, 24]. The main advantage of cellular structure over solid structure is that cellular structure is designed so that the material is added to the structure only when it needs to be used for specific applications such as medical application (bone scaffold, implant and etc.), aerospace and automotive industries. Since the use of cellular structures saves expensive materials and, as a result, reduces the final cost, construction time and energy consumption, innovative design and fabricating methods are used for these structures [25]. These structures due to their high performance, high strength-to-weight ratio [26, 27], low heat conduction properties [28, 29], superior energy absorption [30] and excellent thermal and acoustic insulation [26, 31, 32] have attracted much attention in the aerospace, automotive, and biomedical industries. Medical applications of cellular structures include their use for femoral stem implant using powder-bed fusion [33], dental implants [34] and tissue engineering [35]. The parameters of permeability, surface-to-volume ratio and pore size play a major role in bone implant success [36]. Auxetic cellular material are a type of cellular materials which provide unique properties due to their negative Poisson's ratio. For clarifying properties of auxetic cellular materials, two well-known types of cellular materials with different architecture have briefly been reviewed in following sections.

1.6.4.1 Re-entrant honeycomb model

To investigate the behavior of a conventional honeycomb cellular structure, Gibson et al used a conventional two-dimensional model [8]. As it can be seen in Figure 1.6.4 when the unit cells are stretched horizontally the vertical ribs tend to move outwards resulting auxetic properties. It should be noted that in many honeycomb structures, oblique ribs are prone to bend due to the interaction of the struts with each other, and part of the auxetic behavior of the structure is due to the bending of the oblique ribs [37]. Based on their model, Poisson's ratio and Young's modulus in the direction of applying force are expressed as follows:

$$\nu_{12} = \frac{sin\theta(h/l + sin\theta)}{cos^2\theta} \tag{1.6.1}$$

$$E_1 = k\frac{(h/l + sin\theta)}{bcos^3\theta} \tag{1.6.2}$$

$$k = E_s b\left(\frac{t}{l}\right)^3 \tag{1.6.3}$$

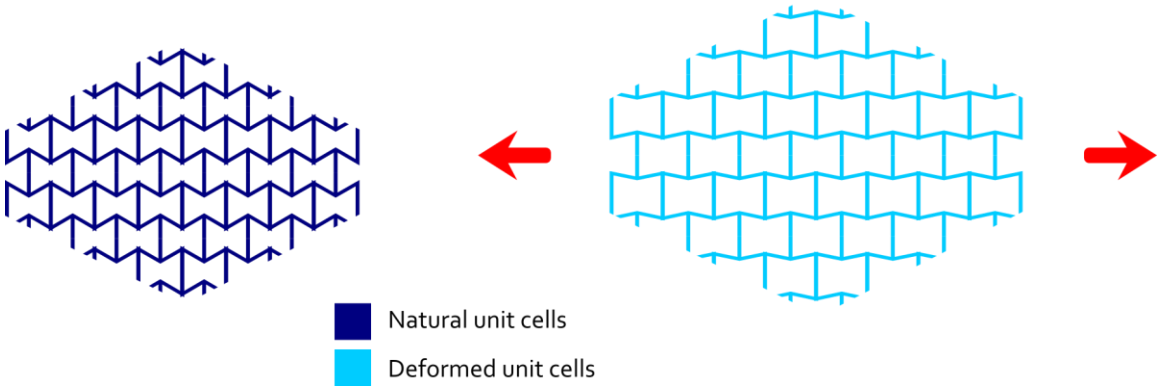

FIGURE 1.6.4 Illustration of auxeticity of re-entrant honeycomb structure

Where as shown in Figure 1.6.5, h, l, b, θ are respectively the half of the length of vertical struts, the oblique struts length, the out-of-plane thickness of the struts and the angle between the vertical and oblique struts. E_s is Young modulus of the basis material from which unit cells are made.

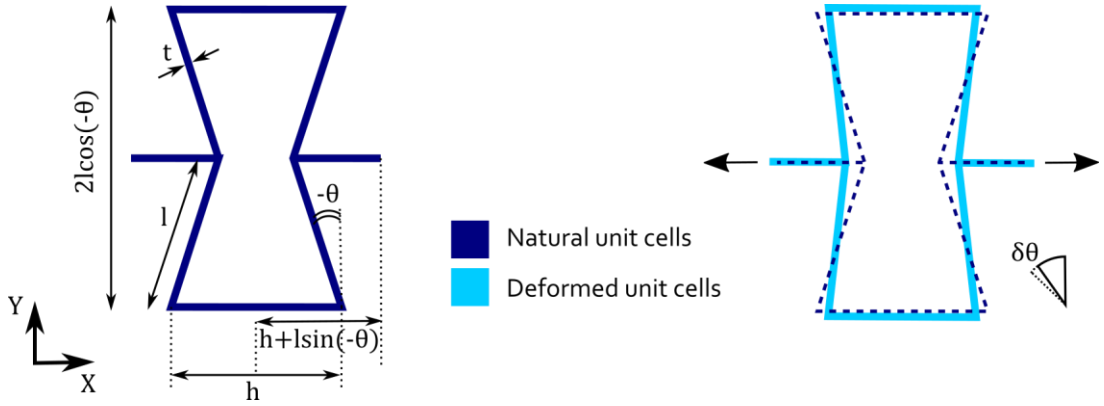

FIGURE 1.6.5 Single cell of a re-entrant honeycomb structure and its defined parameters [38]

1.6.4.2 Rotating square model

Another early category of auxetic structures is the rotating polygonal model. This model has been extensively investigated by Grima Alderson et al [39-41]. Rafsanjani et al [42] also conducted studies in the development of this model. Grima et al [39] presented a new model in which by placing rigid squares next to each other and connecting their vertices by hinges,

a new structure is obtained that exhibits auxetic behavior. A unit cell of the rotating square is depicted in Figure 1.6.6. It is worth mentioning that in designing this model, two basic assumptions have been considered. First, it is assumed that the squares are not deformable in the directions of applying load and the rotating squares are resistance to shear.

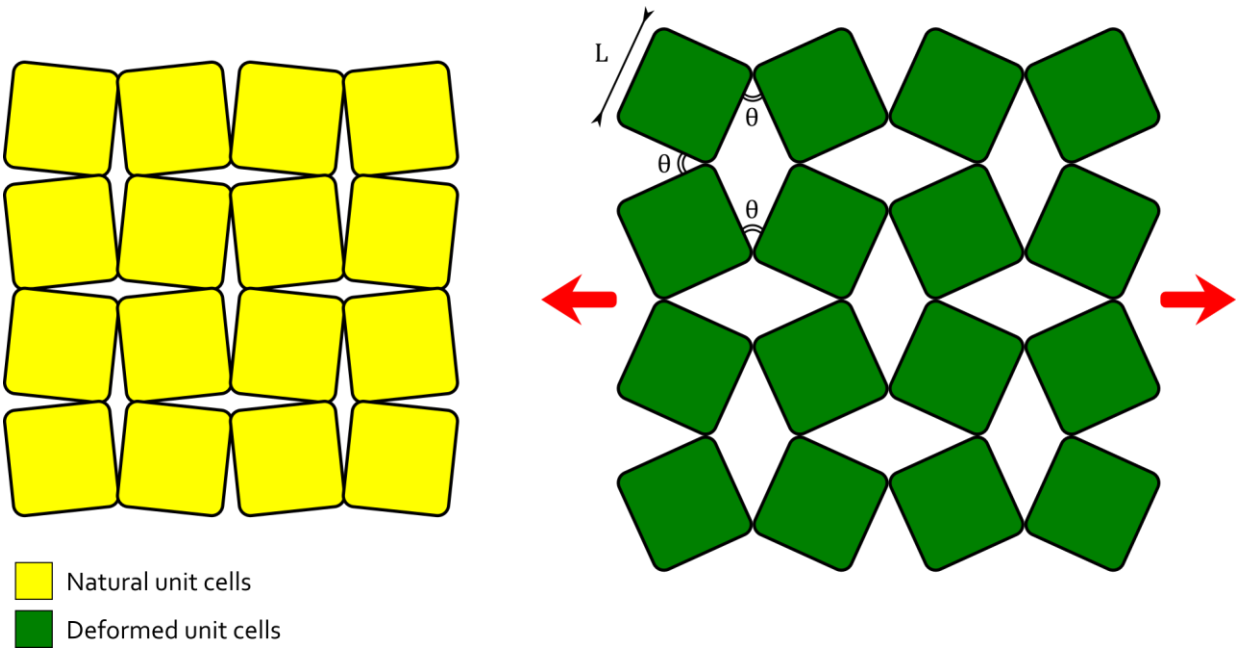

FIGURE 1.6.6 Illustration of auxeticity of rotating square structure

Considering the two aforementioned assumptions and applying the mathematical relations, Young's modulus, Poisson's ratio and compliance matrix of the rotating squares model can be presented as follows:

$$\nu_{12} = \nu_{21} = -1 \tag{1.6.4}$$

$$E_1 = E_2 = k_h \frac{8}{l^2} \cdot \frac{1}{1 - sin\theta} \tag{1.6.5}$$

$$S = \begin{pmatrix} S_{11} & S_{12} & 0 \\ S_{21} & S_{22} & 0 \\ 0 & 0 & 0 \end{pmatrix} = \frac{1}{E} \begin{pmatrix} 1 & 1 & 0 \\ 1 & 1 & 0 \\ 0 & 0 & 0 \end{pmatrix} \tag{1.6.6}$$

Where l, k_h, θ are the length of each edge of the square, stiffness coefficient of the hinges and the angle between the squares, respectively and depicted in Figure 1.6.6.

1.7 Medical application of auxetic materials

Due to the unique properties of these substances, auxetic materials are finding their place in various fields like biomedical. In recent years, some potential applications of the auxetic materials in the biomedical field have been reported, which will be discussed below.

Nowadays, materials with a positive Poisson's ratio are mainly used in manufacturing of arterial prostheses. In such conventional materials, when pressure of the blood flowing in vessels opens the lumen of blood vessels the wall thickness of the prostheses reduced. However results of using a material with a negative Poisson's ratio such as PTFE will be in reverse [43]. It follows that, as blood flow passes through the vessel and the lumen of the vessel increases under blood pressure, the thickness of the prosthesis wall increases and as a result, the possibility of its wall rupture decreases (Figure 1.7.1).

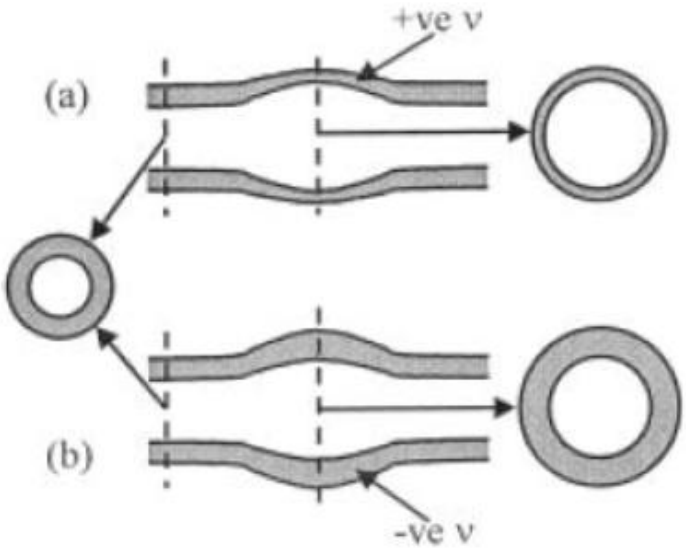

FIGURE 1.7.1 Schematic of deformation in artificial blood vessel: **(a)** conventional material **(b)** auxetic material [44]

Smart bandages shown in Figure 1.7.2 are another application of auxetic materials in the biomedical industries [45]. The micro proes between fibers of such smart bandages are impregnated by anti-inflammatory agents. When the infected wound becomes swollen, the auxetic fibers of the bondage are stretched. As a result of stretching, a controlled amount of anti-inflammatory agent is released on the wound. Therefore it speeds up the wound healing process. As the swelling of the wound heals, the bandage return to its original shape and the release of anti-inflammatory substance stops followed by closure of microfilament pores.

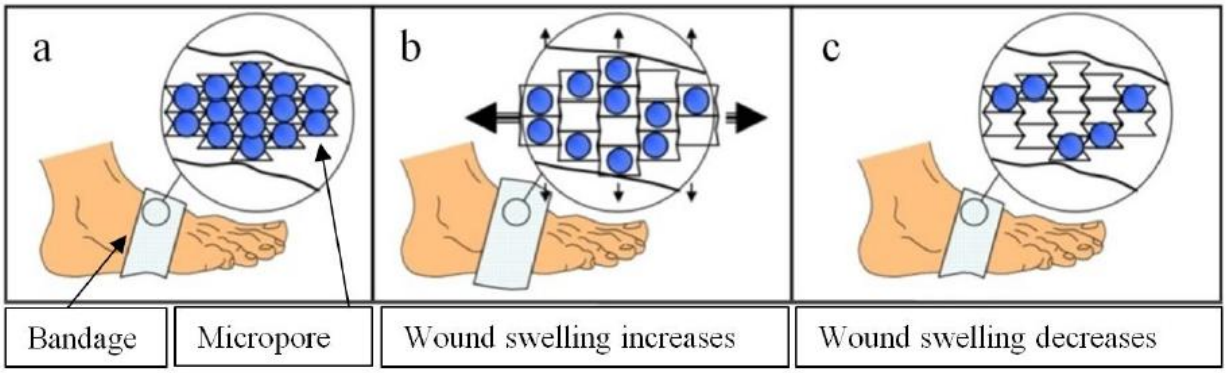

FIGURE 1.7.2 Schematic functionality of a smart bondage made by auxetic fibers containing anti-inflammatory agents [45]

Another application of auxetic material in biomedical field refer to a dilator which can be used in coronary angioplasty by implementing an expandable sheath made by an auxetic material [46] (Figure 1.7.3). Applying tension to the auxetic sheath make it expand laterally and open the coronary artery. auxetic stents have been proposed based on the similar concept [47].

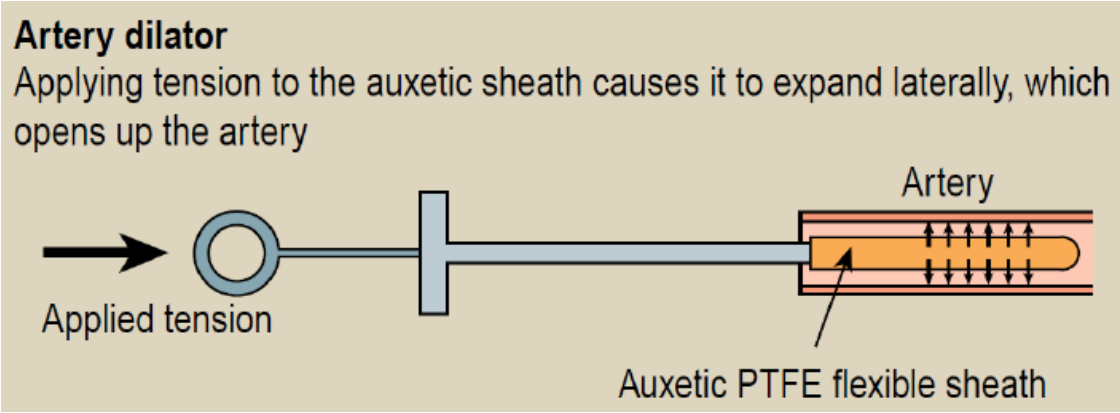

FIGURE 1.7.3 Dilator with an auxetic end sheath. Opening of the artery can be reached by inserting tension force on the finger apparatus which makes the auxetic end sheath expands laterally [46]

Sutures and Ligament-muscle anchors that made by auxetic material and benefit from pull-out resistance have been proposed by Simkins et al [48]. When a conventional suture or anchor subjected to tensile stress it becomes thinner as shown in Figure 1.7.4 (b). Therefore, it moves away from the surrounding material, which leads to the failure of the interface between stature and biomaterial. However an anchor made of auxetic material expands when stretched and locks in the surrounding biological material to prevent interface failure (Figure 1.7.4 (c)).

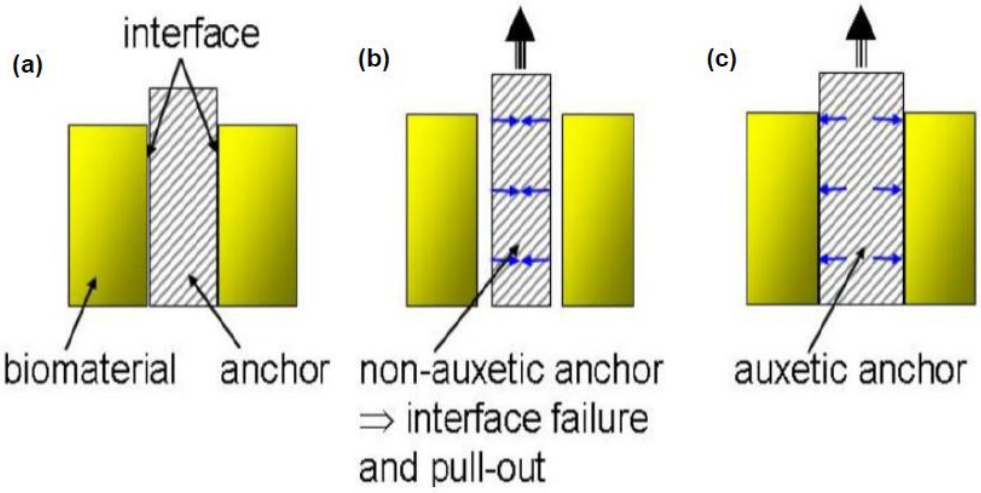

FIGURE 1.7.4 Different behavior of the conventional and auxetic medical stature under pull-out tension [48]

Esophageal cancer is the ninth most common cancer in the world, which is caused by a tumor in a patient's esophagus that causes obstruction and difficulty passing and digesting food. Therefore, in order to remove the obstruction and relieve the patient's pain, auxetic stent can be used. As demonstrated in Figure 1.7.5, Ali et al [49] designed and fabricated an auxetic film and developed it as an auxetic stent to relieve esophageal cancer pain and prevent further dysphagia.

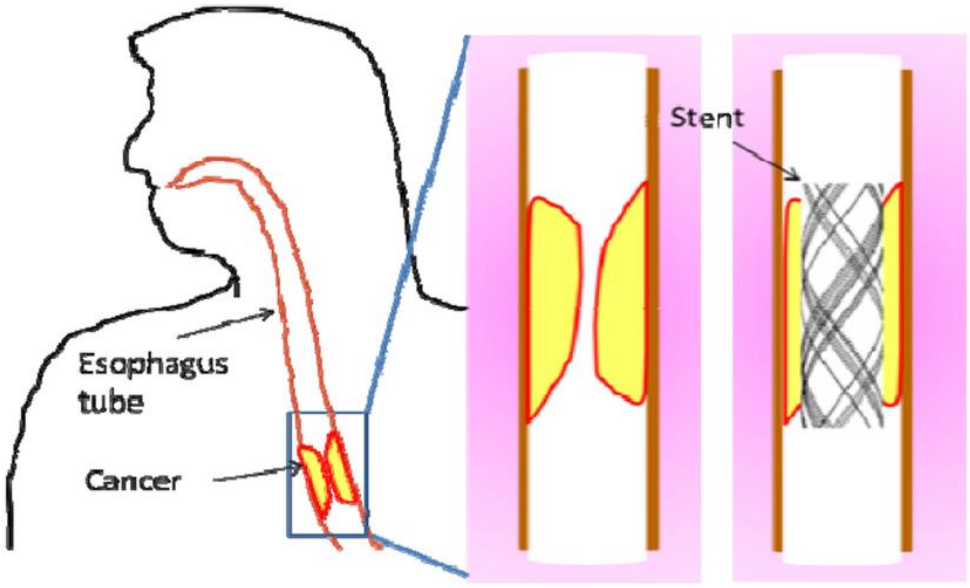

FIGURE 1.7.5 An auxetic stent used for remaining open the obstructed part of the esophagus [16]

Auxetic structures can be used in the design of angioplasty stents [50] and annuloplasty rings [51]. Cardiovascular disease is one of the most important health concerns in the world and requires considerable attention for its prevention and treatment. Due to the fact that the vascular system of the body has anisotropic properties [52], the implementation of commercially available isotropic coronary stents leads to a mismatch between the anisotropic-isotropic properties of the stent and the arterial wall. Therefore, good mechanical adhesion is not achieved. For this reason, it seems that the use of an auxetic stent, which has inherently anisotropic characteristic can eliminate this mismatch between the stent and the arterial wall and provide good mechanical adhesion. Amin et al [52] for the treatment of coronary heart disease developed the coronary stent demonstrated in Figure 1.7.6 based on an auxetic geometry which allows the stent to give negative Poisson's ratio. They stated that the auxetic stent would have desirable adhesion to the arterial wall due to its anisotropic mechanical properties. They concluded that when the stent is expanded by the balloon catheter, it stretches in both radial and longitudinal directions, and the stent does not show any foreshortening. In addition, it seems that the auxetic property of the stent has a significant effect on maintain of luminal patency and avoids the problem of stent migration.

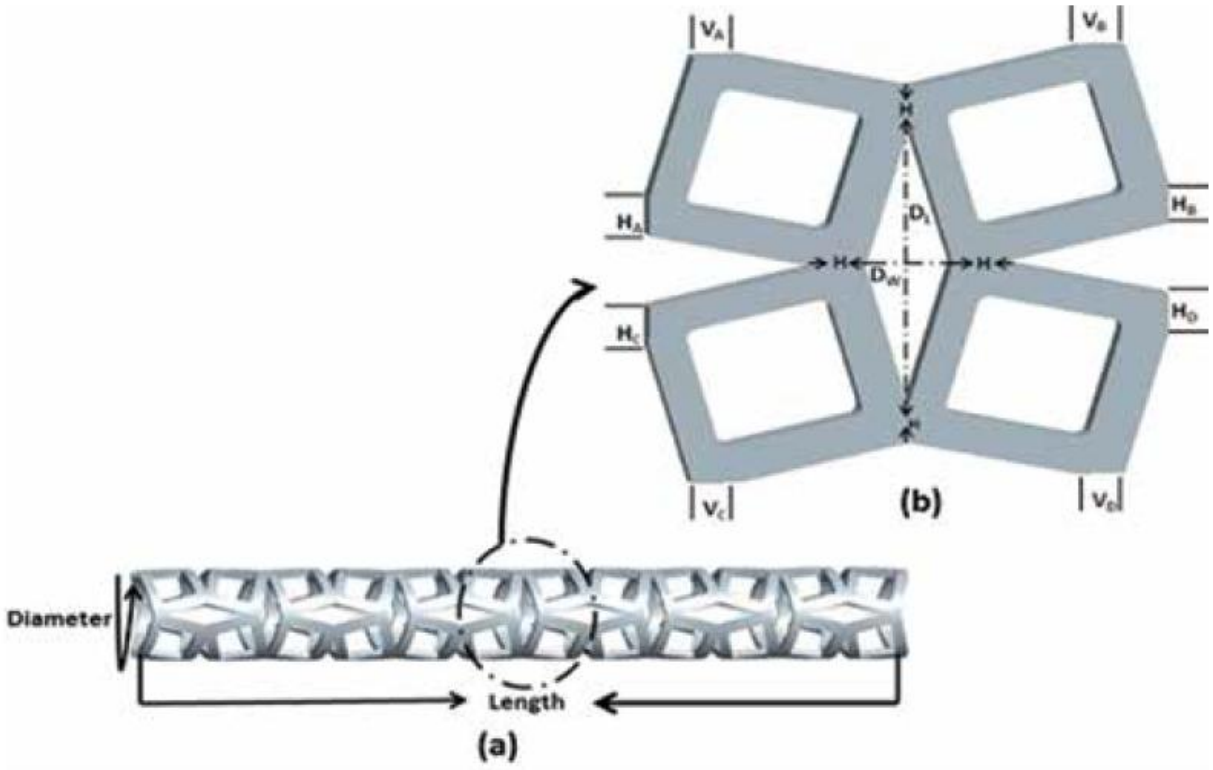

FIGURE 1.7.6 (a) 3D schematic of the auxetic coronary stent exploiting rotating square model, (b) magnified single unit cell of the coronary stent [52]

Another application of the auxetic structure refer to the total hip replacement, where hip stems can be created by using the logical pattern of auxetic and non-auxetic materials as depicted in Figure 1.7.7 to create a unique feature of compressive stress on both side of hip implants stem [52]. When the hip stems are bent, lateral side of the implant is stretched while the medial side is compressed. When stems are made only by conventional materials, the medial side of the hip implant which is under pressure will expand laterally, thus putting pressure on the surrounding bone tissue. Compression of the implant surface to the surrounding bone tissue is desirable because while eliminating the possibility of implant failure, it increases the stimulation of bone remodeling and also prevents the entry of wear particles into the areas between the surrounding bone tissue and implant, which increases the risk of interface failure. However, the lateral side of the implant which is under tension shrinks transversely and therefore tends to move away from the surrounding bone tissue. As a result, the tensile stress created between the surface of the implant and the surrounding bone causes the interface failure. The entrance of the wear particles can also easily occur into the area between the bone and the implant which in turns can cause an inflammatory reaction which leads to osteolysis. It seems the only way to address the problem is to use a material with a negative Poisson's ratio on the side that is under tension. In this way, it is pulled laterally and can increase the probability of implant success.

FIGURE 1.7.7 Combination of conventional and auxetic material (top) which leads to peripheral compression around hip stems (below) [53]

Polyurethane open cell foams are commonly used to make seat cushion pads [55]. A common open cell foam with a positive Poisson's ratio has an uneven distribution of normal stresses during indentation, which localizes the maximum stress around the contact area. However, a uniform stress distribution with lower maximum stress will be provided by implementing an auxetic foam with negative Poisson's ratio. These features make auxetic foam pads an excellent option as a cushion pads for patients suffering from disability or poor medical condition. Moreover, the two properties of mechanical stress distribution and mechanical flexibility of these pads make them suitable for use in knee prostheses [55].

1.8 Buckling of a structure

The sudden collapse of a structural member that has been subjected to a compressive axial load is called buckling. When the compressive axial load exceeds a threshold (critical load), a sudden lateral deflection occurs in the structure. That means the buckling load is obtained when this sudden lateral deflection occurs under axial pressure. From this point on, the structure enters the post-buckling phase. Under these conditions, the load-bearing capacity of the structure usually decreases and the structure shows relatively larger changes in response to relatively smaller loads. The post-buckling behavior of the structure depends significantly on its characteristics. This means that the structure can regain its load-bearing capacity, which is lost after reaching the critical load, in the post-buckling area. But in some cases, the structure fails and as a result collapses completely. Considering the buckling load in structural design is of great importance. It follows that when designing the structure, it should be considered that the critical buckling load of the structure should be more than the maximum load on it to prevent the structure from entering the buckling phase and the possible collapse. In general, narrow structures such as columns, shells and thin plates are prone to go under buckling. It should be noted that buckling instability depends solely on the geometry of the structure, and other nonlinear properties (such as nonlinearity of materials) have no effect on its formation.

In order to investigate the behavior of a structure under buckling compressive load, load displacement diagrams are usually used. Same diagrams are also implemented to study the behavior of the structure in the post-buckling area. Figure 1.8.1 shows the schematic buckling and post-buckling behavior of the structure in terms of in-plane displacement. The same diagram but in terms of out-of-plane displacement is drawn in Figure 1.8.2

1.8.1 Load vs in-plane displacement

Bucking behavior in shell structures (structures in which the thickness of at least one dimension is much smaller than the other dimensions) is accompanied by a sudden decrease in post-buckling strength. It should be pointed out that the slope of the load displacement

curve in the post-buckling region can be negative or positive, which determines the stability of the structure in the post-buckling regime. This means that a positive slope refers to the post-buckling strength of the structure even after reaching a critical point, while a negative slope indicates that the structure loses its strength completely and will simply collapses. It is worth mentioning that in the post-buckling regime, after reaching a certain amount of axial displacement (snap), the structure regains its post-buckling strength and can withstand loads even more than the critical load.

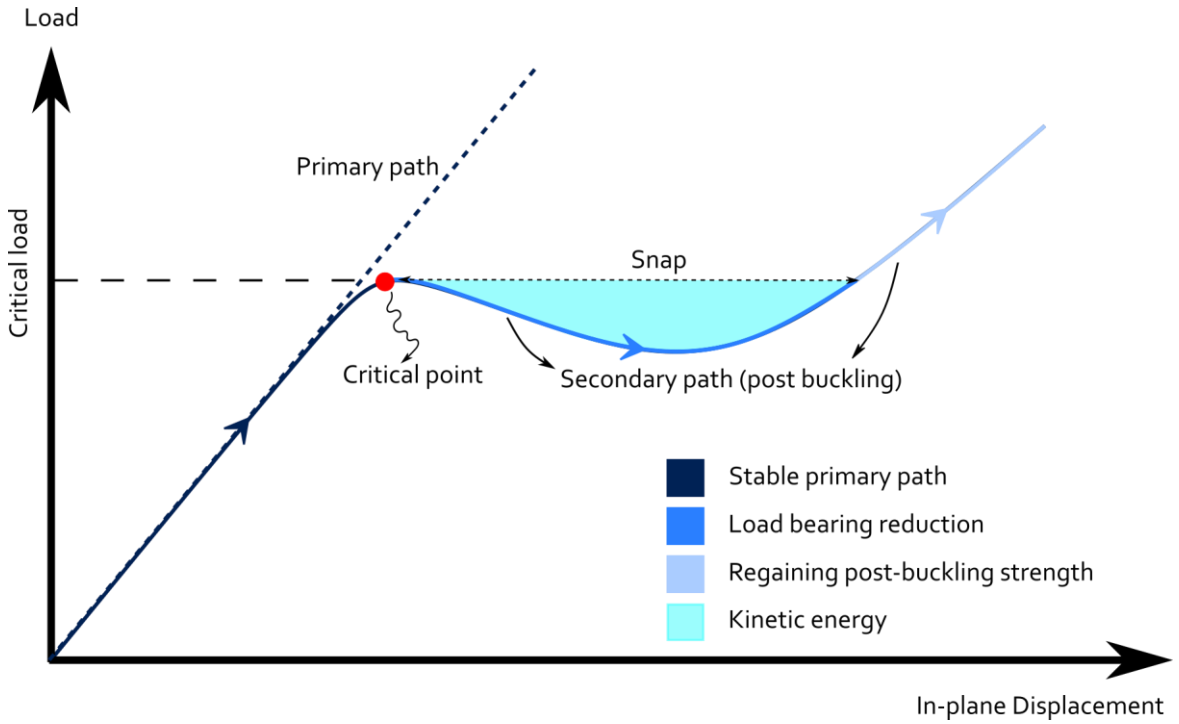

FIGURE 1.8.1 Schematic curve of buckling and post-buckling behavior of a structure in terms of in-plane displacement

1.8.2 Load vs out-of-plane displacement

As it is mentioned above, when a shell structure is subjected to axial compressive load, after reaching the critical load, it loses its load bearing capacity and then undergoes a significant lateral displacement. This lateral displacement usually occurs locally. Moreover when the structure reaches the critical point, it releases its strain energy accumulated by applying axial load in the form of kinetic energy. In the post-buckling area, after reaching a certain amount of lateral displacement (snap), the structure regains its load-bearing capacity and can withstand loads even beyond the critical load.

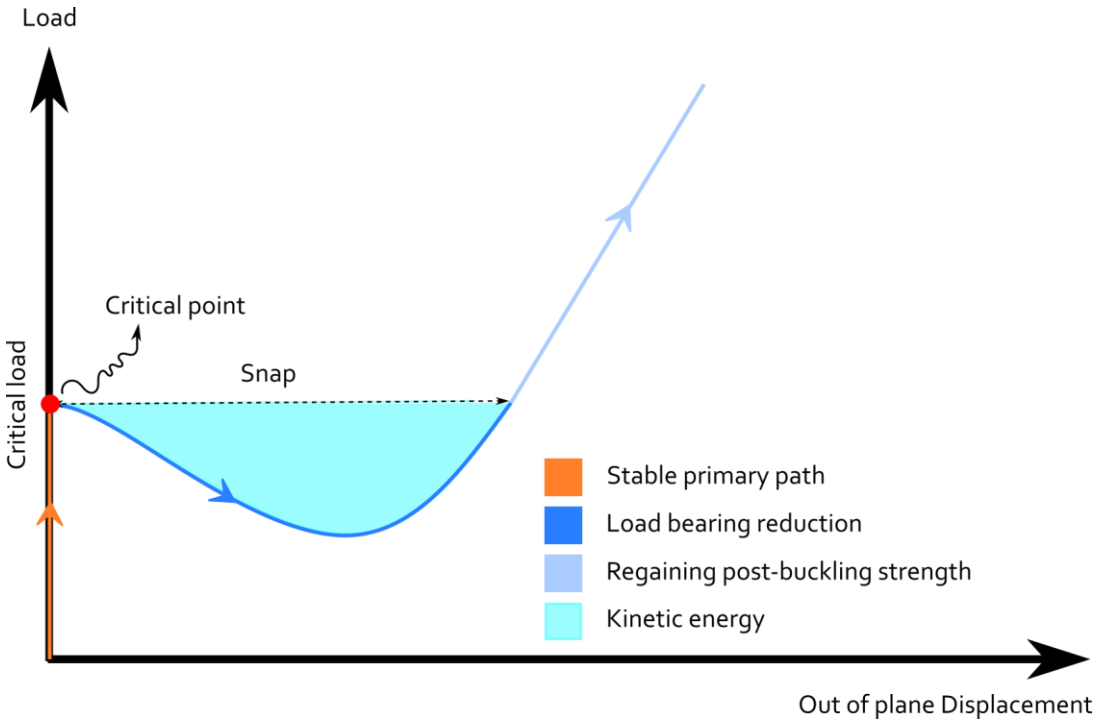

FIGURE 1.8.2 Schematic curve of buckling and post-buckling behavior of a structure in terms of out-of-plane displacement

1.8.3 Buckling of cellular structures

One of the biggest weaknesses of cellular structures is their buckling instability when they are under the action of compressive stress, which leads to premature collapse in cellular structures. The critical buckling load required for the collapse of the cellular structure is far less than the critical buckling load of the basis material that makes up the cellular structure. Structural parameters of cellular structures play an important role in the performance of the structures. Static and dynamic properties of the structures can be improved by Structural parameters or, conversely, their improper design can jeopardize the stability of the structures [56]. As a result, determining the optimal cellular structure parameters is essential for a particular application. Qianqian et al [57] studied 1D lattice truss composite structures in uniaxial compression by developing theoretical and numerical finite element methods and found that the length of the cellular column significantly effects the buckling modes of the structure. Magnucka-Blandzi [58] analyzed the buckling behavior of a pores plate under uniformly distributed compressive stress. The dependency of the buckling behavior of a 2D cellular structure on geometrical shapes has been investigated by Overvelde et al [59] and the authors expressed that geometry of the structure effects the buckling behavior of the soft porous structures. The effect of cellular structure geometry, out-of-plane thickness of the

plate and different boundary condition on the buckling behavior of functionally graded porous plate has been investigated by Jabbari et al [60]. Tang et al [61] revealed that different patterns of porosity distribution have different effects on the critical buckling load of the pores structure. Pihler et al [62] demonstrated that buckling behavior of a cellular structure can be significantly affected by that the pore size of the cellular structure. Aamer et al [56] studied uniform and variable-density cellular columns. They investigated buckling and post-buckling behavior of such columns and expressed improved critical buckling load resistance due to innovative construction of cellular column in which the beams located in the outer sides of the column are thicker than internal beams. In another survey, the same author found that height of the column and size of the unit cell can significantly affect the critical buckling load [63].

1.9 Buckling of a rectangular auxetic plate

Consider a plate of edges a and b and thickness h which is subjected to compressive load as depicted in Figure 1.9.1 The critical buckling load for such a plate in the case of uniaxial compression is [64]:

$$F_{cr} = \frac{\pi^2 D}{b^2} \cdot \left(\frac{a}{b} + \frac{b}{a}\right)^2 \tag{1.9.1}$$

Where D is bending stiffness of the plate and can be expressed as:

$$D = \frac{Eh^3}{12(1-\nu^2)} \tag{1.9.2}$$

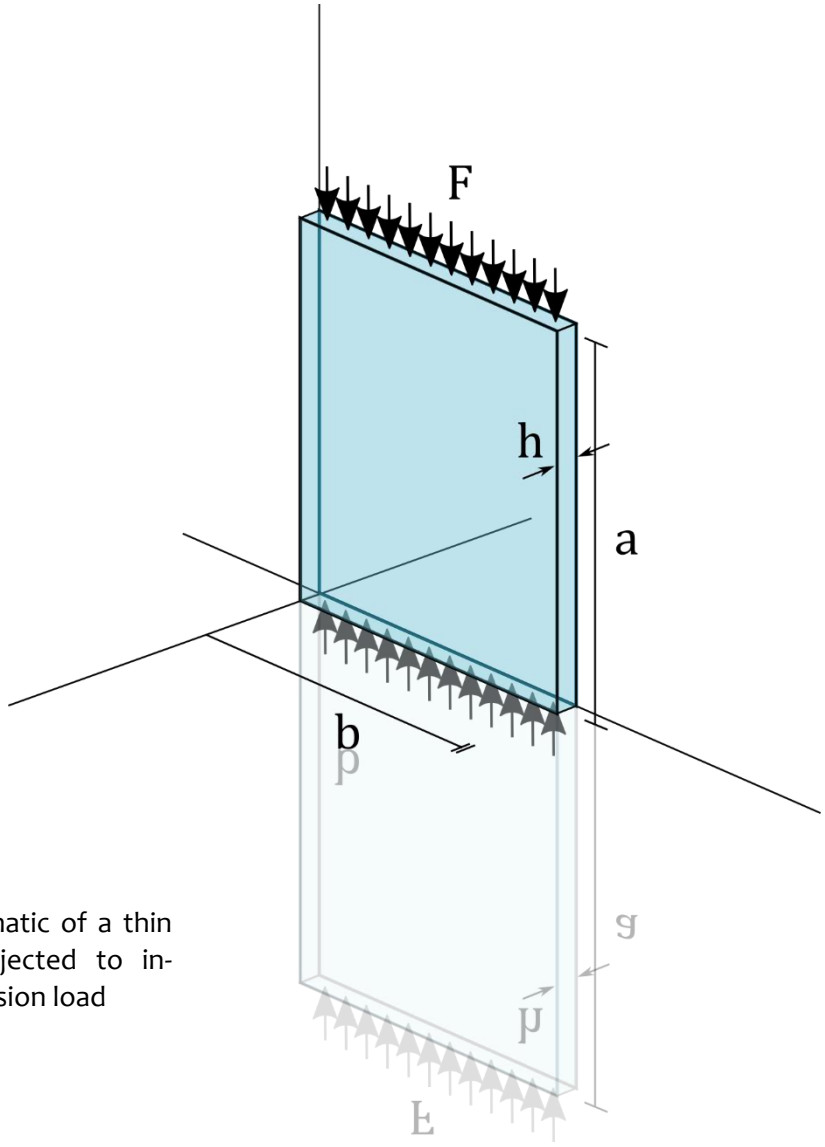

FIGURE 1.9.1 3D schematic of a thin rectangular plate subjected to in-plane uniaxial compression load

Obrecht et al [65] investigated the buckling behavior of a flattish rectangular plate under uniaxial compressive and shear stresses. The numerical results depicted in Figure 1.9.2 show how the critical stresses (normalized to the critical stresses at the Poisson's ratio equals to 0.3) change with respect to Poisson's ratio variations between 0.5 and around -0.9. As can be seen from the graph, when the Poisson's ratio approaches to minus one, the critical stress increases significantly. In fact, the order of magnitude of the increase is such great that it hardly happens in practice.

They suggested that a significant weight efficiency could be achieved by designing a macroscopic structure made of conventional non-auxetic materials. The critical force (normalized by weight) as a function of α (corresponding to the Poisson's ratio) is plotted in Figure 1.9.3. As it can be seen, critical loads and hence the critical stresses have different trend from what is shown in Figure 1.9.2 (related to a thin homogeneous auxetic plate). Here the maximum critical load occurs at a relatively small negative α. Moreover, the maximum load at this point is almost three times greater than the magnitude of critical load at $\alpha = +30$ which indicates weight efficiency can be increased by designing an auxetic structure with non-auxetic materials.

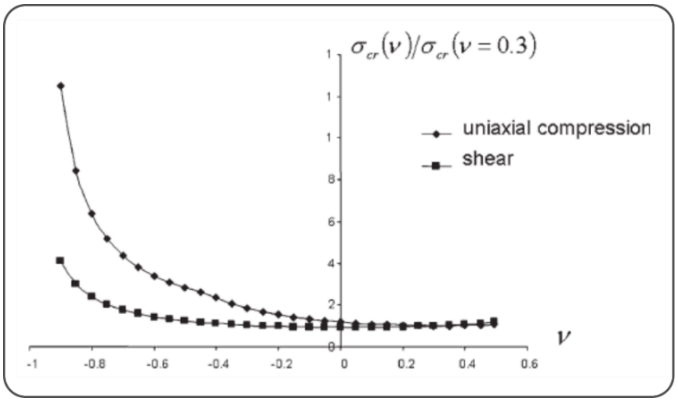

FIGURE 1.9.2 Variation of critical buckling stress of a flattish plate with respect to Poisson's ratio under uniaxial compression and shear

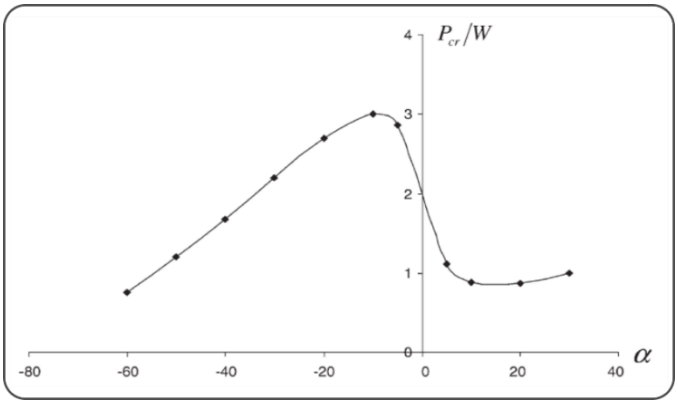

FIGURE 1.9.3 Dependence of the weight-normalized critical buckling load on the unit cell angle α

1.10 Buckling of a cylindrical auxetic shell

The critical buckling load of a cylinder shell of radius R and thickness h under compressive axial pressure as illustrated in Figure 1.10.1 is:

$$F_{cr} = \frac{Eh^2}{R\sqrt{3(1-\nu^2)}} \tag{1.10.1}$$

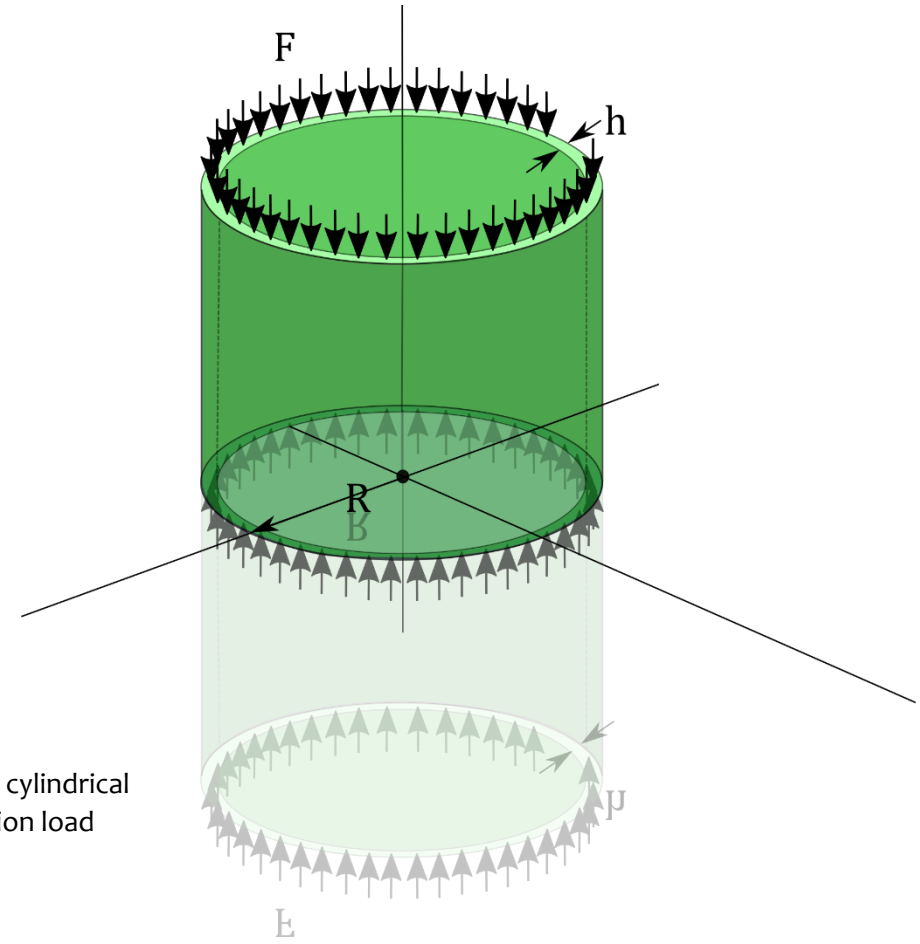

FIGURE 1.10.1 Buckling of a cylindrical shell under axial compression load

The critical load as a function of Poisson's ratio is shown in Figure 1.10.2. While it is clear from the Eq 1.10.1 and can be seen in the Figure, the critical buckling load is symmetric around $v = 0$.

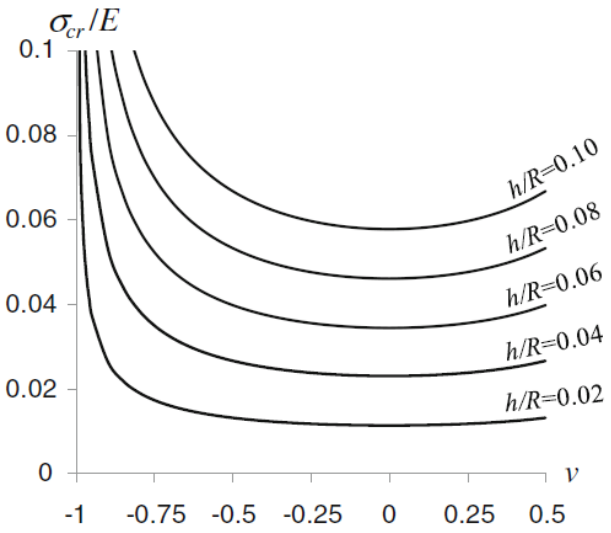

FIGURE 1.10.2 Dependence of critical buckling load (normalized by Young modulus) on Poisson's ratio in different thickness to radius proportion

1.11 Research questions

As described in part 1.6.4, the use of cellular structures has many advantages over solid structures. Due to these advantages, such structures are finding their place in various fields, such as biomedical industries. Moreover, since cellular structures allow the penetration of surrounding tissues into their porous space, the use of such structures with a high resistance to weight ratio will provide better stabilization of medical implants in the surrounding tissues. On the other hand buckling instability is one of the biggest weaknesses of such structures when they are under the action of compressive stress, which leads them to undergo premature collapse. The two aforementioned facts about cellular structure show the importance of the buckling analysis performed in this study on cellular plate and cylindrical structures. The motivation of this study is to find out how a structure with a desired buckling strength and stability can be designed by adjusting the structural parameters. In fact, we are trying to answer to the following questions:

- How does the auxetic property change the mechanical buckling behavior of a cellular plate and cylinder?

- How does changing the geometric parameters of a structure affect its buckling behavior and critical load?

- Do the structural parameters have similar effects on the buckling and post-buckling behavior of two different geometries of plate and cylinder?

- How the post-buckling slope of a structure (which indicates its stability) can be tuned by designing its structural parameters?

- Are the effects of geometric parameters on the mechanical behavior of the structure interdependent? How?

1.12 Study outline

In order to answer the above questions, we investigated on both plate and cylindrical models separately. For this purpose, we used the cellular structure model proposed by Gibson et al. to create our cellular models. We designed three primary reference models for cellular plates and two primary reference models for cellular cylindrical structures. Then for studying each of these five reference models numerical finite element method in ABAQUS has been implemented. In order to validate the numerical method, reference models were fabricated by additive manufacturing technology and subjected to buckling test. After verifying the numerical results extracted from the finite element method, we created other models by changing the geometric parameters of both plate and cylindrical structures to investigate how variable geometric parameters can tune buckling and post buckling behavior of the both plate and cylindrical cellular structures. A total of 84 solid models in plate geometry and 45 solid models in cylindrical geometry were designed in SOLIDWORKS and simulated in ABAQUS software. After performing numerical solution on all models, the relevant results were extracted and investigated to reveal the effect of geometric parameters on the buckling and post-buckling behavior of the plate and cylindrical cellular structures.

Chapter 2

Materials & Methods

In this chapter, we intend to describe in detail the models created by changing the geometric parameters of the structure. For this purpose, we used the cellular structure model proposed by Gibson et al. which has briefly described in section 1.6.4.1. In fact, we designed our models in both plane and cylindrical geometries consisting of re-entrant honeycomb unit cells shown in Figure 1.6.5. In the following, we comprehensively explain this type of cellular model and the corresponding conventional and auxetic cellular plates and cylinder designed by variable structural parameters

2.1 Auxetic cellular plate

Auxetic cellular plates are designed as rectangular patterns of single re-entrant honeycomb unit cells shown in Figure 2.1.1. As you can see in the Figure below, an enlarged image of a cell unit with its structural parameters is displayed. As it mentioned earlier, dependency of buckling and post-buckling behavior of the structure on these geometric parameters in macroscopic scale is investigated.

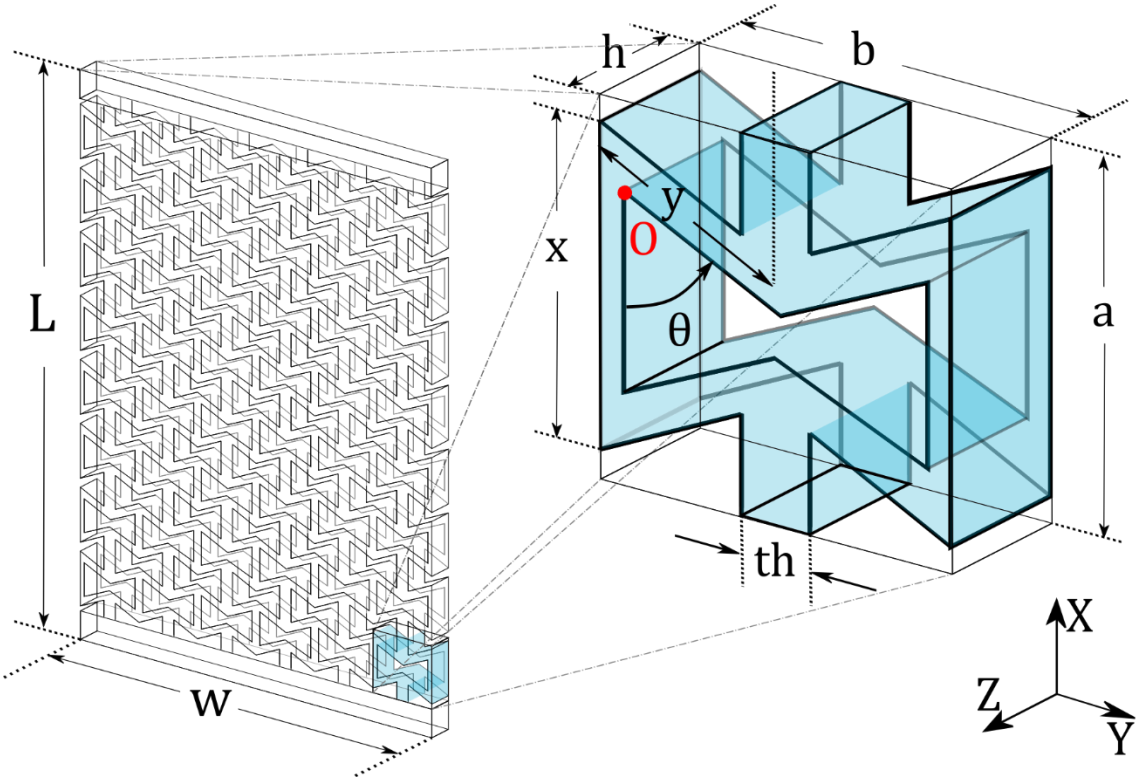

FIGURE 2.1.1 Three-dimensional schematic of an auxetic cellular plate and a magnified image of a unit cell characterized by geometric parameters

Now let's define each of these independent parameters:

$\boldsymbol{h}$: The out-of-plane thickness of the plate along the axis Z. It should be noted that since there is only one unit cell in the thickness of the plate, then both plate and unit cell have identical out-of-plane thicknesses.

$\boldsymbol{th}$: The in-plane thickness of all cell members including diagonal and vertical struts.

$\boldsymbol{x}$: The length of the vertical struts

$\boldsymbol{y}$: The length of the diagonal struts

$\boldsymbol{\theta}$: The angle between the diagonal and vertical struts. θ is the value of the angle that the diagonal strut makes with the vertical strut by rotation around the point O.

$\boldsymbol{L}$: The length of the plate. This is the direction in which compressive stresses are applied on the plate

$\boldsymbol{w}$: The width of the plate.

It is worth mentioning that in order to design structures with different Poisson's ratios, each unit cell is limited to a reference cube with dimensions of a, b and h (see Figure 2.1.1). In fact, variation of the angle θ, which it turn changes the unit cell from conventional honeycomb to the auxetic one occurs in a constant height-to-width ratio a/b of the unit cells. The plate models are designed as rectangular arrangements of the defined unit cells. It consists of n unit cells in length and m in width. By doing a simple mathematics these two parameters can be determined as the following:

$$n = L/a \tag{2.1.1}$$

$$m = w/b \tag{2.1.2}$$

Another parameter that has been investigated is the size of the unit cells. As mentioned earlier, each unit cell is housed inside a reference rectangle of dimensions a and b. Now suppose we multiply the sides of this rectangle by a constant. The resulting rectangle will have sides equal to a' and b'. $R = a'/a = b'/b$ is the constant which determines the size of the unit cells. As a result, by changing the R, the shape of the reference rectangle will be preserved and only the ratio of the corresponding sides will change.

In order to calculate the analytical Poisson's ratio and Young modulus of the unit cell we used the expression provided by Gibson et al. If the applied force is in the direction of the vertical struts, ie in the direction 1 in Figure 2.1.2, the Poisson's ratio and Young modulus in the direction of the applied force can be obtained from Equation 1.6.1. and 1.6.2 respectively. However since we have considered a different definition of θ, these two equation can be rewritten by change of the variables as the following:

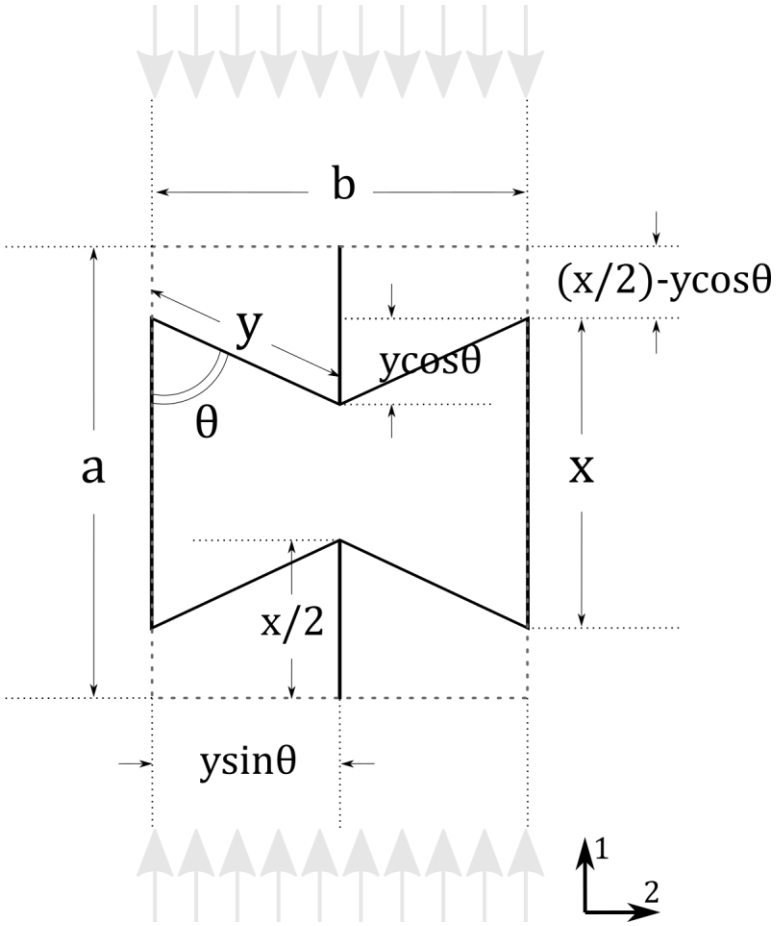

FIGURE 2.1.2 2D schematic of a re-entrant unit cell under axial compression load

$$\theta \to -\frac{\pi}{2} + \theta, \qquad h \to x, \qquad l \to y$$

$$\nu_{12} = \frac{\varepsilon_2}{\varepsilon_1} = -\frac{cos\theta(x/y - cos\theta)}{sin^2\theta} \tag{2.1.3}$$

$$E_1 = k\frac{(x/y - cos\theta)}{bsin^3\theta} \tag{2.1.4}$$

$$k = E_s b\left(\frac{t}{l}\right)^3 \tag{2.1.5}$$

In order to analyze the dependence of buckling and post-buckling behavior of the structure on the structural parameters, three reference models of an auxetic cellular plate characterized by the values in Table 2.1.1 were defined.

TABLE 2.1.1 Values of the geometric parameters used for the references models of cellular plate

	θ^o	h (mm)	a/b	th (mm)	R	L (mm)	W (mm)
Model 1	48	5	1.5	0.51	1	130.05	92.31
Model 2	88	5	1.5	0.51	1	130.05	92.31
Model 3	120	5	1.5	0.51	1	130.05	92.31

Based on the three reference models, another 81 cellular plates were created. The later models are characterized by range of variations in the out-of-plane thickness h, in the angle θ, in the ratio a/b, in the in-plane thickness th, in the scaling parameter R and in the width w of the plate. In the following sections, we will comprehensively expound each of these structural parameters and their corresponding models.

2.1.1 Models created by change of the Poisson's ratio

The change in the Poisson's ratio is a consequence of a change of the angle θ. When $\theta < \pi/2$, the Poisson's ratio possess negative value and the structure gives auxetic properties. As the theta increases to $\pi/2$, the auxeticity of the model decreases and the Poisson's ratio tends to zero. Then, by increasing θ and passing beyond $\pi/2$, the Poisson's ratio becomes positive and the structure enters to the non-auxetic phase. In order to obtain both auxetic and conventional models, a relatively wide range of the angle θ $(48 \leq \theta \leq 120)$ has been covered. The mentioned interval is divided into 9 equal parts. It follows that the angle can possess 10 (2 boundary values and other 8 values in the interval) different values in total as summarized in table 2.1.1.

As mentioned earlier and also shown in the Figure 2.1.2, all unit cells designed for different angles are bounded inside a rectangle with length a and width b. This is because the final cellular plates have the identical length and width, regardless of the value of their unit cells angle. For this purpose, using simple mathematical equations and what is presented in the Figure 2.1.2, the length of the vertical and oblique struts of the unit cell can be obtained as a function of the angle θ. Then we have:

$$2ysin\theta = b$$

$$\Rightarrow y = \frac{b}{2sin\theta} \tag{2.1.6}$$

$$x + 2\left(\frac{x}{2} - ycos\theta\right) = a$$

$$\Rightarrow 2x - 2ycos\theta = a$$

$$\Rightarrow x = \frac{a}{2} + ycos\theta \qquad (2.1.7)$$

In the primary models the values of a and b are constant and equal to 7.5 and 5, respectively. It should be noted that, these two parameters are not always constant and will be changed when the effect of their variation is studied. By substitution the values of a, b and θ in $Eq.(2.1.6)$ and $Eq.(2.1.7)$ the value of vertical and oblique struts corresponding to each angle can be obtained. After that by implementing $Eq.(2.1.3)$ the corresponding Poisson's ratio can be determined (see Table 2.1.1). By changing Poisson's ratio a set of ten cellular plates were designed. Values of structural parameters with respect to variations of Poisson's ratio are summarized in the Figure 2.1.3. Values of the reference models are highlighted by the blue color.

θ^o	$X_{(mm)}$	$Y_{(mm)}$	υ
48	6.11	3.43	-1.35
56	5.54	3.07	-1.01
64	5.06	2.83	-0.73
72	4.65	2.68	-0.49
80	4.27	2.58	-0.26
88	3.91	2.55	-0.05
96	3.55	2.56	0.16
104	3.19	2.63	0.37
112	2.79	2.75	0.61
120	2.35	2.94	0.87

TABLE 2.1.1 Ten different values of the angle between the vertical and oblique struts and the corresponding Poisson's ratio

2.1.2 Models created by change of the out-of-plane thickness

The out-of-plane thickness is another important parameter that has been investigated in our study. Beside $h = 5\ mm$ which is considered for the reference models other five values have been chosen to figure out how the change of the out-of-plane thickness can modify buckling and post-buckling behavior of the models. It should be noted that the $h = 26\ mm$ is considered only for five models with $\nu = -1.35, -0.49, -0.05, 0.37, 0.87$. However, other

thicknesses regardless of the value of the Poisson ratio have been applied to all models. It follows that, another 45 models were obtained by changing the thickness h. Values of the structural parameters with respect to variations of the out-of-plane thickness are shown in Figure 2.1.4. The blue color values refer to the reference models.

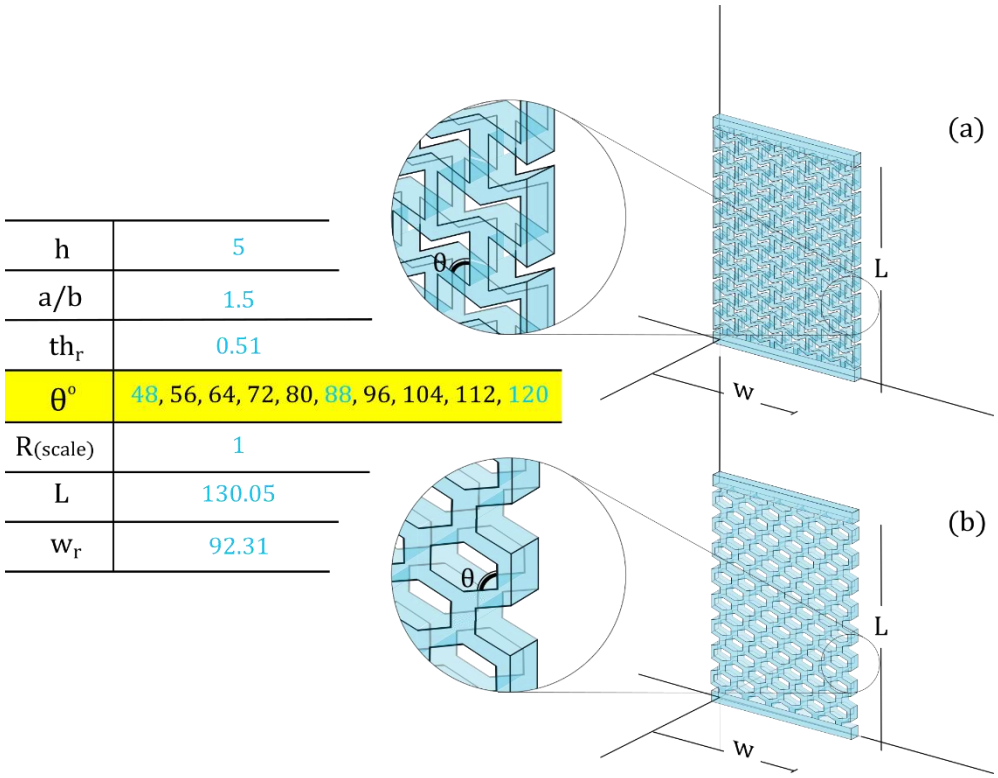

FIGURE 2.1.3 3D schematic of the plate models created by changing the angle θ: **(a)** auxetic plate **(b)** conventional honeycomb plate

2.1.3 Models created by change of the in-plane thickness

As mentioned above, the in-plane thickness is actually the thickness of the oblique and vertical struts of the unit cells. Here, the effect of variation of in-plane thickness was studied only in two models with maximum and minimum Poisson's ratio, ie $\nu = -1.35, 0.87$. Considering four thicknesses of $th = 0.1275\ mm, 0.255\ mm, 0.3825\ mm, 0.6375\ mm$ for these Poisson's ratio, other 8 models were designed. Values of the structural parameters with respect to variations of the in-plane thickness are represented in Figure 2.1.5. It is worth mentioning that in order to have better understanding and comparison, instead of the numerical value of the thickness we used the fraction th/th_r, which is the ratio of the thickness of a secondary model to the thickness of the reference model. For instance, since the in-plane thickness of the references models equal to $th_r = 0.51\ mm$ then $th/th_r = 0.25$ and $th/th_r = 1.25$ refer to the thickness of 0.1275 and 0.6375 respectively.

th_r	0.51
a/b	1.5
h	1, 2.5, 5, 7.5, 10, 26*
θ^o	48, 56, 64, 72, 80, 88, 96, 104, 112, 120
R(scale)	1
L	130.05
w_r	92.31

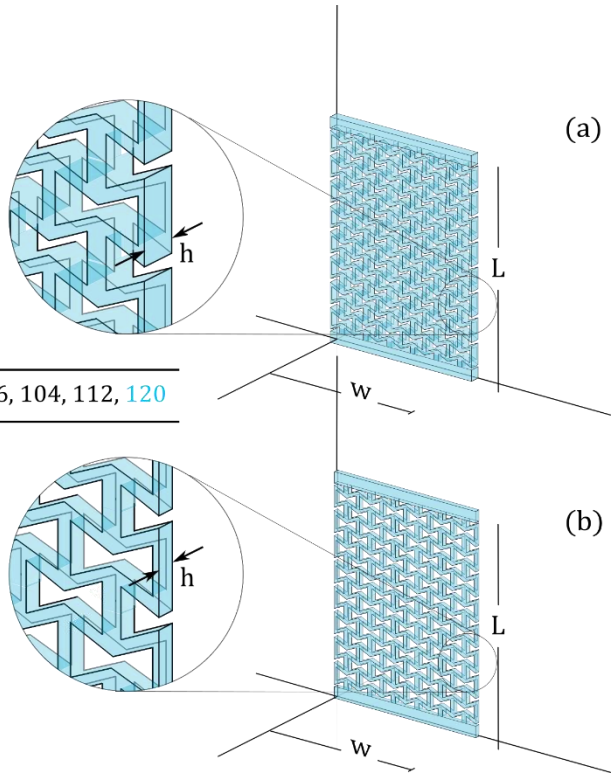

FIGURE 2.1.4 3D schematic of the plate models created by changing the out-of-plane thickness. The auxetic plate depicted in **(a)** is two times thicker than the one shown in **(b).** * $h = 26$ is considered only on five models with $\theta^\circ = 48, 72, 88, 104, 120$

h	5
a/b	1.5
θ^o	48, 120
th/th_r	0.25, 0.5, 0.75, 1, 1.25, 1.5
R(scale)	1
L	130.05
w_r	92.31

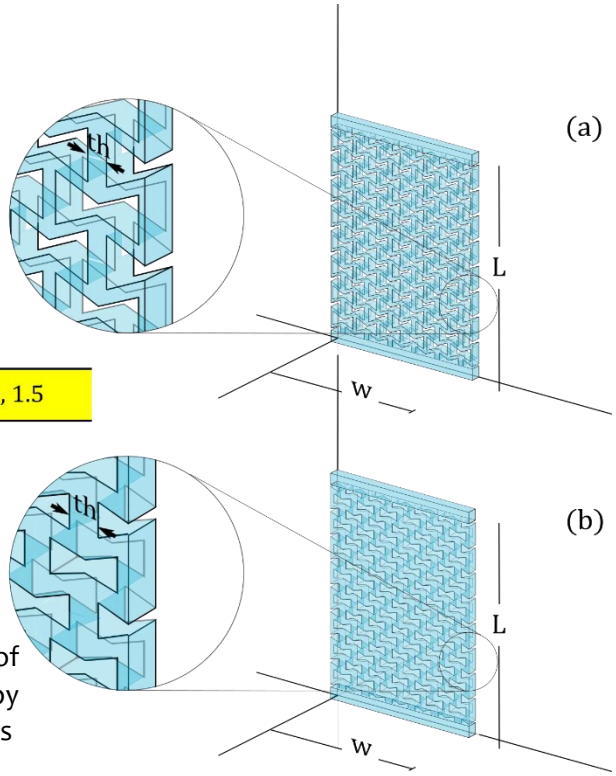

FIGURE 2.1.5 3D schematic of the plate models created by changing the in-plane thickness

2.1.4 Models created by change of the width of the plate

Three other different width ($w = 46.155\ mm, 184.62\ mm, 369.24\ mm$) for only two cellular plate with maximum and minimum Poisson's ratio ($\nu = -1.35, 0.87$) have been considered to investigate how the width of a plate can play a role in tuning of the buckling and post-buckling behavior of a cellular re-entrant honeycomb plate. Variation of the width of the plate gives 6 new models. Like what mentioned about the in-plane thickness, here again the fraction w/w_r, which is the ratio of the width of a secondary model to the width of the reference model, has been implemented. For instance, since the plate width of the references model equals to $w_r = 92.31\ mm$, then $w/w_r = 0.5$ and $w/w_r = 4$ refer to the width of 46.155 and 369.24 respectively. Values of the structural parameters with respect to variations of the plate width are demonstrated in Figure 2.1.6.

h	5
a/b	1.5
θ^o	48, 120
w/w_r	0.5, 1, 2, 4
$R_{(scale)}$	1
L	130.05
th_r	0.51

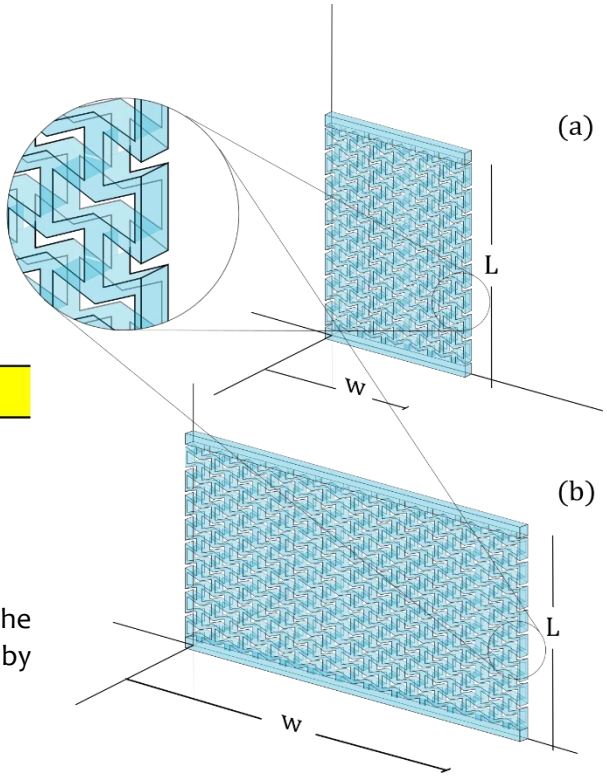

FIGURE 2.1.6 3D schematic of the plate models created by changing the plate width

2.1.5 Models created by change of the scaling parameter

Three different scaling parameters ($R = 0.75, 1.5, 3$) only for the two maximum and minimum Poisson's ratio ($\nu = -1.35, 0.87$) is considered which in turn offers 6 new models. Figure 2.1.7 represented the values of the structural parameters with respect to different scaling values.

h	5
a/b	1.5
th_r	0.51
R(scale)	0.75, 1, 1.5, 3
θ^o	48, 120
L	130.05
w_r	92.31

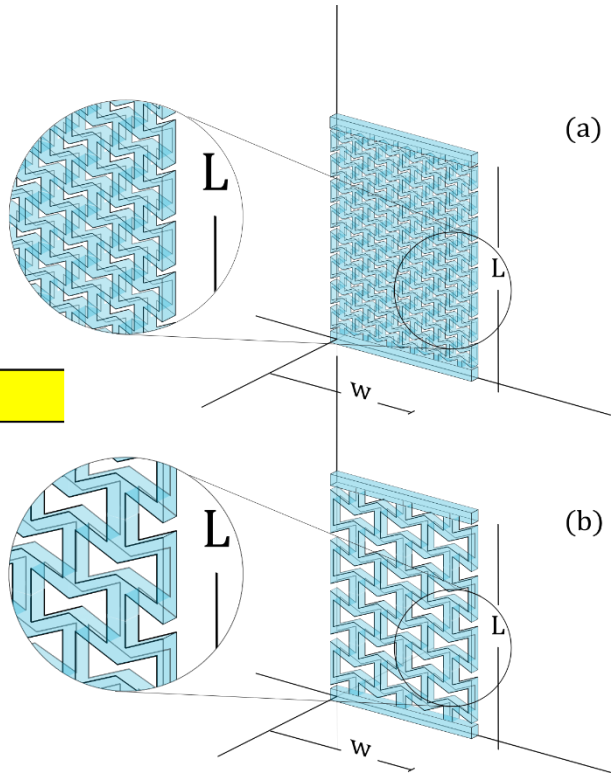

FIGURE 2.1.7 3D schematic of the plate models created by changing the scale R. Unit cells of the auxetic plate depicted in **(a)** is two times smaller than the one shown in **(b)**

2.1.6 Models created by change of the ratio a/b

In order to prevent the mutual interfusion of diagonal struts of a unit cell, the following constraint is imposed to its angle (see also Figure 2.1.2):

$$ycos\theta < x/2 \Rightarrow \theta < Arccos\,(x/2l) \tag{2.1.8}$$

The value of b is kept constant and the ratio a/b is changed by only changing the parameter a. Thus, by increasing and decreasing the numerical value of a, two different $a/b = 1, 2$ used for five different Poisson's ratios ($\nu = -1.35, -0.73, 0.05, 0.37, 0.87$). It should be noted that due to the geometric constraint presented in $Eq.\,(2.1.8)$, it is not possible to design a model with $\theta = 48$ and $a/b = 1$. The values of the structural parameters with respect to variation of the ratio a/b is demonstrated in Figure 2.1.8.

h	5
th_r	0.51
a/b	1*, 1.5, 2
θ^o	48, 64, 88, 104, 120
R(scale)	1
L	130.05
w_r	92.31

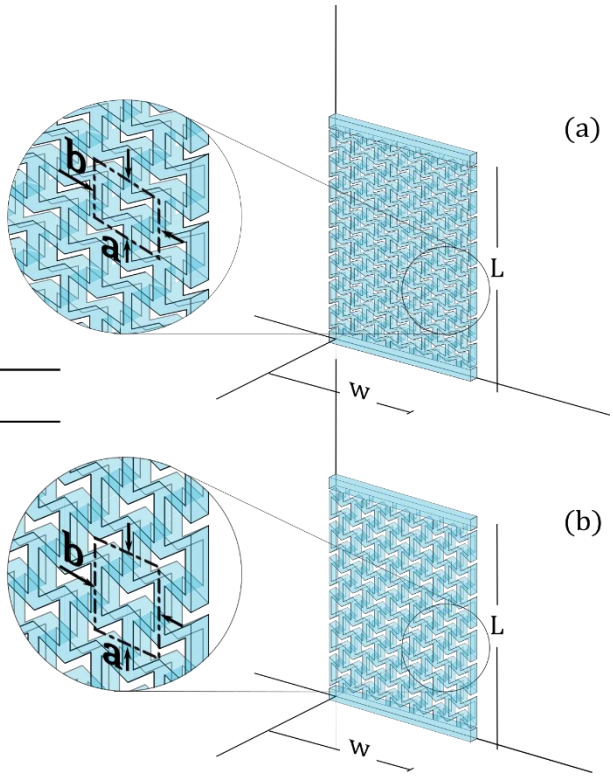

FIGURE 2.1.8 3D schematic of the plate models created by changing the ratio a/b.
* $a/b = 1$ is not applied to $\theta^\circ = 48$ due to the geometric restriction

In order to investigate the behavior of the structure under the influence of buckling force, each of the three reference models were subjected to compressive load as depicted in Figure 2.1.9. First, the models were analyzed numerically and then we performed buckling test on the reference models to validate the numerical approach. In the following sections both numerical and experimental approaches are comprehensively discussed.

2.1.7 Numerical simulation

The commercial finite element software ABAQUS/Explicit was implemented to study buckling and post-buckling behavior of the conventional and auxetic cellular plates designed in the Computer-Aided Design software SOLIDWORKS. Linear buckling analysis is firstly conducted by applying unit compressive force on the top of the plate and extracting its displacements as an output. By considering the first mode shape, calling the extracted data and applying 12% strain with imperfection scale factor of 1, non-linear general static analysis executed to obtain post-buckling behavior of the structures. Isotropic elastic material with $E = 3500\ MPa$ and $\upsilon = 0.3$ is assigned to the models. In all simulations the lower surface of the structure could just freely rotate around axis X (see Figure 2.1.7). Rotation around axis X and translation in

the direction Y is the boundary condition which is applied to the top surface of the structure. The solid model was discretized by linear hexagonal element without reduced integration ($C3D8$) with approximate mesh size 1. The mesh size was selected after performing mesh convergence analysis for the reference models.

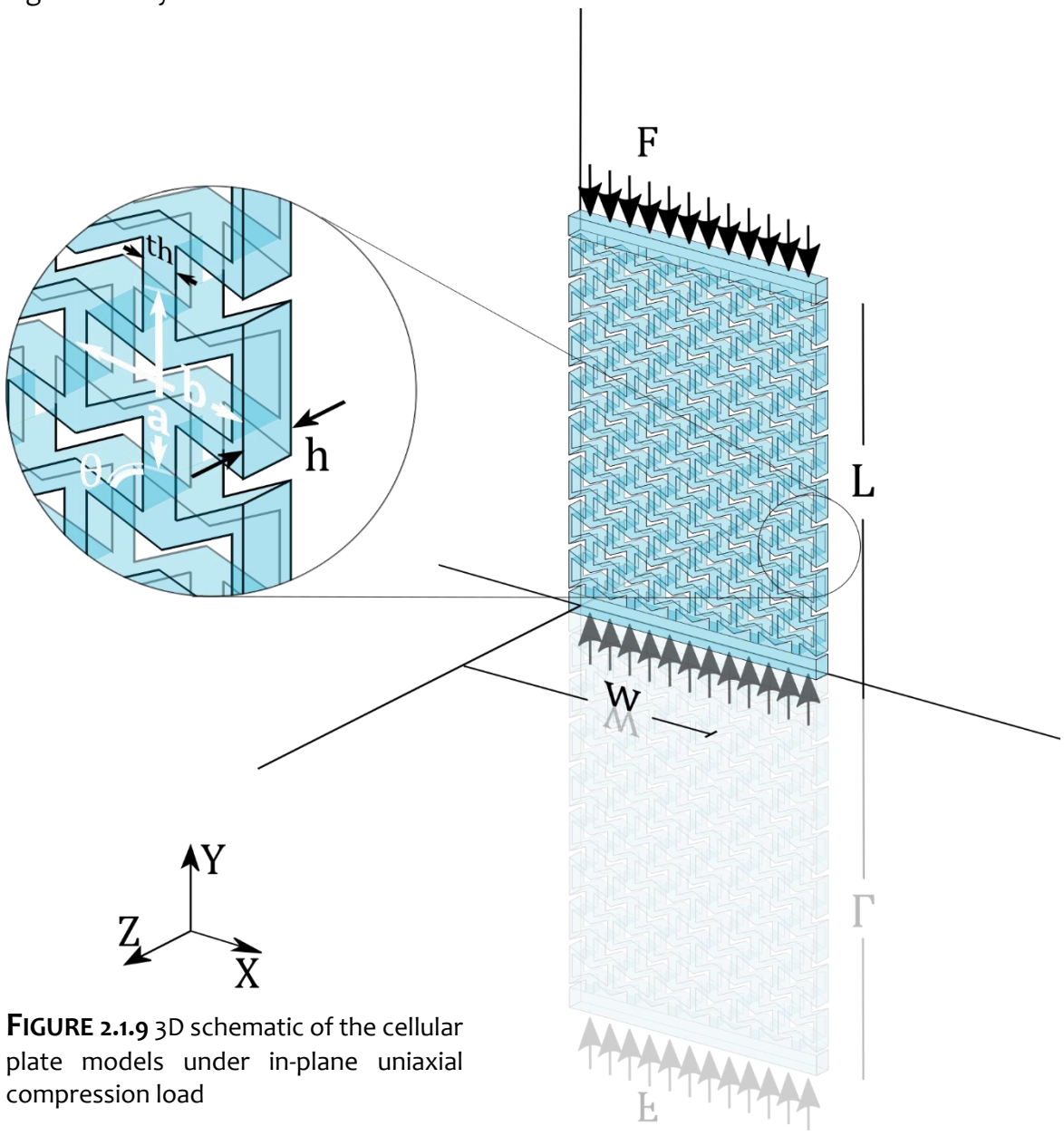

FIGURE 2.1.9 3D schematic of the cellular plate models under in-plane uniaxial compression load

2.1.8 Sample preparation and experimental setup

As it mentioned above we performed buckling test only on the reference models to validate the numerical approach. In order to perform buckling tests in a more efficient and precise manner, a griper which is able to mimic the simulated boundary condition is needed. The gripper consists of two different parts as depicted in Figure 2.1.10. Hard parts which are

printed by Vero Cyan with $E = 2000{\sim}3000\ MPa, \upsilon = 0.3$ and the soft part that is made by black rubberlike material with Shore Hardness 85. The most challenging part of design of such gripper is to allow the sample to rotate around axis X. As it can be seen in Figure 2.1.10 a, the sample is mounted on the solid part and the soft part allows it to rotate around intended axis (Figure 2.1.8 (b)). The soft part of the gripper should be flexible enough allowing models rotate and strong enough not to undergo buckling before buckling of the structure.

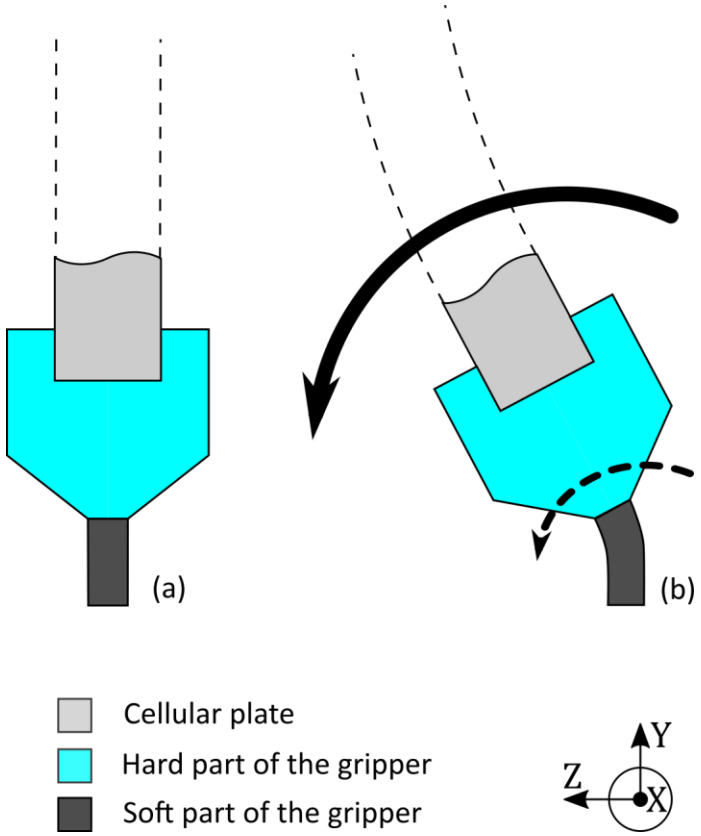

FIGURE 2.1.10 Different parts of the designed gripper. **(a)** Before loading: plate mounted on the gripper and **(b)** after loading: rotation of the sample around axis X due to use of soft material

Cellular plates were fabricated by additive manufacturing technology and printed by Ultimaker 3D printer with the PLA (infill40%, $E = 3500\ MPa, \upsilon = 0.3$). Three samples are fabricated in three different colors white ($\upsilon < 0$), green ($\upsilon = 0$) and red ($\upsilon > 0$) based on dimensions of the reference models (Figure 2.1.11). Samples are mounted on grippers and all together are connected to the loading machine equipped with a 100 N load cell allowing us to perform a uniaxial buckling test and measure the axial force with respect to the axial compressive displacement. For each sample quasi static compression test with strain rate of $0.002\ s^{-1}$ were conducted.

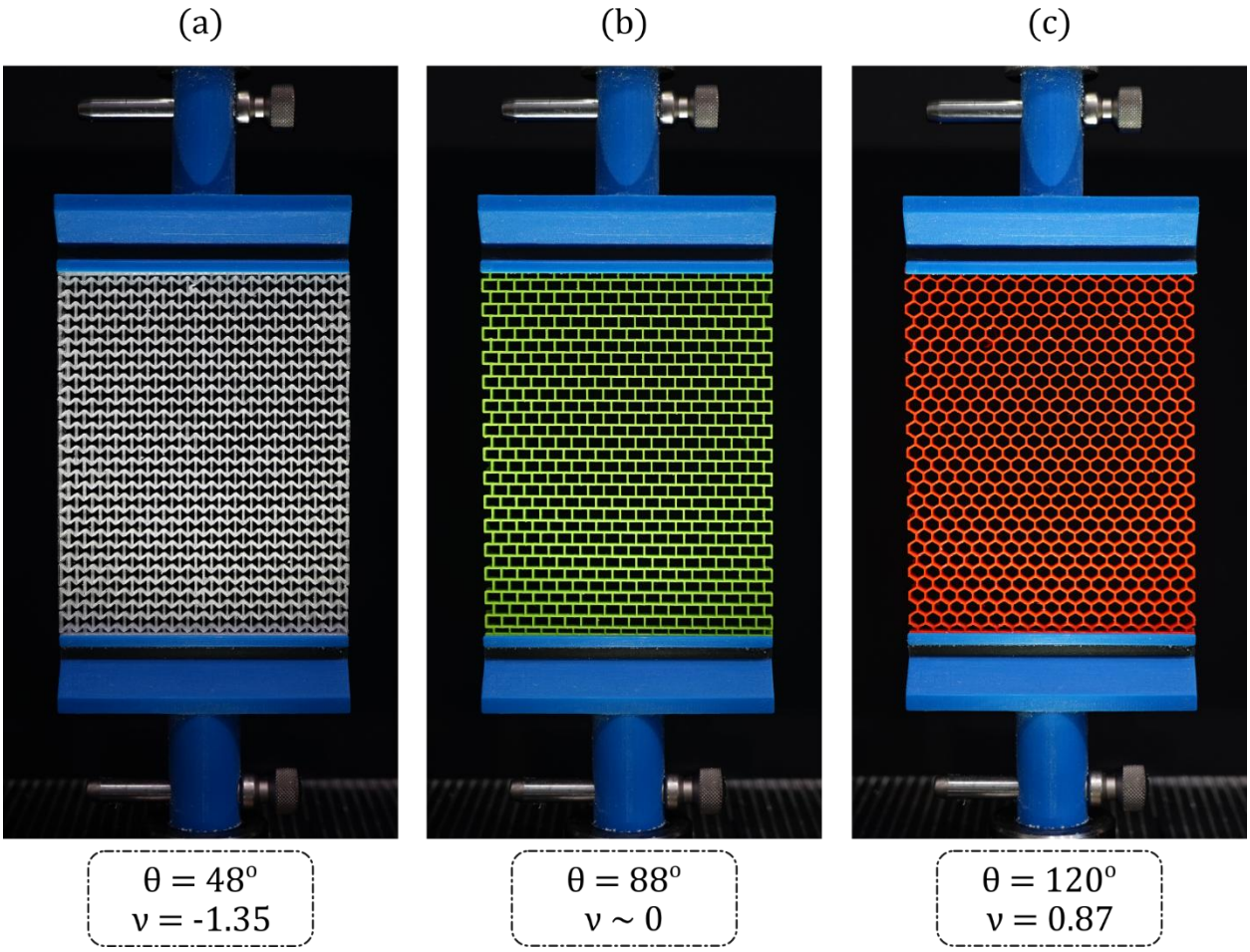

FIGURE 2.1.11 Three fabricated cellular plate samples for buckling test before loading: **(a)** auxetic plate with negative Poisson's ratio, **(b)** auxetic plate with almost zero Poisson's ratio and **(c)** conventional honeycomb plate with positive Poisson's ratio

It worth mentioning that each experiment performed three times with the same setup and conditions (like measuring tools, time period etc.) to prove repeatability of our experimental setup. It verifies that the results are true and are not just by chance.

So far, we described cellular plate and its structural parameters, models made, numerical and experimental approaches. Similar to the plate models, the role of structural parameters on the buckling and post-buckling behavior of a cylindrical structure has been investigated and will be discussed in more details in the following sections.

2.2 Auxetic cellular cylinder

Auxetic cellular cylinder are designed as cylindrical patterns of single re-entrant honeycomb unit cells. In fact if the auxetic cellular plate depicted in Figure 2.1.1 is wrapped around the tube with outer radius, membrane thickness h and length of L shown in Figure 2.2.1, an auxetic cellular cylinder will be created.

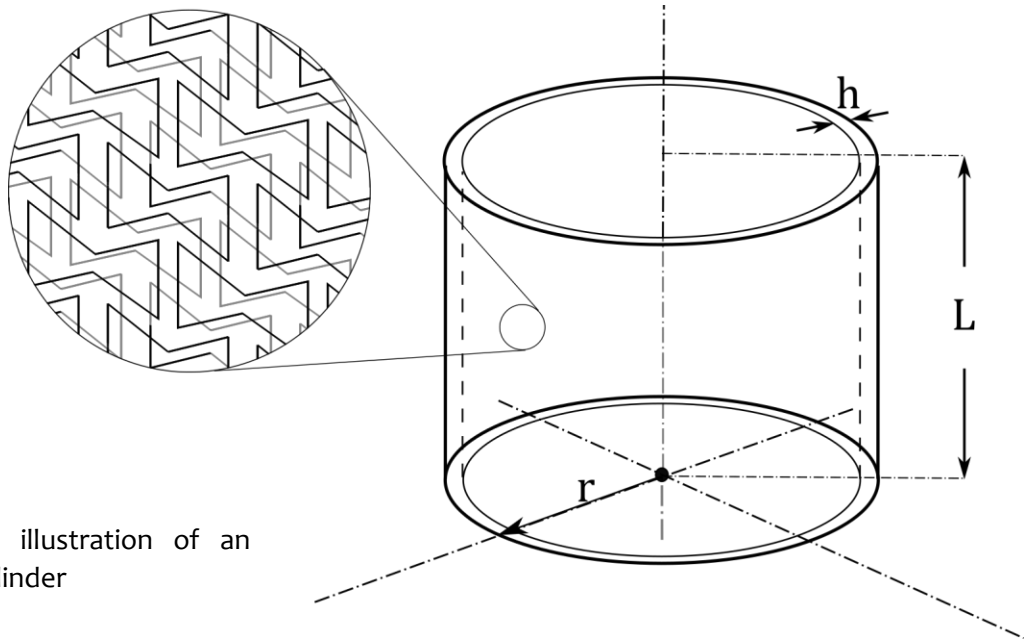

FIGURE 2.2.1 3D illustration of an auxetic cellular cylinder

In order to analyze the dependence of buckling and post-buckling behavior of the cellular cylinder on the structural parameters, two reference models characterized by the values in the table 2.2.1 were defined.

TABLE 2.2.1 Values of the geometric parameters used for the cellular cylindrical reference models

	θ^o	h (mm)	a/b	r (mm)	R	L (mm)
Model 1	48	5	1.5	28.648	1	112.5
Model 2	120	5	1.5	28.648	1	112.5

Based on the two reference models, another 43 cellular cylinder models were created. The models are characterized by range of variations in the membrane thickness h, in the angle θ, in the ratio a/b and in the scaling parameter R. In the following sections, each of these structural parameters and their corresponding models will be comprehensively described.

2.1.1 Models created by change of the Poisson's ratio

As it obvious variation in the Poisson's ratio is a consequence of the change of the angle θ. In order to obtain both auxetic and conventional cellular cylindrical models, a relatively wide range of the angle θ $(48 \leq \theta \leq 120)$ has been also covered for the cylindrical geometry. By choosing the other three Poisson's ratio $(\nu = -0.49, -0.05, 0.37)$ a set of five auxetic and conventional cylinders were designed. Values of structural parameters with respect to variations of Poisson's ratio are summarized in the Figure 2.2.2. Values of the reference models are highlighted by the green color.

a/b	1.5
h	5
θ°	48, 72, 88, 104, 120
R(scale)	1
L	112.5

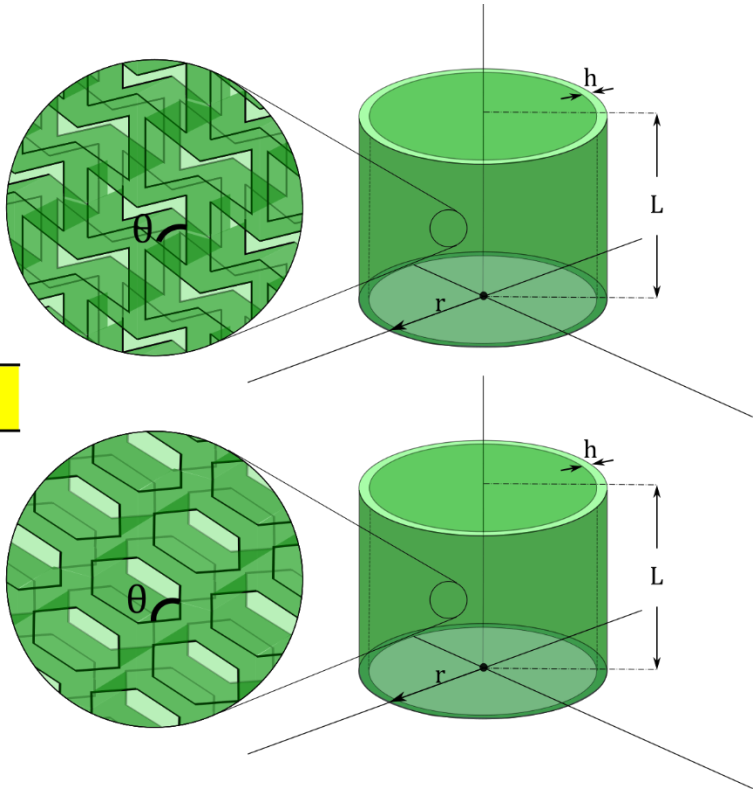

FIGURE 2.2.2 3D schematic of the cylinder models created by changing the angle θ. **(a)** auxetic cylinder **(b)** conventional honeycomb cylinder

2.2.2 Models created by change of the membrane thickness

Another significant parameter that has been investigated in our study is the thickness of the cylinder membrane. Similar to the plate models, $h = 5\ mm$ is considered for the reference models and other four values $(h = 1\ mm, 2.5\ mm, 7.5\ mm, 10\ mm)$ have been chosen to Figure out how the change of the out-of-plane thickness can tune buckling and post-buckling behavior of the models. It follows that another 20 models were obtained by changing the membrane thickness h. Values of the structural parameters with respect to variations of the membrane thickness are shown in the Figure 2.2.3. Green color values refer to the reference models.

a/b	1.5
θ°	48, 72, 88, 104, 120
h	1, 2.5, 5, 7.5, 10
R(scale)	1
L	112.5

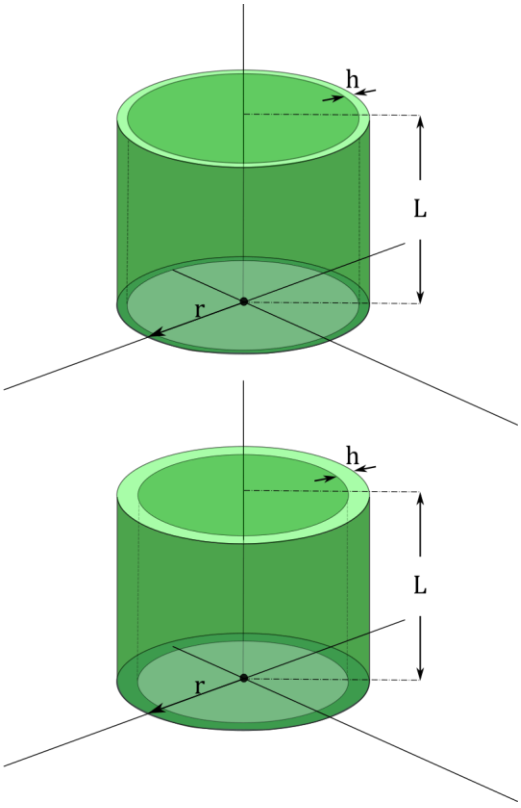

FIGURE 2.2.3 3D schematic of the cylinder models created by changing the cylinder membrane thickness. The auxetic cylinder depicted in **(a)** is two times thinner than the one shown in **(b).**

2.2.3 Models created by change of the scaling parameter

Here again three different scaling parameters ($R = 0.75, 1.5, 3$) but this time for all five Poisson's ratio ($\nu = -1.35, -0.49, -0.05, 0.37, 0.87$) were considered which in turn offers 15 new cellular cylinder models. Figure 2.2.4 demonstrates the values of the structural parameters with respect to different scaling values. Values of the reference models are highlighted by the green color.

2.2.4 Models created by change of the ratio a/b

As it mentioned in the section 2.1.1, the unit cell membranes angle must obey the restriction expressed in $Eq.(2.1.8)$ to avoid compenetration. The ratio of a/b is changed by keeping the value of b constant and only changing the parameter a. Two different ratio $a/b = 1, 2$ used for only 3 different Poisson's ratios ($\nu = -1.35, 0.05, 0.87$). It should be noted that due to the geometric constraint presented in $Eq.(2.1.8)$, design of a model with $\theta = 48$ and $a/b = 1$ is not practical. It follows that variation of the ratio a/b provides five new cellular cylinderical models. Values of the structural parameters with respect to different ratio are represented in Figure 2.2.5. Values of the reference models are highlighted by the green color.

a/b	1.5
h	5
R(scale)	0.75, 1, 1.5, 3
θ°	48, 72, 88, 104, 120
L	112.5

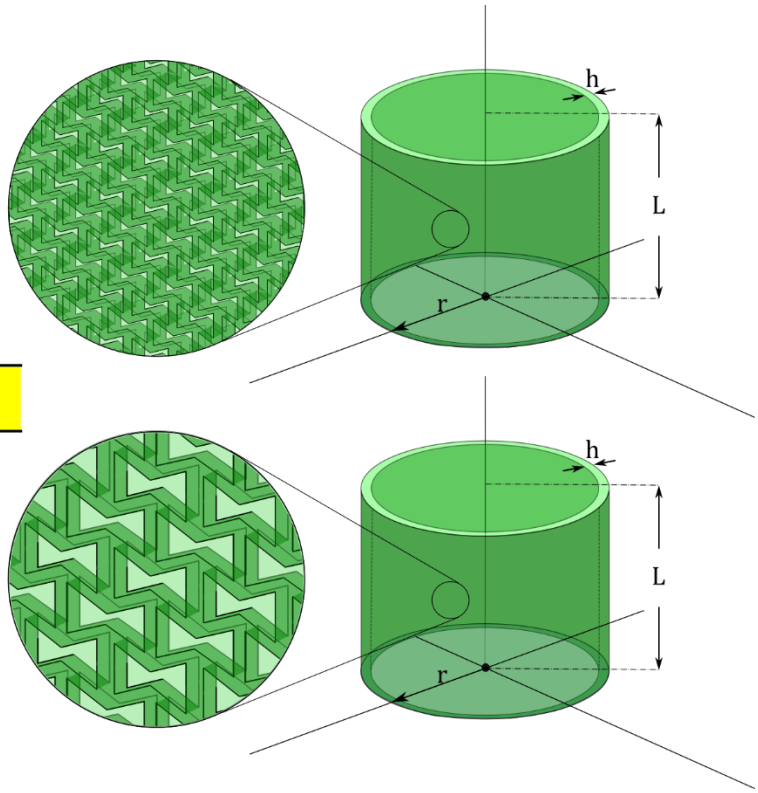

FIGURE 2.2.4 3D schematic of the cylinder models created by changing the scaling parameter R. Unit cells of the auxetic cylinder depicted in **(a)** is two times smaller than the one shown in **(b)**

h	5
θ°	48, 88, 120
a/b	1*, 1.5, 2
R(scale)	1
L	112.5

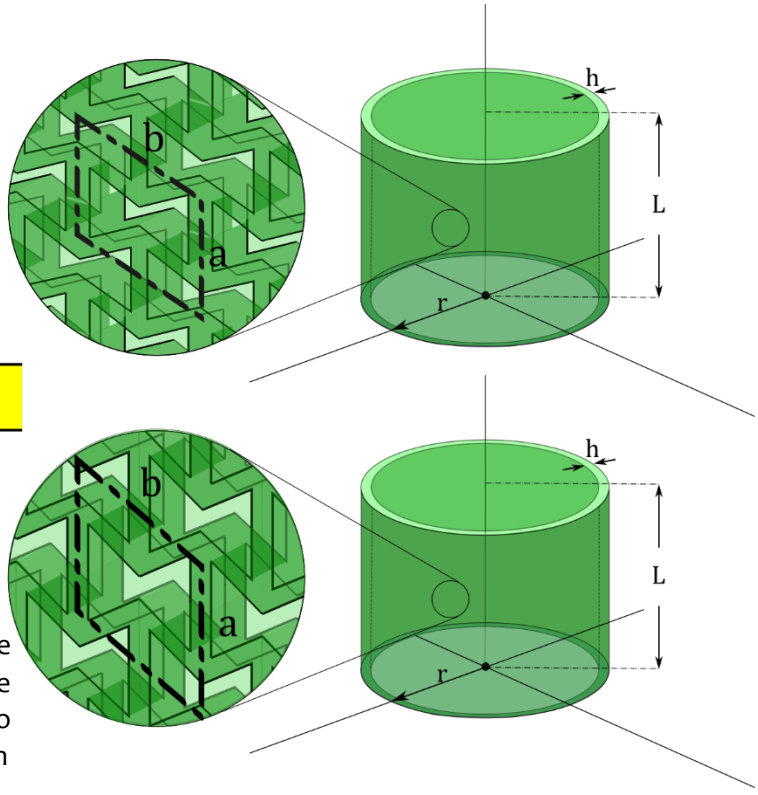

FIGURE 2.2.5 3D schematic of the cylinder models created by changing the ratio a/b * $a/b = 1$ is not applied to $\theta^{\circ} = 48$ due to the geometric restriction

In order to investigate the behavior of the cellular cylinder structure under the influence of buckling force, each of the two reference models were subjected to compressive load as depicted in Figure 2.2.6. First, the models were analyzed numerically and then for repeatability three buckling test were performed on each reference models to validate the numerical approach. In the following sections both numerical and experimental approaches are comprehensively discussed.

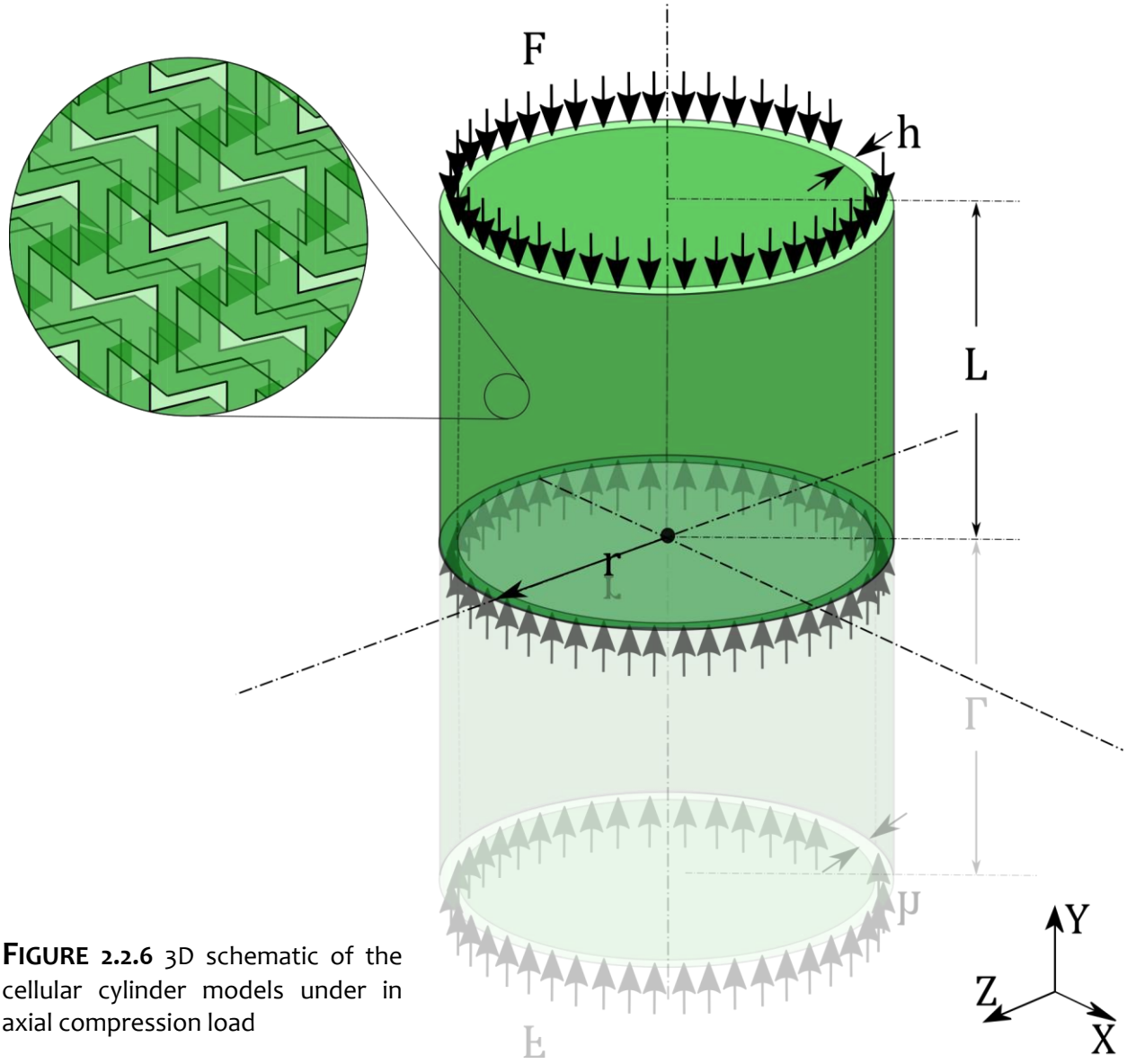

FIGURE 2.2.6 3D schematic of the cellular cylinder models under in axial compression load

2.2.5 Numerical simulation

The commercial finite element software ABAQUS/Explicit was implemented to study buckling and post-buckling behavior of the cellular cylinders designed in the Computer-Aided Design software SOLIDWORKS. Linear buckling analysis is firstly conducted by applying unit

compressive force on the top of the cylinder and extracting its axial displacements as an output. By considering the first mode shape, calling the node coordinates extracted in linear buckling analysis and applying 18% strain with imperfection scale factor of 1, non-linear Risk analysis executed to obtain post-buckling behavior of structures. Neo-Hookean hyper-elastic material with $C_{10} = 0.117733$ and $D_1 = 0$ is assigned to the models. In all simulations the bottom surface of the structure is fixed with ENCASTER boundary condition which provides no degree of freedom. However the top surface of the model has only one degree of freedom moving freely along Y direction (see Figure 2.2.8). The solid model was discretized by linear hexagonal element without reduced integration ($C3D8$) with approximate mesh size 1. The mesh size was selected after performing mesh convergence analysis for the reference models.

2.2.6 Sample preparation and experimental setup

As it mentioned above we performed buckling test only on the reference models to validate the numerical approach. In order to perform buckling in a more efficient and precise manner, a griper which is able to mimic the simulated boundary condition is needed. Samples are mounted on the solid part and undergo compression load. Cellular cylinder were fabricated by 3D printer with the black soft material with shore hardness 80. Two samples with different angles ($\theta = 48$) and ($\theta = 120$) are printed based on dimensions of their corresponding reference models (Figure 2.2.7). Samples are mounted on grippers and all together are connected to the loading machine equipped with a 100 N load cell allowing us to perform a uniaxial buckling test and measure the axial force with respect to the axial compressive displacement. For each sample quasi static compression test with strain rate of $0.002\ s^{-1}$ were conducted.

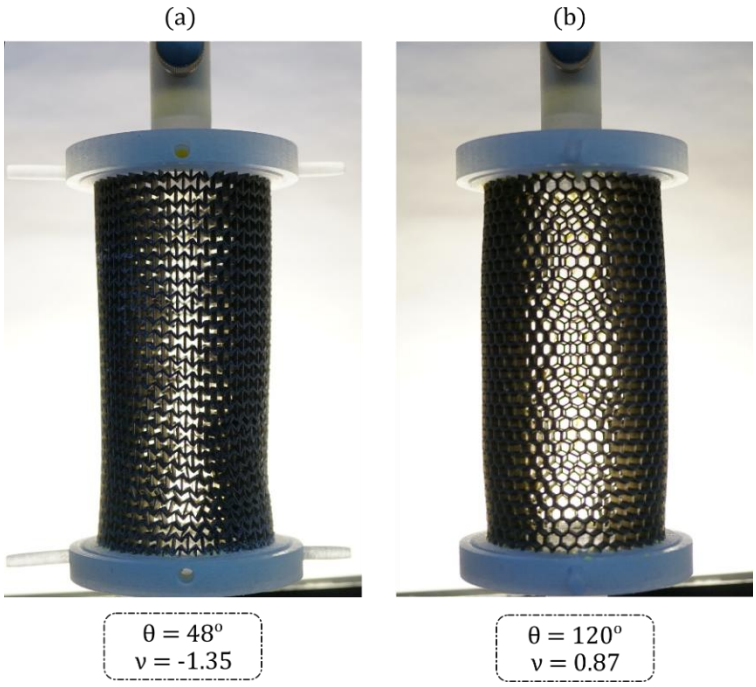

FIGURE 2.2.7 Two fabricated cellular cylinder samples for buckling test before loading: **(a)** auxetic tube with negative Poisson's ratio and **(b)** conventional honeycomb tube

Chapter 3

Results & Discussions

In the previous chapter, we first had an overview of the structural parameters of the fundamental unit cells of the models used in this study. Then, how the models were designed in both plate and cylindrical geometry were studied in more details. It was also mentioned that all models were analyzed by finite element method and the accuracy of the results obtained from the numerical method has been investigated by fabricating reference models and performing mechanical test on them. In this chapter, in order to validate results of the finite element method, they have been compared with the experimental approach and presented together in the following sections. In the later sections, the effect of each of the structural parameters on the buckling behavior of the structure in both plate and cylindrical geometry will be studied. The effects of these structural parameters on each other was also investigated. We will also point out the behavioral differences between cellular and classical bulk structures. Finally, we survey on the post-buckling behavior of structures and discuss how by changing the structural parameters, the slope of the strain stress diagram in the post-buckling area, which indicates the stability of the structure, can be tuned.

3.1 Results of the cellular plate models

In this section, we present the results of numerical and experimental analysis performed on cellular plate models. Then, the results related to changes in the mechanical behavior of cellular plate models while changing the values of structural parameters will be expressed.

3.1.1 Validation of the FEM method

As it mentioned in previous chapter we designed and performed finite element analysis on 84 cellular plate models. In order to validate the numerical method, three reference models were fabricated and underwent buckling experimental setup. The three reference models in the three different colors white ($\upsilon < 0$), green ($\upsilon = 0$) and red ($\upsilon > 0$) with their initial and final states, deformation during buckling test and load displacement diagram are depicted in Figure 3.1.1, Figure 3.1.2 and Figure 3.1.3 respectively. Part (a) of each of these Figures shows the front view of the real fabricated model. In segment (b) how the model deforms during compression load until it reaches to the critical load and buckling and post-buckling regions has been depicted. In this part each frame has been made after one millimeter displacement in the direction of the loading. Section (c) shows the perspective view of the final buckled deformation of the analyzed model in ABAQUS software. Synclastic, cylindrical and anticlastic curvatures are obviously recognizable in the Figures and corresponds to negative, zero and positive Poisson's ratio respectively. The force-displacement data extracted from the ABAQUS simulation and the buckling test are given in the diagram in part (d). The black dots are related to the experimental results and the colored dots are related to the model with the corresponding Poisson's ratio. As can be seen from Section (d) of these Figures, the experimental results for all three reference models follow the simulation results so well, and there is a perfect agreement between the two results. This is evidence of the claim that the numerical finite element analysis used in this study for investigating the buckling and post-buckling behavior of plate cellular structures is highly accurate and reliable.

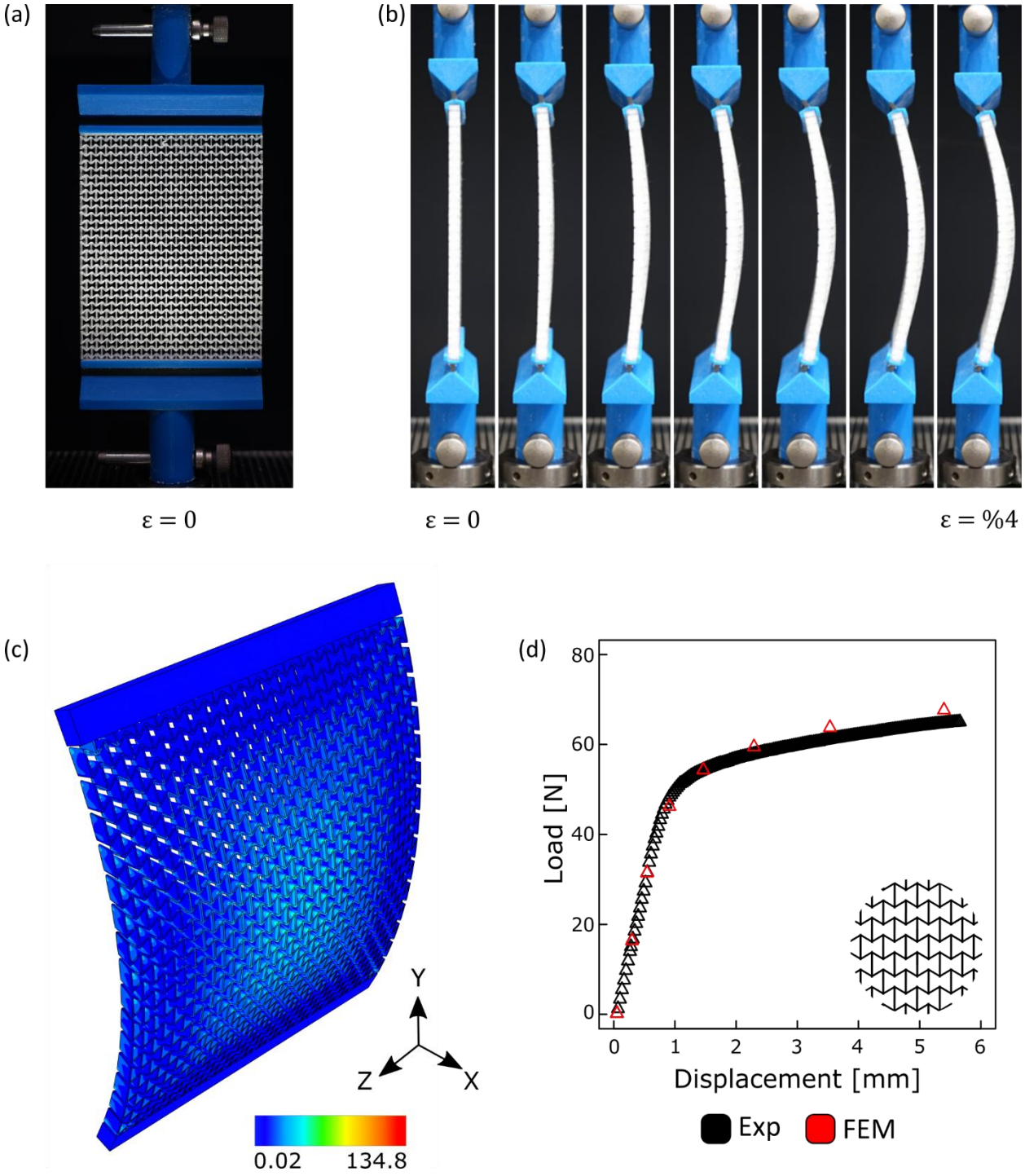

FIGURE 3.1.1 Experimental and numerical results of the auxetic cellular plate with negative Poisson's ratio: **(a)** front view of the real fabricated model mounted on the gripper, **(b)** deformation and buckling of the model under compression load, **(c)** perspective view of the buckled auxetic plate and its final synclastic surface, **(d)** very nice and perfect match between experimental (black) and FEM (red) results in both buckling and post-buckling region

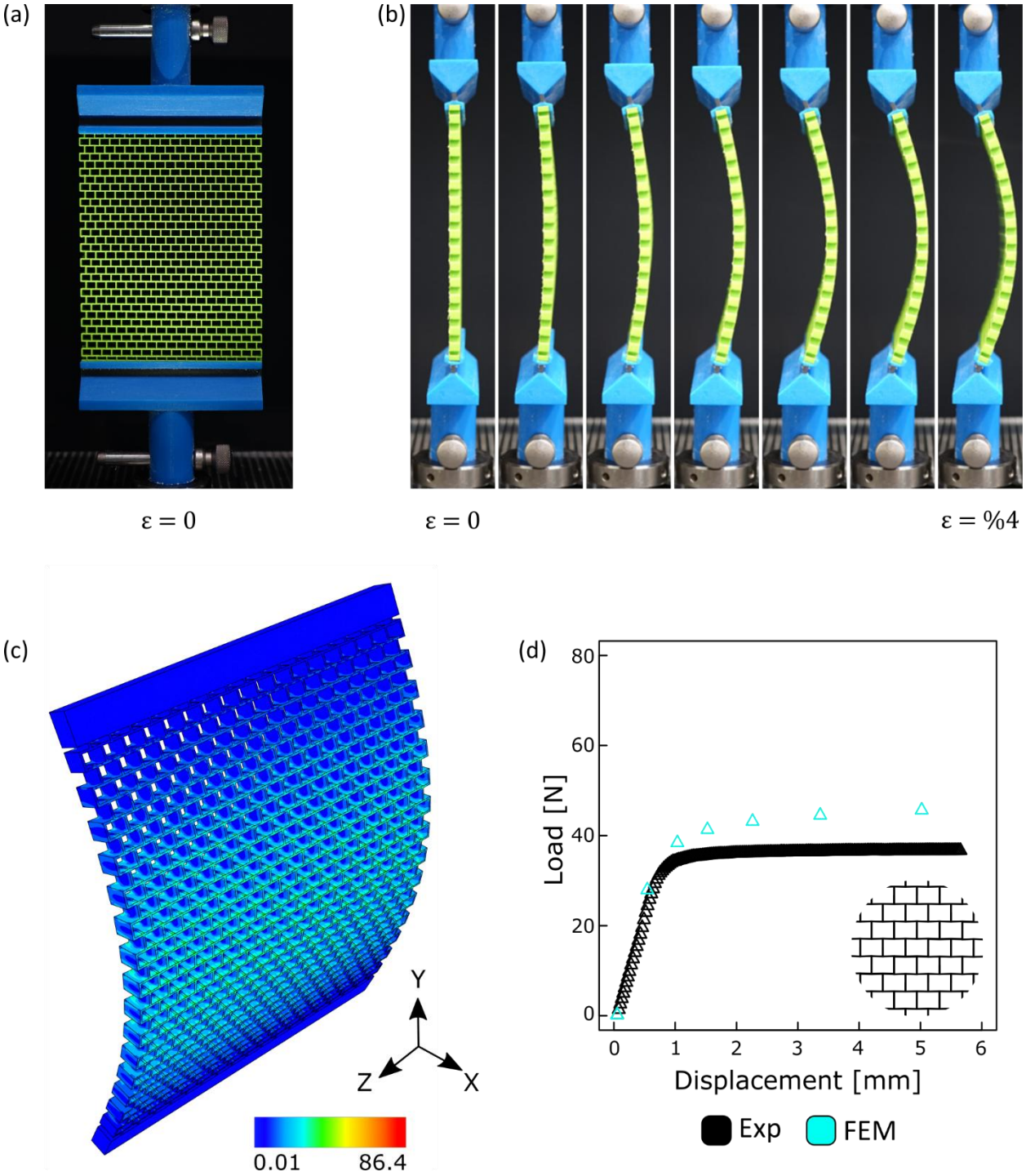

FIGURE 3.1.2 Experimental and numerical results of the auxetic cellular plate with almost zero Poisson's ratio: **(a)** front view of the real fabricated model mounted on the gripper, **(b)** deformation and buckling of the model under compression load, **(c)** perspective view of the buckled auxetic plate and its final cylindrical surface, **(d)** very nice and perfect match between experimental (black) and FEM (cyan) results in both buckling and post-buckling region

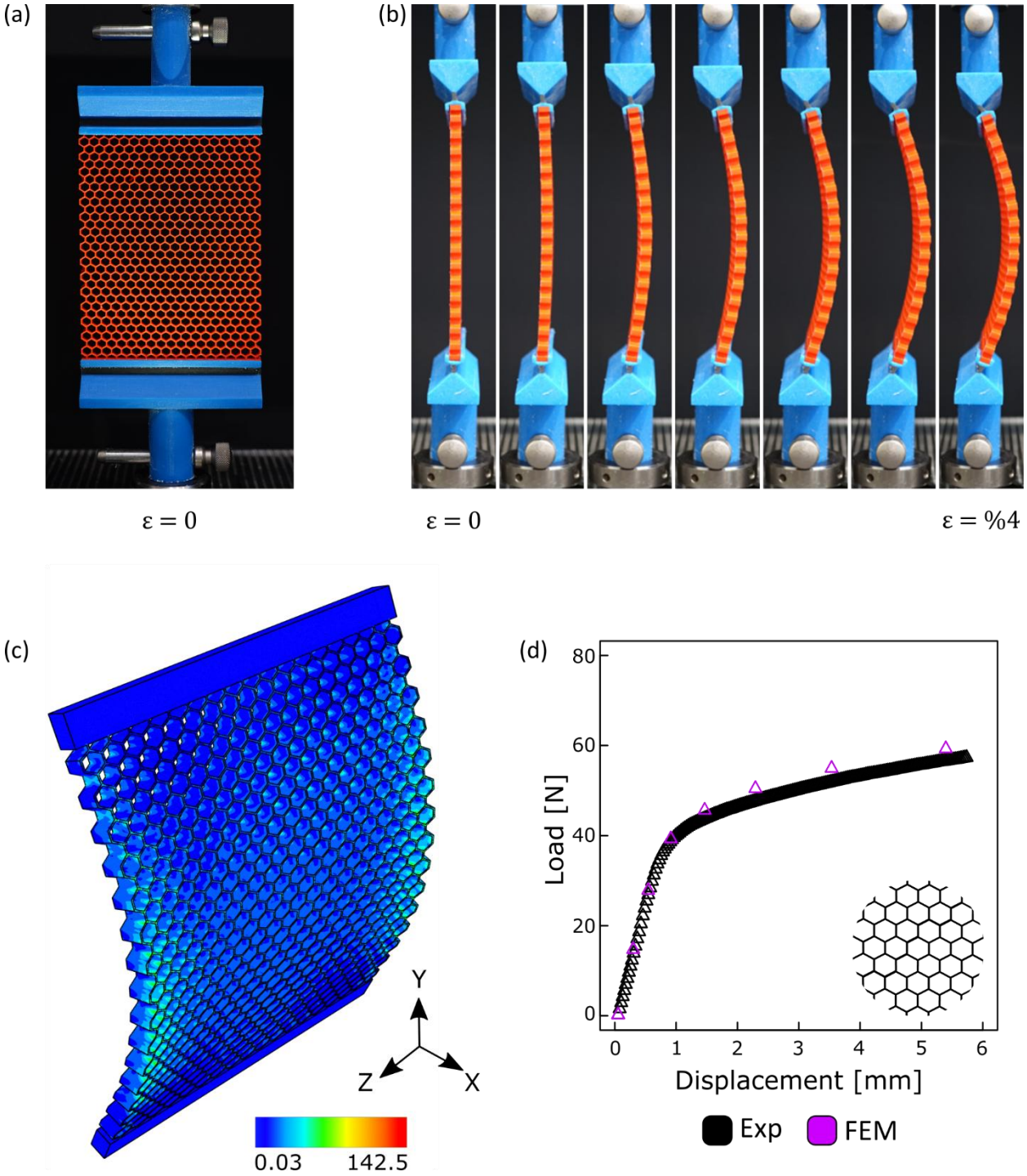

FIGURE 3.1.3 Experimental and numerical results of the conventional cellular plate with positive Poisson's ratio: **(a)** front view of the real fabricated model mounted on the gripper, **(b)** deformation and buckling of the model under compression load, **(c)** perspective view of the buckled conventional plate and its final anticlastic surface, **(d)** very nice and perfect match between experimental (black) and FEM (violet) results in both buckling and post-buckling region

Before discussing the results of changing the structural parameters, we first define the Φ parameter as the following:

$$\Phi = \frac{V_c}{V_b} \tag{3.1.1}$$

Where V_c is the volume of the solid material and V_b is the volume of the solid material plus the volume of the pores. It is well known that the porosity of a structure is defined as follows:

$$porosity = \frac{V_b - V_c}{V_b} \tag{3.1.2}$$

Then it follows that $\Phi = 1 - porosity$ and is related to the solid part of the structure and contributes to the overall mass of the models. For each of the designed models, the value of the parameter Φ is obtained by calculating the volume of the solid part of the model through ABAQUS software and dividing it over the total volume occupied by the structure. Later, in order to eliminate the effect of structure weight on the results, the extracted data are normalized by dividing them to the value of the Φ to provide a set of pure data which are only affected by changing structural parameters. The values of Φ for each models will be presented later in the relevant tables.

As it discussed in chapter two based on the three reference models, another 81 cellular plates were created. The later models are characterized by range of variations in the out-of-plane thickness h, in the angle θ, in the ratio a/b, in the in-plane thickness th, in the scaling parameter R and in the width w of the plate. The results of the numerical analysis for each of the structural parameters are extracted and will be present in the following sections one by one.

3.1.2 Results corresponding to change of the Poisson's ratio

The values of the critical load, the parameter Φ and other structural parameters for the three reference models and the other seven models created by changing the Poisson's ratio are given in Table 3.1.1. As it can be understood from Table 3.1.1, the value of the Φ decreases by increasing the angle θ and Poisson's ratio. In fact, by passing through the auxetic region and entering to the non-auxetic area, the porosity of the structure increases and its weight decreases. Also, the maximum critical load occurs in $\nu = -1.01$. Values of the reference models are highlighted by the blue color.

TABLE 3.1.1 Values of the critical load, the weight parameter Φ and other geometrical parameters for ten models designed by variation of the Poisson's ratio.

θ°	υ	h (mm)	a/b	th (mm)	w (mm)	R	Φ	F_{cr} (N)
48	-1.35	5	1.5	0.51	92.31	1	0.39	31.99
56	-1.01	5	1.5	0.51	92.31	1	0.37	47.26
64	-0.73	5	1.5	0.51	92.31	1	0.35	44.35
72	-0.49	5	1.5	0.51	92.31	1	0.34	41.34
80	-0.26	5	1.5	0.51	92.31	1	0.33	35.73
88	-0.05	5	1.5	0.51	92.31	1	0.31	39.49
96	0.16	5	1.5	0.51	92.31	1	0.31	35.59
104	0.37	5	1.5	0.51	92.31	1	0.30	34.72
112	0.61	5	1.5	0.51	92.31	1	0.29	44.41
120	0.87	5	1.5	0.51	92.31	1	0.26	38.62

As it expressed before, since the Young's modulus (E_c) and the weight of the cell structure change due to variation of the structural parameters, then in order to investigate only the effect of the Poisson's ratio on the structure's mechanical behavior, the critical stresses are normalized by dividing to the E_c and Φ of the corresponding models. The normalized strain stress curves of the ten models presented in the table 3.1.1 are shown in Figure 3.1.4.

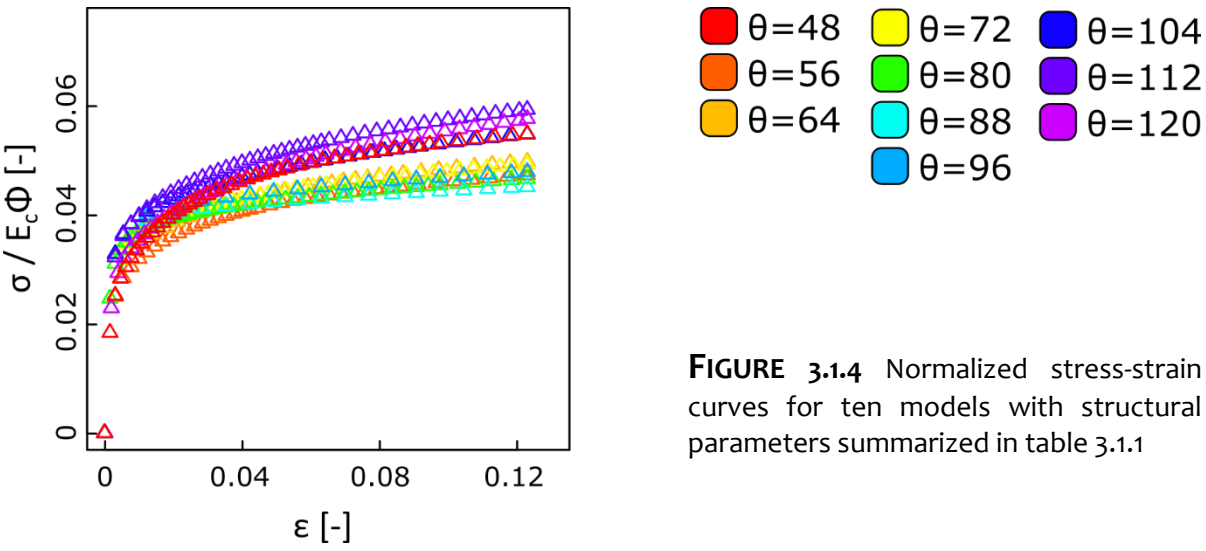

FIGURE 3.1.4 Normalized stress-strain curves for ten models with structural parameters summarized in table 3.1.1

3.1.3 Results corresponding to change of the out-of-plane thickness

The values of critical load, the parameter Φ and other structural parameters for the four sets of ten models with $h = 1\ mm, 2.5\ mm, 7.5\ mm, 10\ mm$ are extracted and presented in the table 3.1.2, table 3.1.3, table 3.1.4 and table 3.1.5, respectively. The same values are given in Table 3.1.6 for those models that were designed with the out-of-plane thickness of $26\ mm$. It is obvious that although the out-of-plane thickness changes however weight parameter Φ will be constant for each Poisson's ratio.

TABLE 3.1.2 Values of the critical load, the weight parameter Φ and geometry parameters for models with $h = 1\ mm$

θ^o	υ	h (mm)	a/b	th (mm)	w (mm)	R	Φ	F_{cr} (N)
48	-1.35	1	1.5	0.51	92.31	1	0.39	0.61
56	-1.01	1	1.5	0.51	92.31	1	0.37	0.86
64	-0.73	1	1.5	0.51	92.31	1	0.35	0.88
72	-0.49	1	1.5	0.51	92.31	1	0.34	0.89
80	-0.26	1	1.5	0.51	92.31	1	0.33	0.90
88	-0.05	1	1.5	0.51	92.31	1	0.31	0.94
96	0.16	1	1.5	0.51	92.31	1	0.31	1.02
104	0.37	1	1.5	0.51	92.31	1	0.30	1.01
112	0.61	1	1.5	0.51	92.31	1	0.29	1.07
120	0.87	1	1.5	0.51	92.31	1	0.26	0.92

TABLE 3.1.3 Values of the critical load, the weight parameter Φ and geometry parameters for models with $h = 2.5\ mm$

θ^o	υ	h (mm)	a/b	th (mm)	w (mm)	R	Φ	F_{cr} (N)
48	-1.35	2.5	1.5	0.51	92.31	1	0.39	5.66
56	-1.01	2.5	1.5	0.51	92.31	1	0.37	8.07
64	-0.73	2.5	1.5	0.51	92.31	1	0.35	7.67
72	-0.49	2.5	1.5	0.51	92.31	1	0.34	7.37
80	-0.26	2.5	1.5	0.51	92.31	1	0.33	6.78
88	-0.05	2.5	1.5	0.51	92.31	1	0.31	7.27
96	0.16	2.5	1.5	0.51	92.31	1	0.31	7.17
104	0.37	2.5	1.5	0.51	92.31	1	0.30	7.11
112	0.61	2.5	1.5	0.51	92.31	1	0.29	8.39
120	0.87	2.5	1.5	0.51	92.31	1	0.26	7.17

TABLE 3.1.4 Values of the critical load, the weight parameter Φ and geometry parameters for models with $h = 7.5\ mm$

θ^o	υ	h (mm)	a/b	th (mm)	w (mm)	R	Φ	F_{cr} (N)
48	-1.35	7.5	1.5	0.51	92.31	1	0.39	94.93
56	-1.01	7.5	1.5	0.51	92.31	1	0.37	143.7
64	-0.73	7.5	1.5	0.51	92.31	1	0.35	135.33
72	-0.49	7.5	1.5	0.51	92.31	1	0.34	125.24
80	-0.26	7.5	1.5	0.51	92.31	1	0.33	105.99
88	-0.05	7.5	1.5	0.51	92.31	1	0.31	118.67
96	0.16	7.5	1.5	0.51	92.31	1	0.31	103.90
104	0.37	7.5	1.5	0.51	92.31	1	0.30	100.35
112	0.61	7.5	1.5	0.51	92.31	1	0.29	131.10
120	0.87	7.5	1.5	0.51	92.31	1	0.26	114.66

TABLE 3.1.5 Values of the critical load, the weight parameter Φ and geometry parameters for models with $h = 10\ mm$

θ^o	υ	h (mm)	a/b	th (mm)	w (mm)	R	Φ	F_{cr} (N)
48	-1.35	10	1.5	0.51	92.31	1	0.39	212.08
56	-1.01	10	1.5	0.51	92.31	1	0.37	324.83
64	-0.73	10	1.5	0.51	92.31	1	0.35	307.52
72	-0.49	10	1.5	0.51	92.31	1	0.34	284.32
80	-0.26	10	1.5	0.51	92.31	1	0.33	239.57
88	-0.05	10	1.5	0.51	92.31	1	0.31	269.54
96	0.16	10	1.5	0.51	92.31	1	0.31	232.15
104	0.37	10	1.5	0.51	92.31	1	0.30	222.84
112	0.61	10	1.5	0.51	92.31	1	0.29	293.50
120	0.87	10	1.5	0.51	92.31	1	0.26	255.71

TABLE 3.1.6 Values of the critical load, the weight parameter Φ and geometry parameters for models with $h = 26\ mm$

θ^o	υ	h (mm)	a/b	th (mm)	w (mm)	R	Φ	F_{cr} (N)
48	-1.35	26	1.5	0.51	92.31	1	0.39	5429.2
72	-0.49	26	1.5	0.51	92.31	1	0.34	7890.5
88	-0.05	26	1.5	0.51	92.31	1	0.31	6428.2
104	0.37	26	1.5	0.51	92.31	1	0.30	7457.6
120	0.87	26	1.5	0.51	92.31	1	0.26	6958.9

The normalized strain stress curves of the 45 models presented in the table 3.1.2, table 3.1.3, table 3.1.4, table 3.1.5 and table 3.1.6 are depicted in Figure 3.1.5.

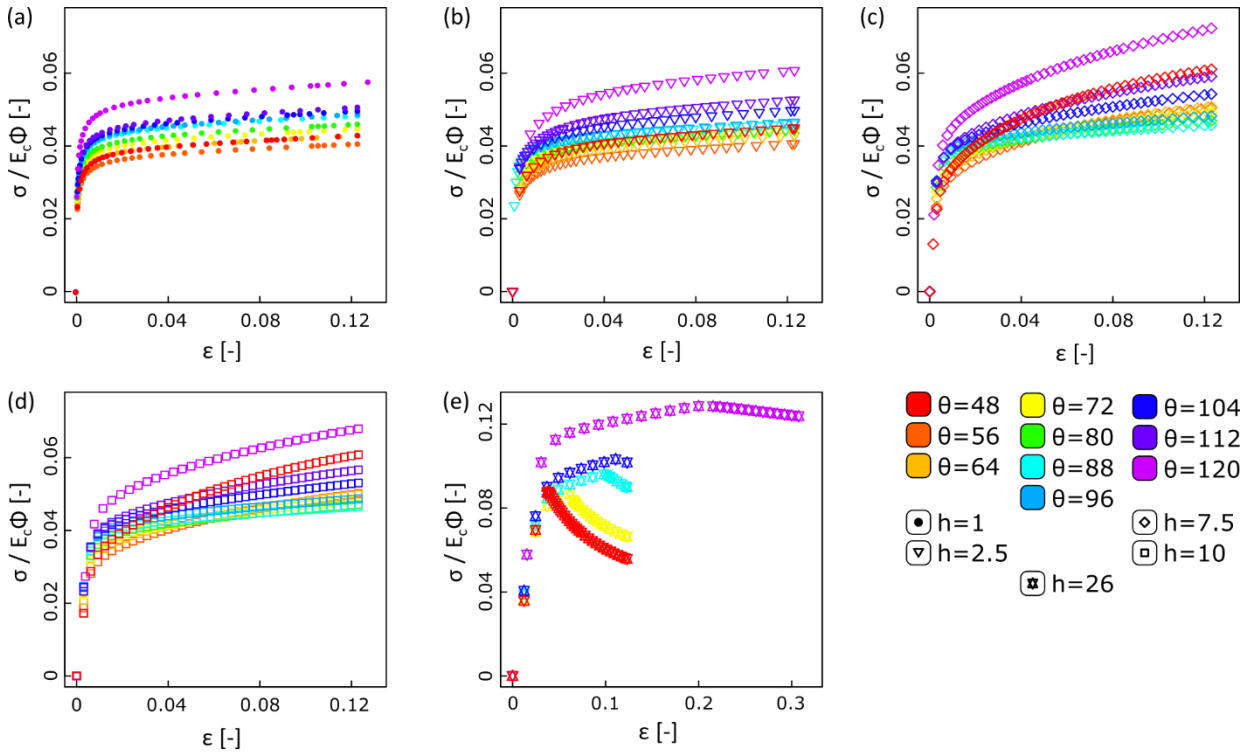

FIGURE 3.1.5 Normalized stress-strain curves for 45 models created by change of out-of-plane thickness: **(a)** $h = 1$, **(b)** $h = 2.5$, **(c)** $h = 7.5$, **(d)** $h = 10$ and **(e)** $h = 26$

From the stress-strain curves shown in the Figure 3.1.4 and Figure 3.1.5, it can be inferred that the slope of these curves in the post-buckling regime changes by the variation of the Poisson's ratio and out-of-plane thickness of the cellular structure. These changes are plotted in the Figure 3.1.6. The dependence of the post-buckling slope on the two parameters of Poisson's ratio and out-of-plane thickness is shown in Figures 3.1.6 (a) and Figures 3.1.6 (b), respectively. As can be seen in Figures 3.1.6 (a), for structures sufficiently slender, the post-buckling slope gradually decreases by increasing the negative Poisson's ratio and reaches to its minimum for the Poisson's ratio of zero. But after passing this turning point and entering to the non-auxetic regime, the post-buckling slope increases again. Another interesting result is that as the out-of-plane thickness of the structure increase, this descending trend from $\nu = -1.35$ to $\nu \approx 0$ and ascending trend from $\nu \approx 0$ to $\nu = -1.35$ occurs with a larger gradient as shown in Figures 3.1.6 (a). Moreover, the post-buckling slope of the structure with zero Poisson's ratio remains almost constant, regardless of the amount of the out-of-plane thickness. However, by increasing out-of-plane thickness, the more one goes to the negative or positive Poisson's ratio, the more the post-buckling slope increases divergently. This means that the more

auxetic or conventional the structure, the greater the effect of variation in the out-of-plane thickness on the post-buckling behavior of the structure. Conversely, the closer the Poisson's ratio of the structure is to zero, the less the post-buckling behavior of the structure is affected by changes of out-of-plane thickness. Figure 3.1.6 (b) shows that the post-buckling slope becomes greater with increasing the out-of-plane thickness, regardless of the value of the Poisson's ratio. However, as mentioned above, this enhancement is more noticeable in structures with maximum and minimum Poisson ratio.

For sufficiently large h, the structure regardless of its Poisson's ratio possess a negative post-buckling slope. This means that the structure loses its strength after buckling and is more unstable.

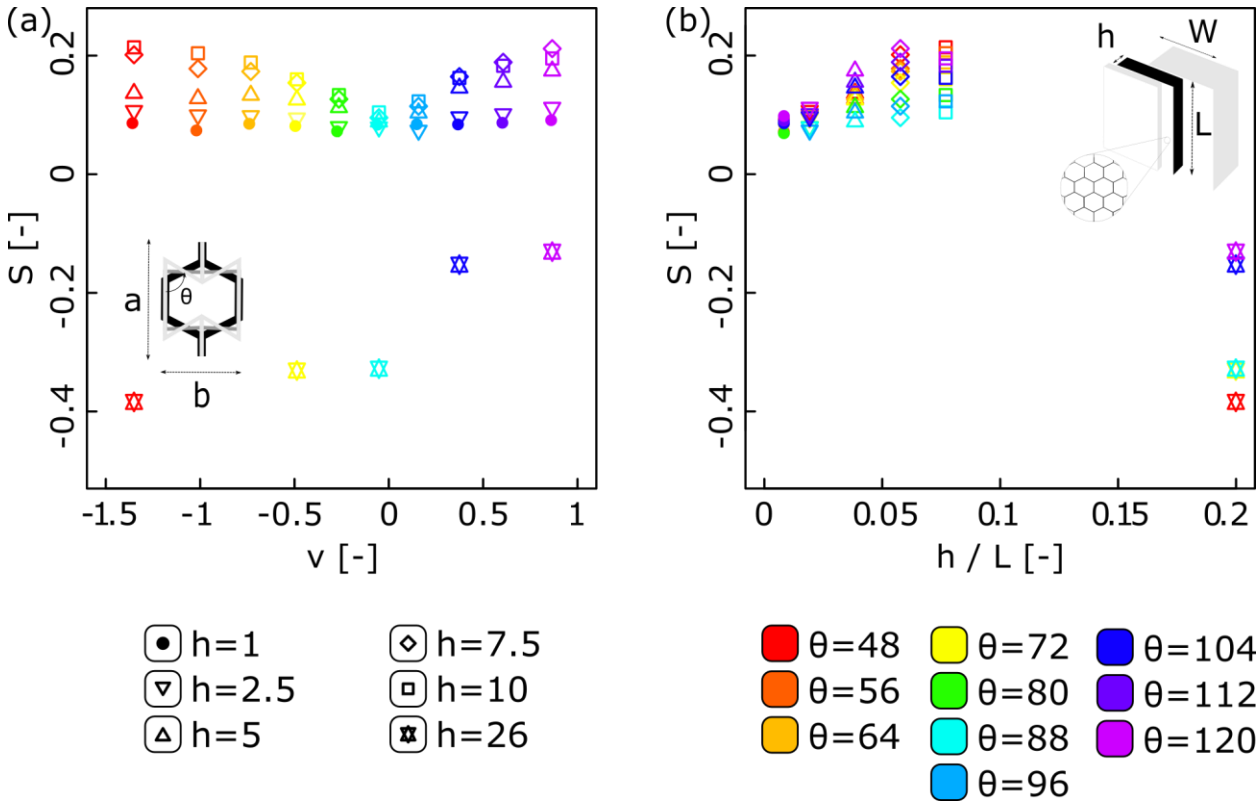

FIGURE 3.1.6 Post-buckling slopes driven from normalized stress-strain curves for models with different: **(a)** Poisson's ratio and **(b)** out-of-plane thickness

The dependence of the stiffness-and-weight-normalized stress on the two parameters of Poisson's ratio and out-of-plane thickness is shown in Figures 3.1.7 (a) and Figures 3.1.7 (b), respectively. The results plotted in the Figure 3.1.7 (a) reveals that for thin cellular plates the value of the normalized critical stress slightly changes but in a constant range. However for very thick plate with $h = 26mm$, the normalized critical stress increases sharply. This is

probably due to the fact that the structure is no longer slender and as a result shows more buckling resistance under compression load. The dependence of the normalized critical stress with respect to the Poisson's ratio also demonstrates that for the thin plate the maximum critical stress occurs mainly in the auxetic region and close to the zero Poisson's ratio (Figure 3.1.7 (b)). This is consistent with the results presented by Obrecht et al. in Figure 1.9.3 in the chapter one. However by approaching to the thicker plates maximum of the normalized critical stress is no longer in the auxetic region and moves toward conventional area.

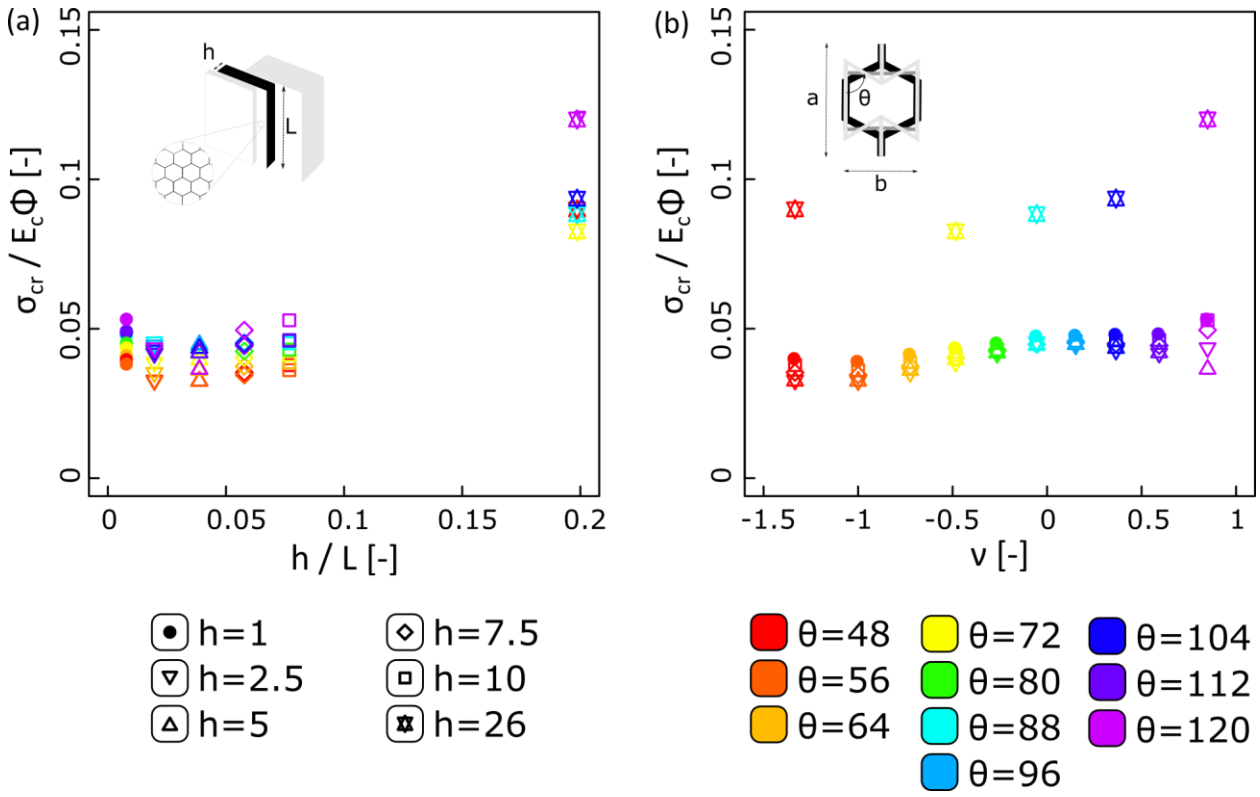

FIGURE 3.1.7 Dependence of the normalized critical stress to: **(a)** out-of-plane thickness and **(b)** Poisson's ratio

3.1.4 Results corresponding to change of the in-plane thickness

Table 3.1.7 presents the values of the critical load, weight parameter Φ and structural parameters for two reference models $\nu = -1.35, 0.87$ and other eight models made by variation of the in-plane thickness. As can be interpreted from last two column of the table 3.1.7, by increasing the in-plane thickness of the cell members, the porosity of the cellular structure decreases and the structure tends to behave like a bulk structure. As a result, the critical load increases significantly in both auxetic and conventional models.

TABLE 3.1.7 Values of the critical load, the weight parameter Φ and other geometrical parameters for cellular plate models created by variation of the in-plane thickness. Reference models are highlighted by the blue color.

th/th_r	θ^o	υ	h (mm)	a/b	w (mm)	R	Φ	F_{cr} (N)
0.25	48	-1.35	5	1.5	92.31	1	0.19	5.89
0.5	48	-1.35	5	1.5	92.31	1	0.26	16.77
0.75	48	-1.35	5	1.5	92.31	1	0.33	27.89
1	48	-1.35	5	1.5	92.31	1	0.39	31.99
1.25	48	-1.35	5	1.5	92.31	1	0.46	77.37
0.25	120	0.87	5	1.5	92.31	1	0.16	4.60
0.5	120	0.87	5	1.5	92.31	1	0.21	13.64
0.75	120	0.87	5	1.5	92.31	1	0.32	30.72
1	120	0.87	5	1.5	92.31	1	0.26	38.62
1.25	120	0.87	5	1.5	92.31	1	0.34	82.86

However the curves shown in Figure 3.1.8 indicates otherwise. In fact, the stiffness and weight-normalized stress strain curves extracted for different in-plate thicknesses, shows that increasing the in-plate thickness of the unit cell members reduces the normalized stress. For instance, according to the Figure 3.1.8 a, when the in-plate thickness of the auxetic cellular plate increases five times from $th/th_r = 0.25$ to $th/th_r = 1.25$, the normalized stress is reduced to approximately one-third of its previous value.

The normalized strain stress curves of the models presented in the table 3.1.7 are depicted in Figure 3.1.8. The blue curves are related to the reference models.

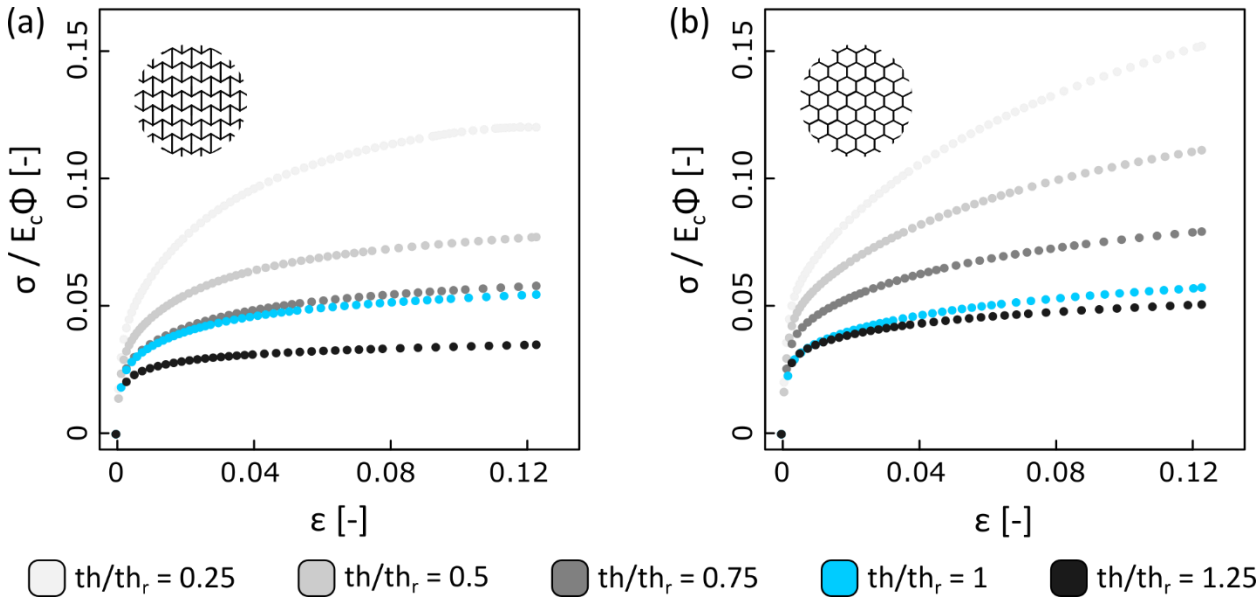

FIGURE 3.1.8 Normalized stress-strain curves for models with different in-plane thickness: **(a)** auxetic cellular plate **(b)** conventional cellular plate

As it is shown in Figure 3.1.8, the post-buckling slope of the both auxetic and conventional cellular and plates varies with changing the in-plane thickness of the unit cells struts. This variation in post-buckling slope is demonstrated in Figure 3.1.9. As can be seen, with increasing the in-plane thickness of the grids members, the slope of the strain stress relation in the post-buckling region decreases. It follows that the post-buckling strength declines and the structure becomes more unstable. The noteworthy point in this diagram is that when the in-plane thickness of the cell members becomes greater, the post-buckling slope of the two auxetic and conventional structures gradually converges to a same value. Therefore in smaller in-plane thickness the auxeticity has practically significant effect on the post-buckling behavior of the structure.

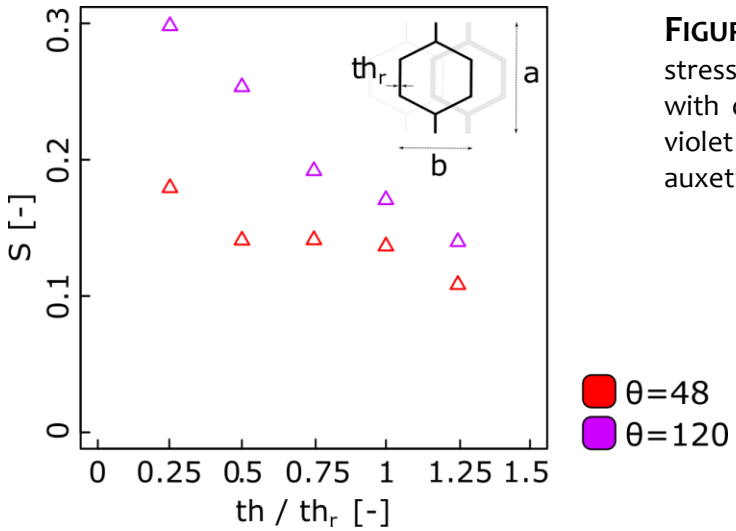

FIGURE 3.1.9 Post-buckling slopes driven from stress-strain curves for cellular plate models with different in-plane thickness: the red and violet triangles in the graph correspond to auxetic and conventional models, respectively

3.1.5 Results corresponding to change of the width of the plate

The values of the critical load, the weight parameter Φ and structural parameters for two reference models $\nu = -1.35, 0.87$ and other six models made by variation of the plate width are presented in the table 3.1.8. As can be interpreted from weight parameter column of the table 3.1.8, by increasing the plate width the weight parameter keeps constant. This is because as the plate width increases, the cellular and bulk volumes increase proportionately and the porosity remains intact as well. However, by increasing the width, the final width of the models become larger than their lengths and the structures gain more strength under axial buckling load.

TABLE 3.1.8 Values of the critical load, the weight parameter Φ and geometrical parameters for cellular plate models created by variation of the plate width

w/w_r	θ^o	υ	h (mm)	a/b	th (mm)	R	Φ	F_{cr} (N)
0.5	48	-1.35	5	1.5	0.51	1	0.39	14.47
1	48	-1.35	5	1.5	0.51	1	0.39	31.99
2	48	-1.35	5	1.5	0.51	1	0.39	131.66
4	48	-1.35	5	1.5	0.51	1	0.39	320.55
0.5	120	0.87	5	1.5	0.51	1	0.26	13.07
1	120	0.87	5	1.5	0.51	1	0.26	38.62
2	120	0.87	5	1.5	0.51	1	0.26	164.19
4	120	0.87	5	1.5	0.51	1	0.26	389.26

As mentioned above, since increasing the width of the plate brings it out from slender state in the axial direction. Therefor strength of the structure along its length becomes higher and the critical load gains dramatically. However, the stiffness and weight-normalized stress strain diagram of the models depicted in Figure 3.1.10 demonstrates that by increasing the plate width in both auxetic and conventional cellular models, the normalized critical stress decrease gradually.

The normalized strain stress curves of the models presented in the Table 3.1.7 are depicted in Figure 3.1.10. The blue curves are related to the reference models.

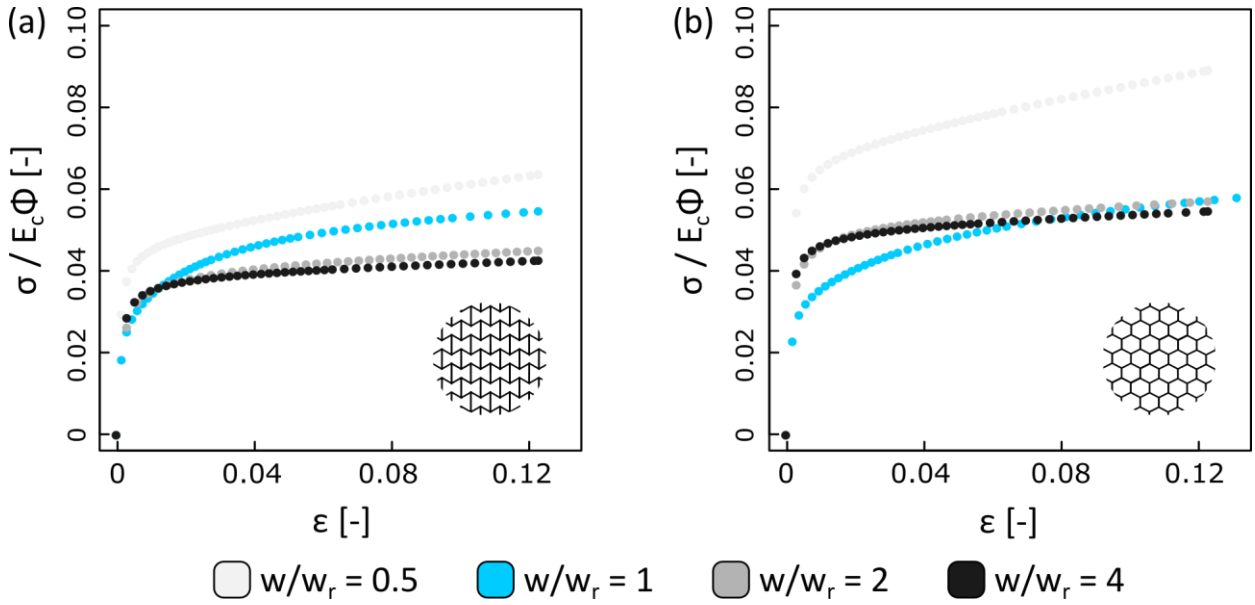

FIGURE 3.1.10 Normalized stress-strain curves for cellular plate models with different plate width: **(a)** auxetic plate **(b)** conventional plate

A closer look of the results obtained from the normalized strain stress curves of models with different width depicted in Figure 3.1.10 reveals that by increasing the plate width, the slope of the curves in the post-buckling area decreases non-linearly. This reduction means a decrease in the post-buckling strength of the structure and an increase in its instability. Post-buckling slope of the auxetic and conventional cellular and plates with different plate width are depicted in Figure 3.1.11. It is worth mentioning that all post-buckling slopes are positive regardless of the width of the plate and its Poisson's ratio.

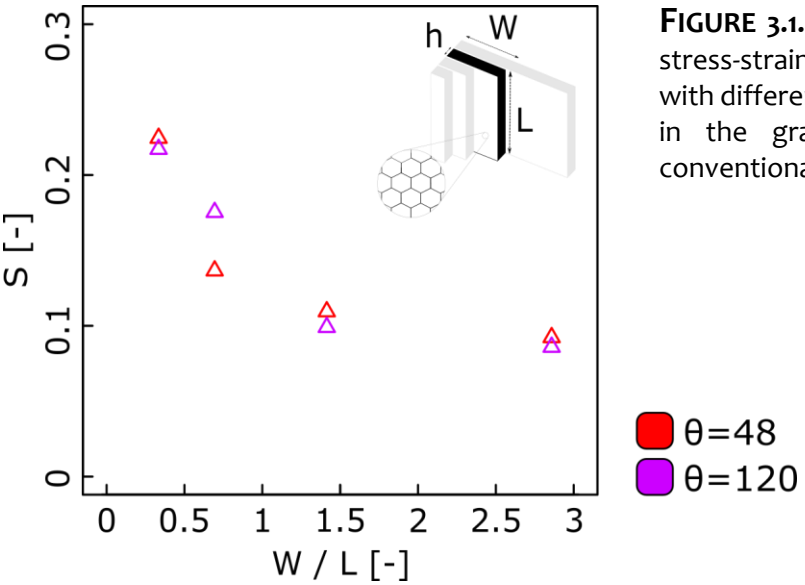

FIGURE 3.1.11 Post-buckling slopes driven from stress-strain curves for cellular plate models with different width: the red and violet triangles in the graph correspond to auxetic and conventional models, respectively

3.1.6 Results corresponding to change of the scaling parameter

Table 3.1.9 exhibits the values of the critical load, the weight parameter Φ and structural parameters for two reference models $\nu = -1.35, 0.87$ and other six models created by changing in the scaling parameter R. As can be interpreted from last two column of the table 3.1.9, by increasing the scaling parameter of the unit cell, the sealed and open pores expand and. It follows that the weight parameter Φ becomes smaller and the structure tends to behave like a more prose structure. As a result, the critical load diminishes significantly in both auxetic and conventional models.

TABLE 3.1.9 Values of the critical load, weight parameter Φ and geometrical parameters for plate models created by variation of the scaling parameter R

R	θ^o	υ	h (mm)	a/b	th (mm)	w (mm)	Φ	F_{cr} (N)
0.75	48	-1.35	5	1.5	0.51	92.31	0.48	80.15
1	48	-1.35	5	1.5	0.51	92.31	0.39	31.99
1.5	48	-1.35	5	1.5	0.51	92.31	0.31	22.12
3	48	-1.35	5	1.5	0.51	92.31	0.22	7.76
0.75	120	0.87	5	1.5	0.51	92.31	0.35	97.61
1	120	0.87	5	1.5	0.51	92.31	0.26	38.62
1.5	120	0.87	5	1.5	0.51	92.31	0.24	27.87
3	120	0.87	5	1.5	0.51	92.31	0.18	10.25

However the stiffness and weight-normalized stress strain curves extracted from different scaling parameters models shown in Figure 3.1.12 reveals a different scenario. In fact, it shows that increasing the scaling parameter of the unit cell leads to an increase in the normalized critical stress. For instance, according to the Figure 3.1.12 a, when dimensions of the unit cell of the auxetic cellular plate becomes four times as great from $R = 0.75$ to $R = 3$, the normalized stress gets almost tripled in value.

The normalized strain stress curves of the models presented in the table 3.1.9 are depicted in Figure 3.1.12. The blue curves are related to the reference models.

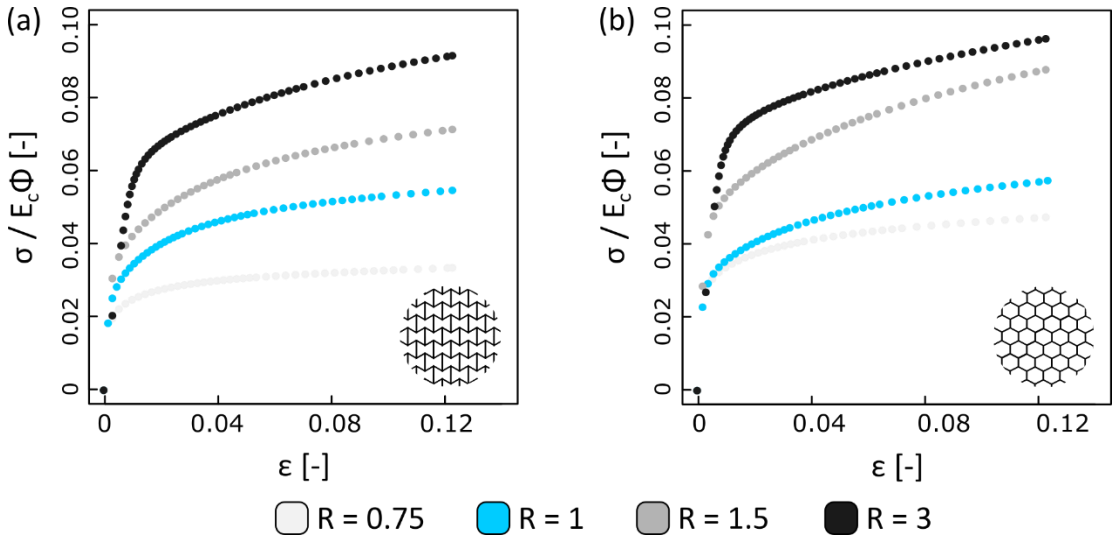

FIGURE 3.1.12 Normalized stress-strain curves for plate models with different scaling parameters: **(a)** auxetic cellular plate **(b)** conventional cellular plate

As it is shown in Figure 3.1.12, the post-buckling slope of the both auxetic and conventional cellular plates varies by alteration the dimensions of the unit cells. This variation in post-buckling slope is demonstrated in Figure 3.1.13. As can be seen, by increasing the scaling value the post-buckling slope for both auxetic and conventional structure becomes greater. The noteworthy point in this diagram is that when the dimensions of the cell unit are reduced, the post-buckling slope of the two auxetic and conventional structures converges to a same value. Like what happens while changing the in-plane thickness of the cells struts. There, as the in-plane thickness increases, post-buckling behavior of the auxetic and conventional plates converges as well. In fact, it seems that when the ratio of the thickness of the members of the unit cell to the dimensions of the unit cell, i.e. th/R, increases, the auxeticity has practically less effect on the post-buckling behavior of the structure.

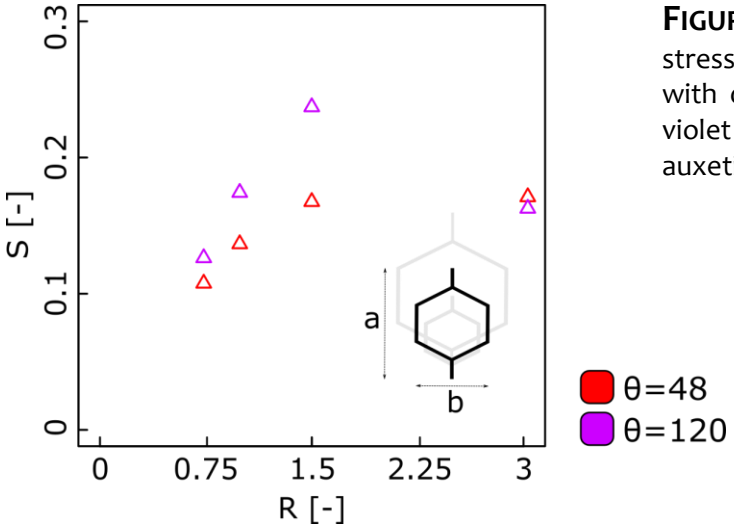

FIGURE 3.1.13 Post-buckling slopes driven from stress-strain curves for cellular plate models with different scaling parameter: the red and violet triangles in the graph correspond to auxetic and conventional models, respectively

3.1.7 Results corresponding to change of the ratio a/b

The values of the critical load, the weight parameter Φ and structural parameters for three reference models $\nu = -1.35, -0.05, 0.87$ and other eleven models made by variation of the ratio a/b are given in the table 3.1.10. As can be interpreted from weight parameter column of the table 3.1.10, by increasing ratio a/b the weight parameter becomes slightly smaller due to expansion of the sealed and open pores of the cellular plates. However the interesting thing is that despite the decrease in the weight of the cellular structure due to the change in the ratio a/b, the critical load increases.

TABLE 3.1.10 Values of the critical load, the weight parameter Φ and geometrical parameters for models created by variation of the ratio a/b. Reference models are highlighted by the blue color.

a/b	θ°	υ	h (mm)	R	th (mm)	w (mm)	Φ	F_{cr} (N)
1	64	-0.73	5	1	0.51	92.31	0.42	34.18
1	88	-0.05	5	1	0.51	92.31	0.36	29.33
1	104	0.37	5	1	0.51	92.31	0.35	32.98
1	120	0.87	5	1	0.51	92.31	0.34	50.13
1.5	48	-1.35	5	1	0.51	92.31	0.39	31.99
1.5	64	-0.73	5	1	0.51	92.31	0.35	44.35
1.5	88	-0.05	5	1	0.51	92.31	0.31	39.49
1.5	104	0.37	5	1	0.51	92.31	0.30	34.72
1.5	120	0.87	5	1	0.51	92.31	0.26	38.62
2	48	-1.35	5	1	0.51	92.31	0.35	63.01
2	64	-0.73	5	1	0.51	92.31	0.31	56.24
2	88	-0.05	5	1	0.51	92.31	0.29	48.81
2	104	0.37	5	1	0.51	92.31	0.28	44.54
2	120	0.87	5	1	0.51	92.31	0.27	66.69

As a result the stiffness and weight-normalized stress strain curves extracted from models with different ratio a/b shown in Figure 3.1.14 restates the same results. In fact, it demonstrates that by increasing the ratio a/b in all cellular models, the normalized critical stress becomes greater.

The normalized strain stress curves of the models presented in the table 3.1.10 are depicted in Figure 3.1.14. The blue curves are related to the reference models.

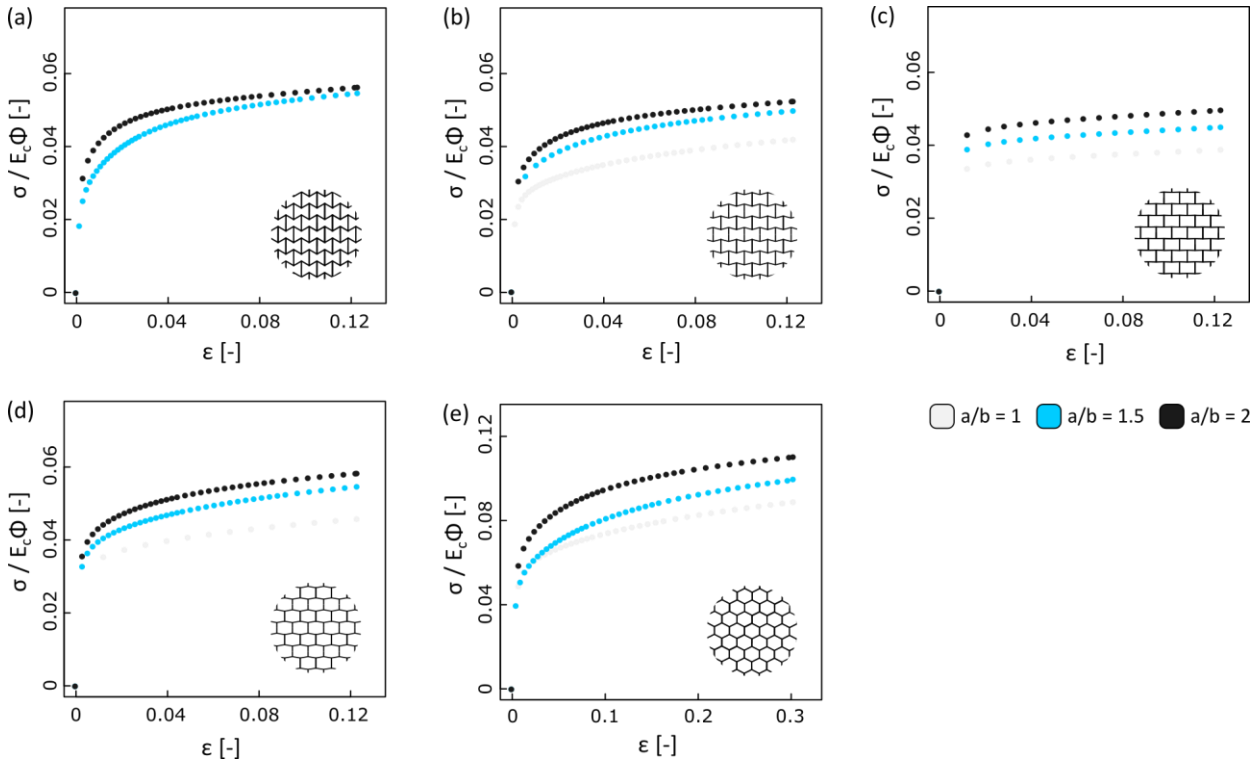

FIGURE 3.1.14 Normalized stress-strain curves for plate models with different ratio a/b:**(a)** auxetic cellular plate with $\upsilon = -1.35$, **(b)** auxetic cellular plate with $\upsilon = -0.73$, **(c)** auxetic cellular plate with $\upsilon = -0.05$, **(d)** conventional cellular plate with $\upsilon = 0.37$, **(e)** conventional cellular plate with $\upsilon = 0.87$

Here again a closer look at the results driven from the normalized strain stress curves of models with different ratio a/b demonstrated in Figure 3.1.14 reveals that the post-buckling slope of the cellular plates varies by alteration ratio a/b of the reference rectangle. This variation in post-buckling slope is depicted in Figure 3.1.15. As can be seen, by increasing the ratio a/b the post-buckling slope of the four models with $\upsilon = -1.35, -0.73, 0.37, 0.87$ becomes smaller. However, although the value of the slope for the model with zero Poisson's ratio seems almost constant but it slightly increases as the ratio a/b grows.

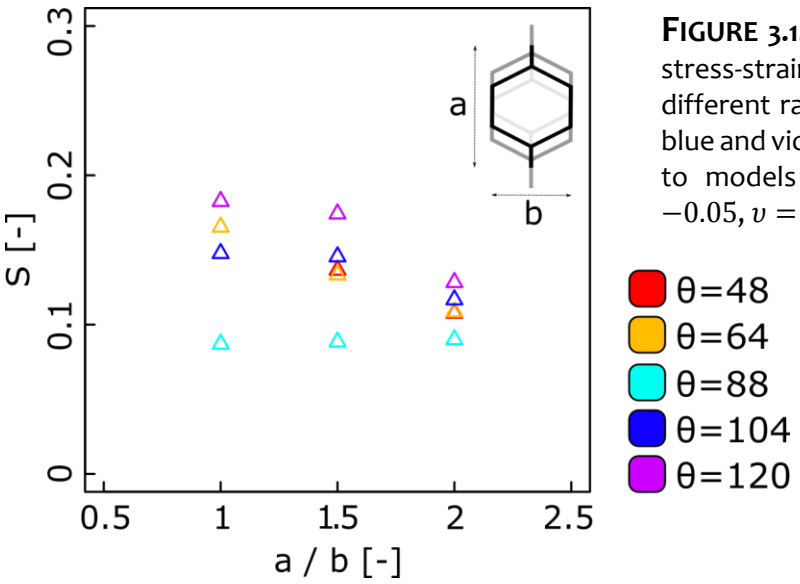

FIGURE 3.1.15 Post-buckling slopes driven from stress-strain curves for plate models with different ratio a/b: the red, orange, cyan, dark blue and violet triangles in the graph correspond to models with $\upsilon = -1.35$, $\upsilon = -0.73$, $\upsilon = -0.05$, $\upsilon = 0.37$and $\upsilon = 0.87$, respectively

3.1.8 Comparison of a cellular plate with a bulk plate

In order to compare the behavior of the cellular plates investigated in our study with a flat bulk plate shown in Figure 1.9.1, the two diagrams in Figure 3.1.16 are presented. In these two diagrams, the dependence of the ratio F_{cr_c}/F_{cr_b} on the Poisson's ratio and the out-of-plane thickness is shown. F_{cr_c} and F_{cr_b} refer to the critical load of a cellular plate and bulk plate under buckling load, respectively. As stated in the chapter one, the critical load for a thin rectangular plate under axial compression load is obtained from $Eq.(1.9.1)$. It should be noted that since the Poisson's ratio for an isotropic and linear elastic material is between -1 and 0.5, then $Eq.1.9.1$ always possess a positive value. However, by substitution Poisson's ratio less than -1, amount of critical load becomes negative, which is not physically meaningful. For this reason, in the plots depicted in Figure 3.1.16, the ratio F_{cr_c}/F_{cr_b} for $\upsilon = -1.35$ is always negative. Also for $\upsilon = -1.01$, the critical load for a bulk plate according to the $Eq.(1.9.1)$ tends to infinity. Therefore, the ratio F_{cr_c}/F_{cr_b}related to the models with $\upsilon = -1.01$ is close to zero. According to the $Eq.(1.9.1)$, the critical load for a bulk plate is proportional to the power of three of the out-of-plane thickness h. While according to the results of our study, this proportion is less for a cellular plate. For this reason, as shown in Figure 3.1.16 (a), by increasing out-of-plane thickness, F_{cr_b} grows faster than F_{cr_c} and then the ratio F_{cr_c}/F_{cr_b} decreases and tends to zero. However, when the plate becomes too thick, the ratio increases again. This is probably due to the fact that by sufficiently increasing of h, the structure is no longer Slander. Under these conditions, the resistance of the cellular structure against buckling increases and more force is needed to reach the critical point.

With a closer look at Figure 3.1.16 b, it can be revealed that the ratio F_{cr_c}/F_{cr_b} reaches its maximum value when the Poisson's ratio approaches to zero and this extreme point decreases by increasing the out-of-plane thickness. An interesting point can be interpreted about thin-walled plates from Figure 3.1.16 (b). As can be seen in the this Figure, an auxetic cellular plate with a thickness of one millimeter and a Poisson's ratio close to zero has a critical load of approximately 70% of the critical load of a bulk plate. However, according to Table 3.1.2, the weight of such a plate is only 31% of the weight of a bulk plate. Therefor the superiority of using such a cellular plate over a bulk plate especially in small thicknesses is well proven.

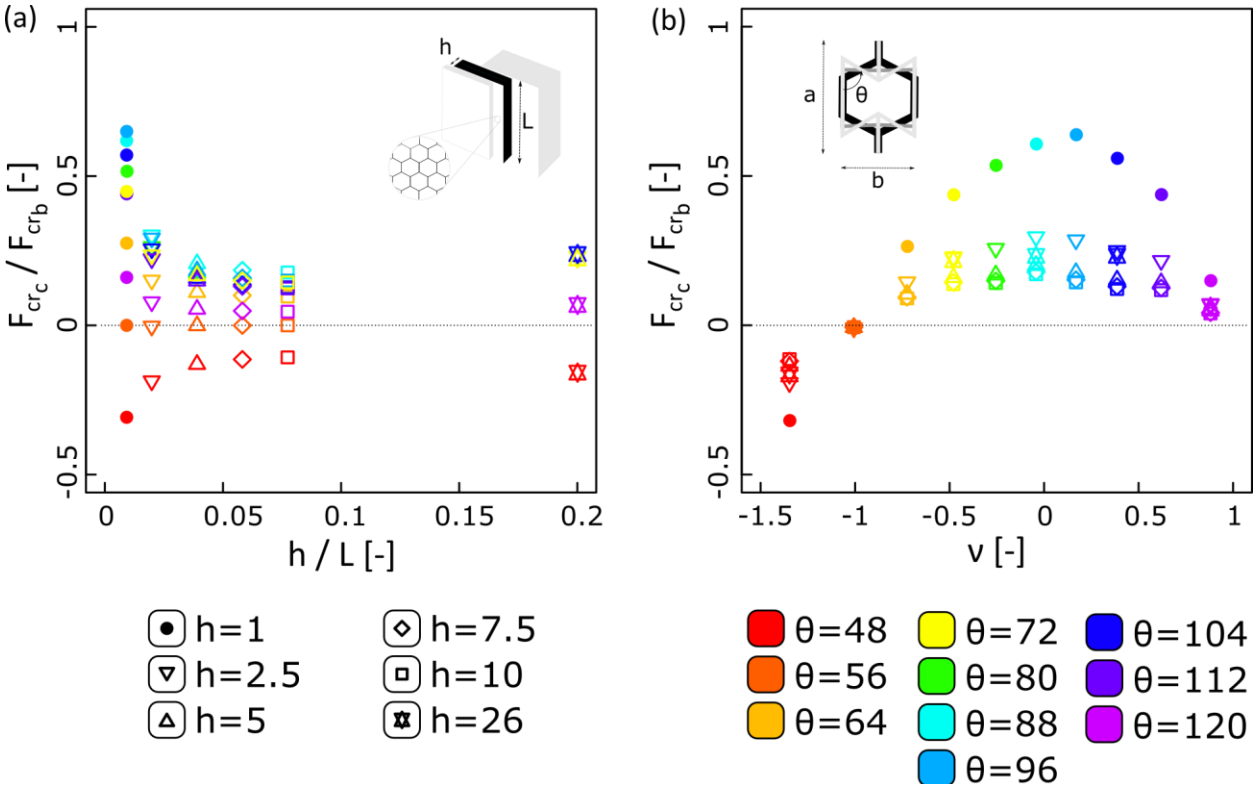

FIGURE 3.1.16 Dependence of the critical load of the cellular plate normalized by the critical load of the bulk plate to: **(a)** out-of-plane thickness and **(b)** Poisson's ratio

3.2 Results of the cellular cylindrical models

In this section, we present the results of numerical and experimental analysis performed on cellular cylindrical models.

3.2.1 Validation of the FEM method

As it discussed in chapter two, we designed and performed finite element analysis on 45 cellular cylindrical models. In order to validate the numerical method, two reference models

were fabricated and subjected to axial compression buckling load. The two reference models and their initial and final states with load displacement diagram are depicted in Figure 3.2.1 and Figure 3.2.2, respectively. In part (a) of these two Figures how the model deforms during compression load until it reaches to the buckling and post-buckling regime has been presented. Section (b) shows the perspective view of the final buckled structure of the analyzed model in Abacus software. The force-displacement data extracted from the Abacus simulation and the buckling test are given in the diagram in part (c). The black dots are related to the experimental results and the colored dots are related to the model with the corresponding Poisson's ratio. As can be seen in section (c) of these Figures, the experimental results for the both reference models follow the simulation results so well, and there is a perfect agreement between the two results. This is evidence of the claim that the finite element method implemented in this study for investigating the buckling and post-buckling behavior of cellular cylindrical structures is highly accurate and reliable.

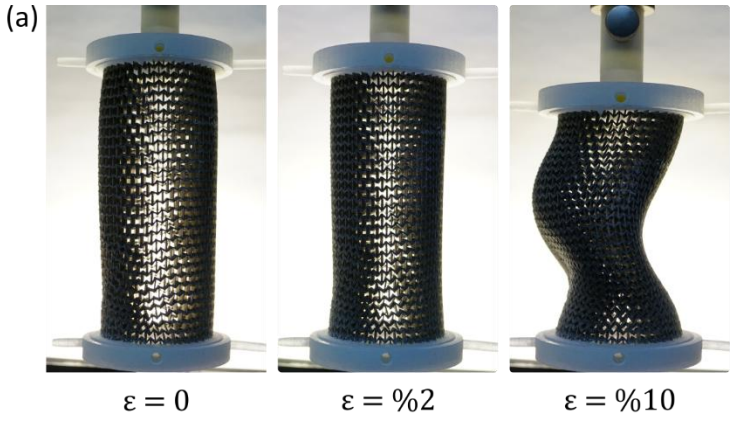

FIGURE 3.2.1 Experimental and numerical results of the auxetic cellular cylinder with negative Poisson's ratio: **(a)** front view of the real fabricated model mounted on the gripper, **(b)** perspective view of the buckled auxetic cylinder and its final deformed shape, **(c)** very nice and perfect match between experimental (black) and FEM (red) results in both buckling and post-buckling regions.

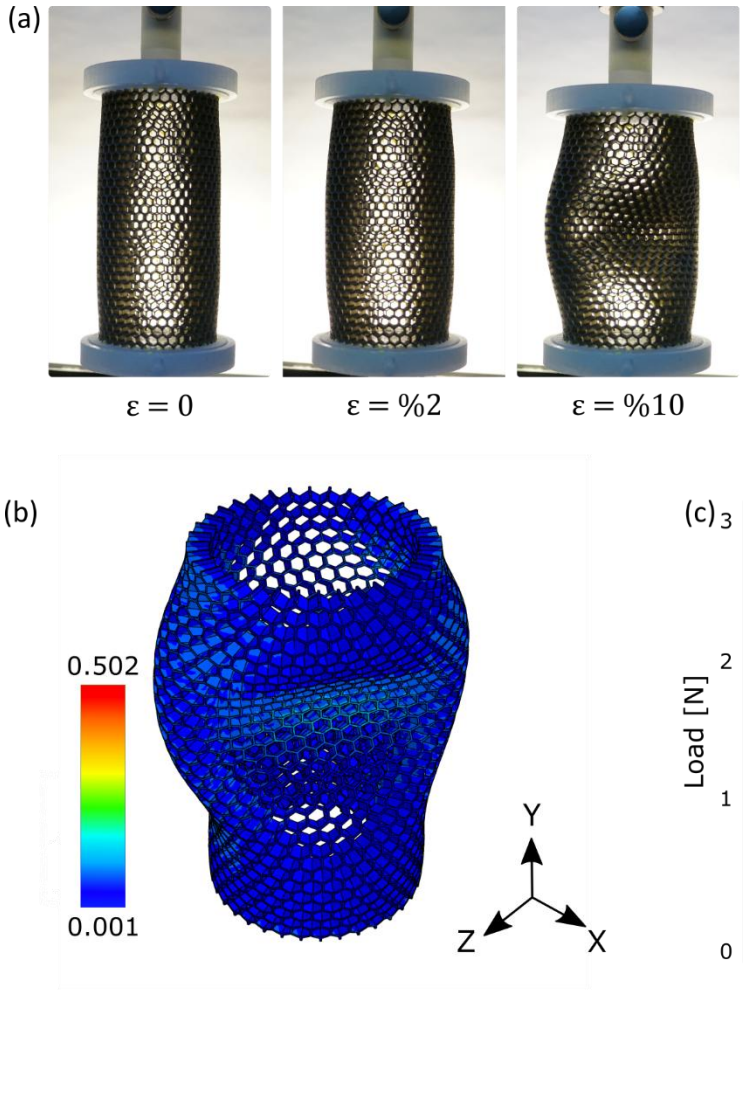

FIGURE 3.2.2 Experimental and numerical results of the conventional cellular cylinder with positive Poisson's ratio: **(a)** front view of the real fabricated model mounted on the gripper, **(b)** perspective view of the buckled conventional cylinder and its final deformed shape, **(c)** very nice and perfect match between experimental (black) and FEM (violet) results in both buckling and post-buckling regions.

As it mentioned before in chapter two based on the two reference models of the cellular cylinder another 43 models were designed and analyzed. The later models are characterized by range of variations in the out-of-plane thickness h, in the angle θ, in the ratio a/b and in the scaling parameter R. The results of the numerical analysis for each of the structural parameters are extracted and in the following sections will be discussed.

3.2.2 Results corresponding to change of the Poisson's ratio

The values of critical load, the parameter Φ and other structural parameters for the two reference models and the other three models created by changing the Poisson's ratio are presented in table 3.2.1. As it can be understood from table 3.2.1, similar to the plate models the value of the Φ decreases by increasing the angle θ and Poisson's ratio. In fact, by passing through the auxetic region and entering to the non-auxetic area, the porosity of the structure

increases and its weight decreases. By comparing the data given in table 3.2.1, it can be understood that, auxetic cylindrical structures show less resistance to buckling. This is because when an auxetic cylinder compressed and its length decreases, due to the auxitic properties, the radius of the structure also decreases, and as a result, the structure becomes more slender. It follows that the structure becomes more prone to buckling. In contrast, conventional cylindrical structures become thicker when compressed due to their positive Poisson's ratio, which in turn increases their buckling resistance.

TABLE 3.2.1 Values of the critical load, the weight parameter Φ and other geometrical parameters for cellular cylindrical models designed by variation of the Poisson's ratio.

θ^o	υ	h (mm)	a/b	R	r (mm)	L (mm)	Φ	F_{cr} (N)
48	-1.35	5	1.5	1	28.65	112.5	0.31	0.84
72	-0.49	5	1.5	1	28.65	112.5	0.25	1.48
88	-0.05	5	1.5	1	28.65	112.5	0.22	2.16
104	0.37	5	1.5	1	28.65	112.5	0.21	2.71
120	0.87	5	1.5	1	28.65	112.5	0.20	3.54

Similar to what have been done on cellular plat models, since the Young's modulus (E_c) and the weight of the cell structure change due to variation of the Poisson's ratio, then in order to investigate only the effect of the Poisson's ratio on the structure's behavior, the critical stresses are normalized by dividing to the E_c and Φ of the corresponding models. The normalized strain stress curves of the models presented in Table 3.2.1 are shown in Figure 3.2.3.

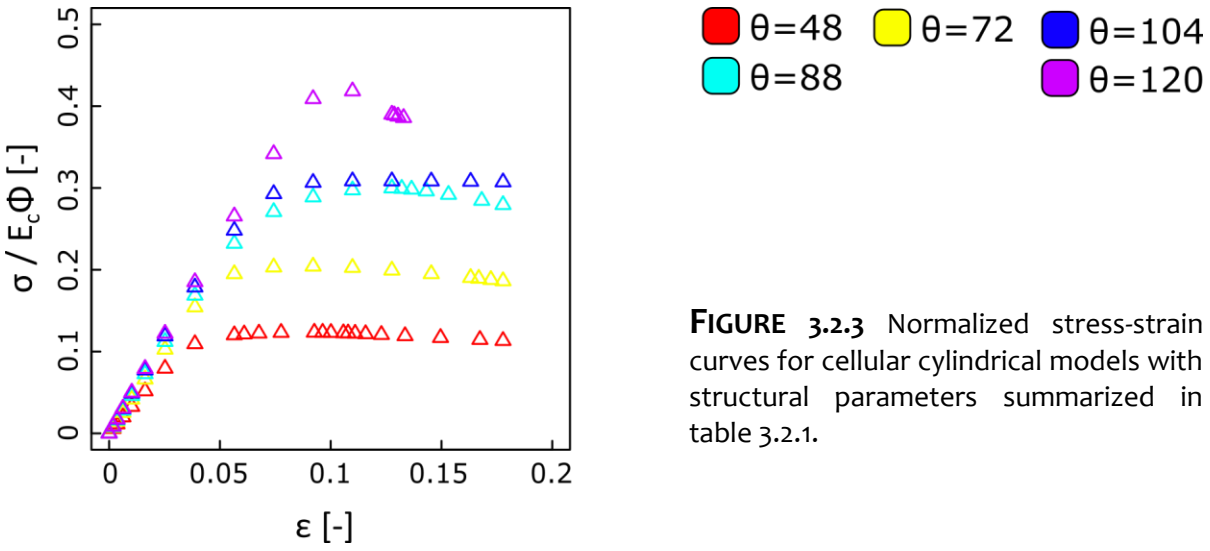

FIGURE 3.2.3 Normalized stress-strain curves for cellular cylindrical models with structural parameters summarized in table 3.2.1.

3.2.3 Results corresponding to change of the membrane thickness

The values of the critical load, the parameter Φ and other structural parameters for the four sets of ten models with $h = 1\ mm, 2.5\ mm, 7.5\ mm, 10\ mm$ are extracted and presented in the table 3.2.2, table 3.2.3, table 3.2.4 and table 3.2.5. It is obvious that although the cylinder membrane thickness changes however weight parameter Φ remains almost constant for each Poisson's ratio.

TABLE 3.2.2 Values of the critical load, weight parameter Φ and geometry parameters for cellular cylindrical models with $h = 1\ mm$

θ^o	υ	h (mm)	a/b	R	r (mm)	L (mm)	Φ	F_{cr} (N)
48	-1.35	1	1.5	1	28.65	112.5	0.31	0.10
72	-0.49	1	1.5	1	28.65	112.5	0.24	0.16
88	-0.05	1	1.5	1	28.65	112.5	0.22	0.22
104	0.37	1	1.5	1	28.65	112.5	0.21	0.25
120	0.87	1	1.5	1	28.65	112.5	0.20	0.36

TABLE 3.2.3 Values of the critical load, weight parameter Φ and geometry parameters for cellular cylindrical models with $h = 2.5\ mm$

θ^o	υ	h (mm)	a/b	R	r (mm)	L (mm)	Φ	F_{cr} (N)
48	-1.35	2.5	1.5	1	28.65	112.5	0.32	0.29
72	-0.49	2.5	1.5	1	28.65	112.5	0.25	0.49
88	-0.05	2.5	1.5	1	28.65	112.5	0.22	0.68
104	0.37	2.5	1.5	1	28.65	112.5	0.21	0.92
120	0.87	2.5	1.5	1	28.65	112.5	0.20	1.22

TABLE 3.2.4 Values of the critical load, weight parameter Φ and geometry parameters for cellular cylindrical models with $h = 7.5\ mm$

θ^o	υ	h (mm)	a/b	R	r (mm)	L (mm)	Φ	F_{cr} (N)
48	-1.35	7.5	1.5	1	28.65	112.5	0.32	1.53
72	-0.49	7.5	1.5	1	28.65	112.5	0.25	2.31
88	-0.05	7.5	1.5	1	28.65	112.5	0.22	3.30
104	0.37	7.5	1.5	1	28.65	112.5	0.21	4.51
120	0.87	7.5	1.5	1	28.65	112.5	0.20	7.22

TABLE 3.2.5 Values of the critical load, weight parameter Φ and geometry parameters for cellular cylindrical models with $h = 10\ mm$

θ^o	υ	h (mm)	a/b	R	r (mm)	L (mm)	Φ	F_{cr} (N)
48	-1.35	10	1.5	1	28.65	112.5	0.31	2.19
72	-0.49	10	1.5	1	28.65	112.5	0.25	3.21
88	-0.05	10	1.5	1	28.65	112.5	0.22	4.28
104	0.37	10	1.5	1	28.65	112.5	0.21	5.54
120	0.87	10	1.5	1	28.65	112.5	0.20	9.35

The normalized strain stress curves of the 20 models presented in the table 3.2.2, table 3.2.3, table 3.2.4 and table 3.2.5 are depicted in Figure 3.2.4.

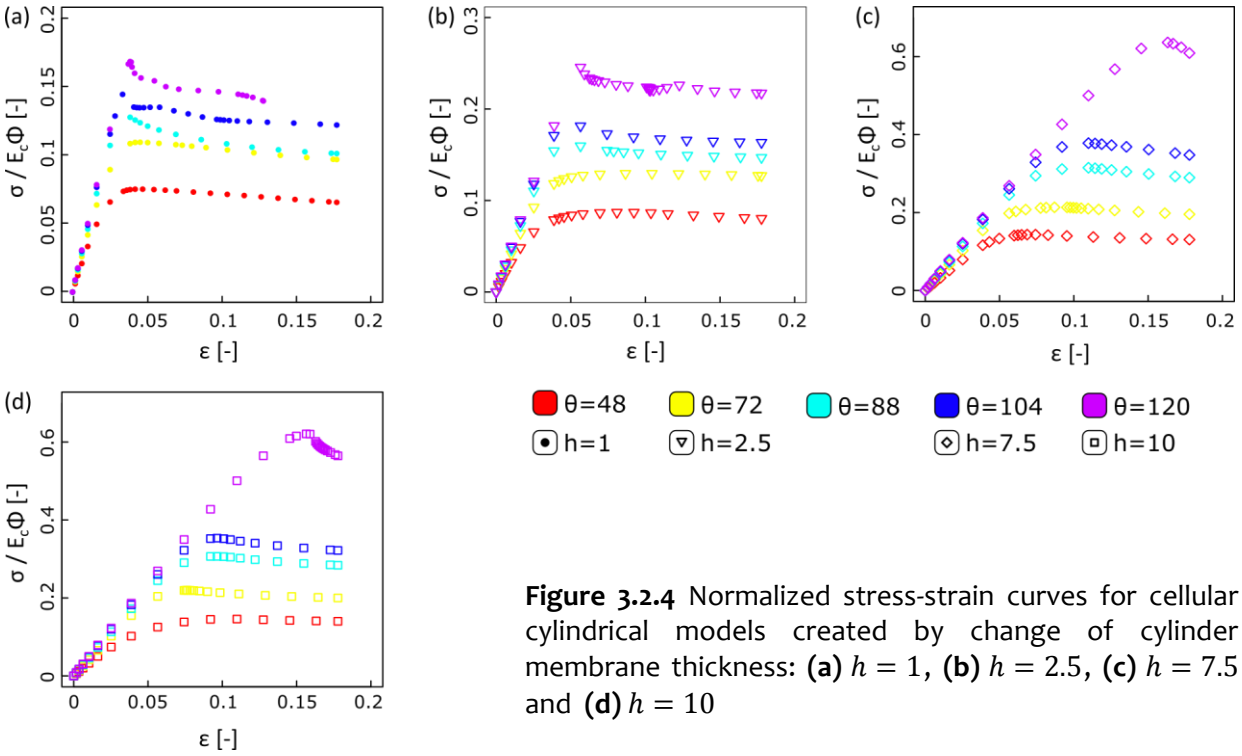

Figure 3.2.4 Normalized stress-strain curves for cellular cylindrical models created by change of cylinder membrane thickness: **(a)** $h = 1$, **(b)** $h = 2.5$, **(c)** $h = 7.5$ and **(d)** $h = 10$

From the normalized stress strain curves shown in the Figure 3.2.3 and Figure 3.2.4, it can be inferred that the slope of these curves in the post-buckling regime changes by the variation of the Poisson's ratio of the cellular cylinder and its membrane thickness. These changes are plotted in the Figure below. The dependence of the post-buckling slope on the two

parameters of Poisson's ratio and the cylinder membrane thickness is shown in Figures 3.2.5 (a) and Figures 3.2.5 (b), respectively. As can be seen in Figures 3.2.5 (a), in contrast with plate models, all cylindrical models have negative post-buckling slope. The post-buckling slope gradually decreases by increasing the Poisson's ratio and reaches to its minimum for the maximum Poisson's ratio. Figure 3.2.5 (b) shows that as the thickness of the cylinder membrane increases, the reduction in post-buckling slope occurs more rapidly.

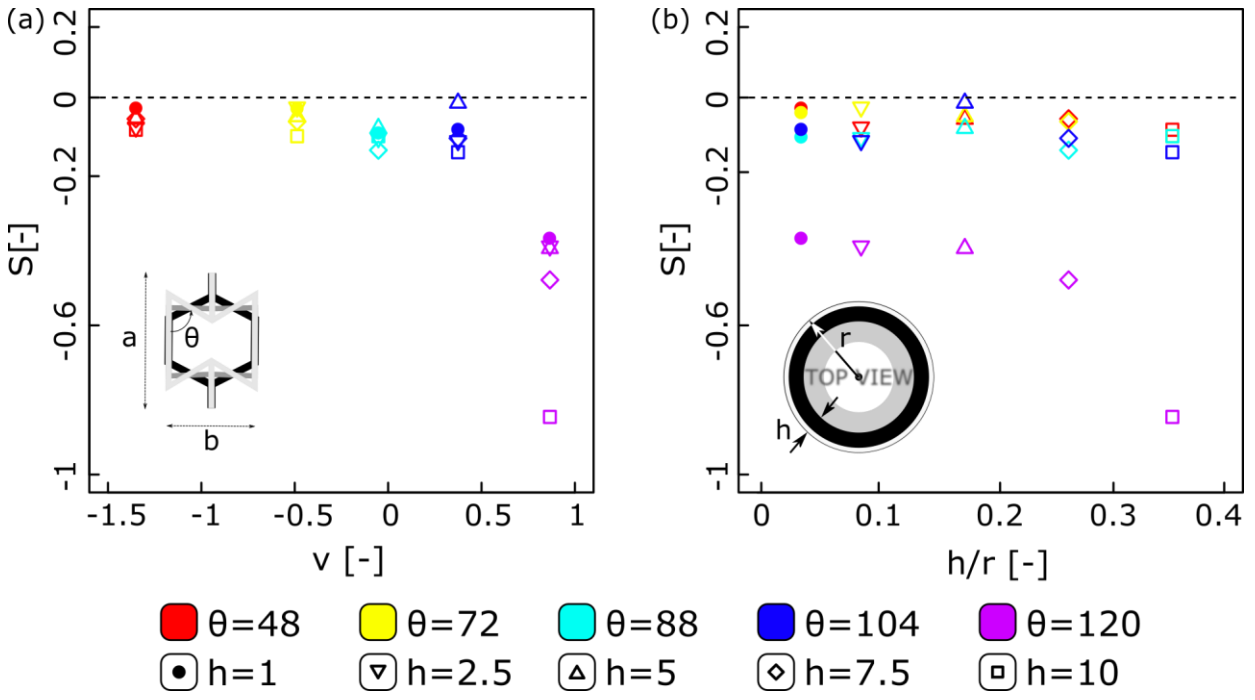

FIGURE 3.2.5 Post-buckling slopes driven from normalized stress-strain curves for cellular cylindrical models with different: **(a)** Poisson's ratio and **(b)** membrane thickness

The dependence of the stiffness-and-weight-normalized stress on the two parameters of Poisson's ratio and membrane thickness is shown in Figures 3.2.6 (a) and Figures 3.2.7 (b), respectively. The results plotted in the Figure 3.2.6 (a) reveals that by increasing membrane thickness of the cellular cylinder the value of the normalized critical stress increase regardless of its Poisson's ratio value. However, the increase in stiffness-and-weight-normalized is more noticeable in structures with maximum Poisson ratio (Figure 3.2.6 (b)).

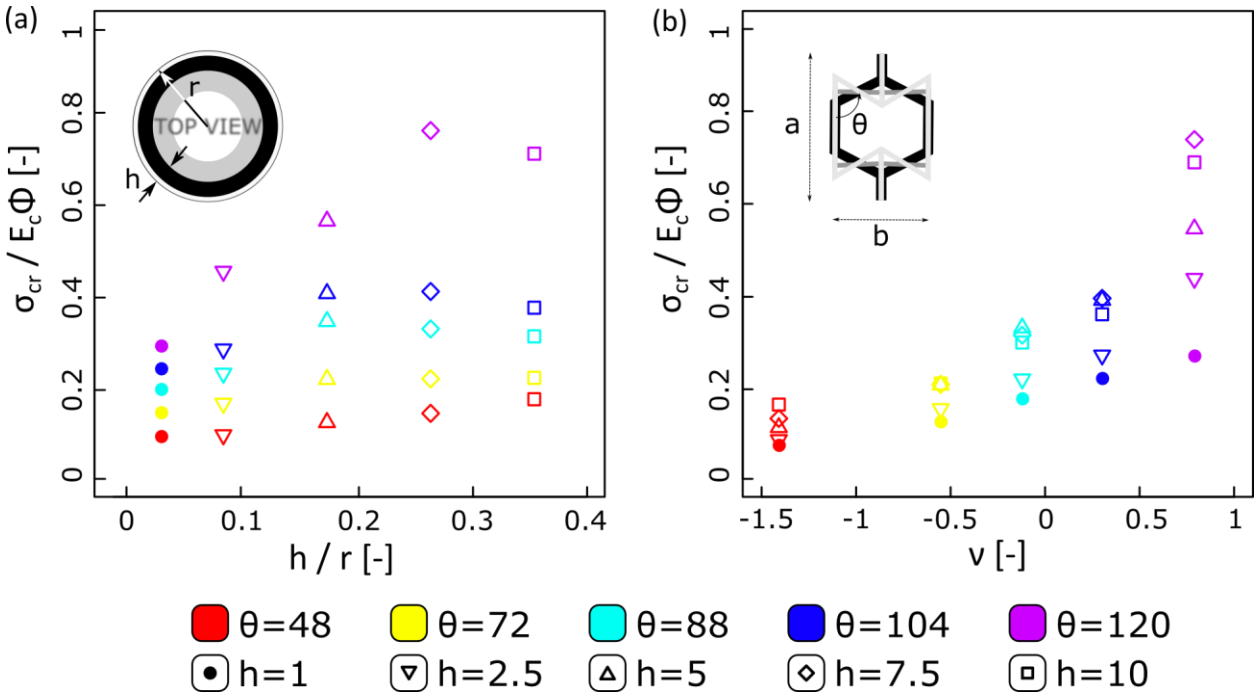

FIGURE 3.2.6 Dependence of the normalized critical stress for the cellular cylindrical models to: **(a)** membrane thickness and **(b)** Poisson's ratio

3.2.4 Results corresponding to change of the scaling parameter

Table 3.2.6 exhibits the values of the critical load, weight parameter Φ and structural parameters for two reference models with $\nu = -1.35, 0.87$ and other 18 models created by changing in the scaling parameter R. As can be understood from last two column of the table 3.2.6, by increasing the scaling parameter of the unit cell, the sealed and open pores expand. It follows that the weight parameter Φ becomes smaller and the structure tends to behave like a more prose structure. As a result, the critical load decreases significantly in all models. However the stiffness and weight-normalized stress strain curves extracted from different scaling parameters models shown in Figure 3.2.7 reveals a different scenario. In fact, it shows that increasing the scaling parameter of the unit cell leads to an significant increase in the normalized critical stress. For instance, according to the Figure 3.2.7 c, when dimensions of the unit cell of the cellular plate with zero Poisson's ratio increases from $R = 0.75$ to $R = 3$, the normalized stress becomes four times as great in value.

The normalized strain stress curves of the five models presented in the table 3.2.6 are depicted in Figure 3.2.7. The green curves are related to the reference models. Reference models are highlighted by the green color.

TABLE 3.2.6 Values of the critical load, the weight parameter Φ and geometrical parameters for cellular cylindrical models created by variation of the scaling parameters R.

R	θ^o	υ	h (mm)	a/b	r (mm)	L (mm)	Φ	F_{cr} (N)
0.75	48	-1.35	5	1.5	28.65	112.5	0.41	2.12
0.75	72	-0.49	5	1.5	28.65	112.5	0.32	3.11
0.75	88	-0.05	5	1.5	28.65	112.5	0.29	3.41
0.75	104	0.37	5	1.5	28.65	112.5	0.27	4.19
0.75	120	0.87	5	1.5	28.65	112.5	0.26	6.56
1	48	-1.35	5	1.5	28.65	112.5	0.31	0.84
1	72	-0.49	5	1.5	28.65	112.5	0.24	1.48
1	88	-0.05	5	1.5	28.65	112.5	0.22	2.16
1	104	0.37	5	1.5	28.65	112.5	0.21	2.71
1	120	0.87	5	1.5	28.65	112.5	0.20	3.54
1.5	48	-1.35	5	1.5	28.65	112.5	0.21	0.29
1.5	72	-0.49	5	1.5	28.65	112.5	0.17	0.43
1.5	88	-0.05	5	1.5	28.65	112.5	0.15	0.56
1.5	104	0.37	5	1.5	28.65	112.5	0.14	1.06
1.5	120	0.87	5	1.5	28.65	112.5	0.14	1.72
2	48	-1.35	5	1.5	28.65	112.5	0.11	0.06
2	72	-0.49	5	1.5	28.65	112.5	0.09	0.08
2	88	-0.05	5	1.5	28.65	112.5	0.08	0.10
2	104	0.37	5	1.5	28.65	112.5	0.07	0.15
2	120	0.87	5	1.5	28.65	112.5	0.07	0.28

As it is shown in Figure 3.2.7, the post-buckling slope of the cellular cylinder varies by alteration the dimensions of the unit cells. This variation in post-buckling slope is demonstrated in Figure 3.2.8.

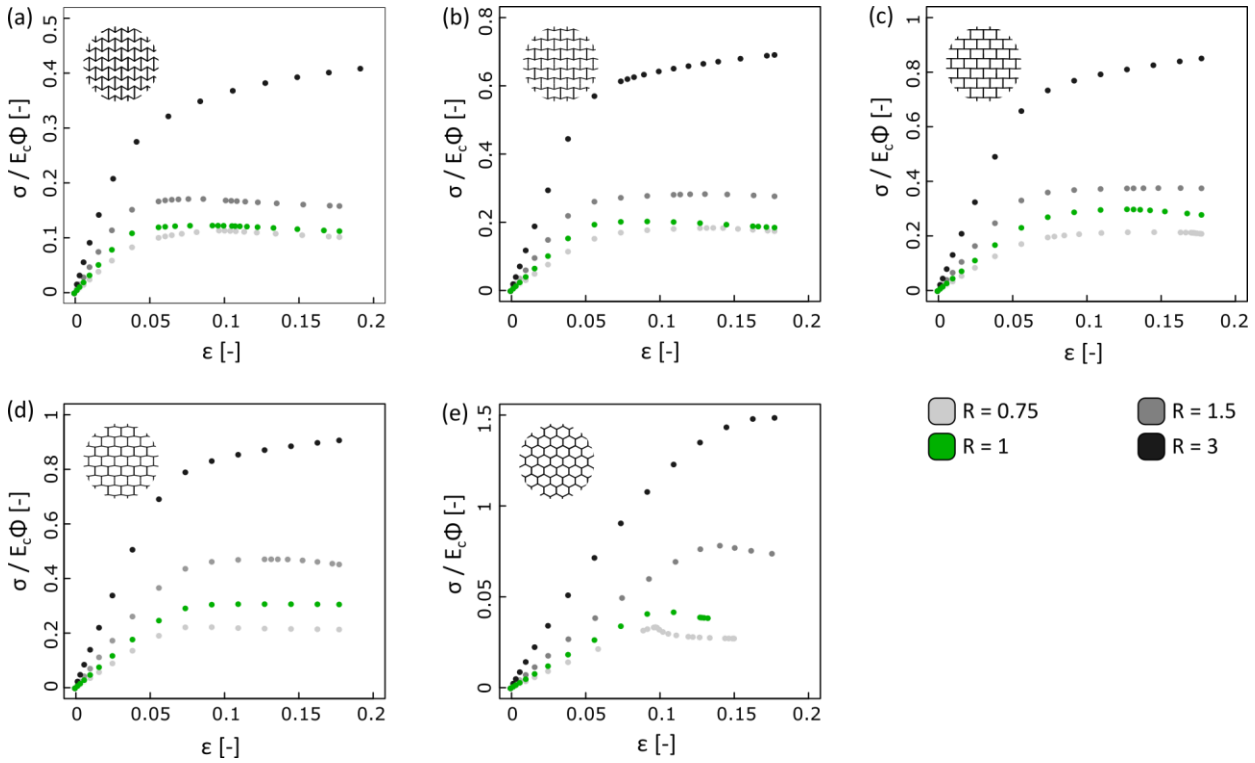

FIGURE 3.2.7 Normalized stress-strain curves with different scaling parameters for cellular cylindrical models with: **(a)** $\upsilon = -1.35$, **(b)** $\upsilon = -0.49$, **(c)** $\upsilon = -0.05$, **(d)** $\upsilon = 0.37$, **(e)** $\upsilon = 0.87$

As can be seen, by increasing the scaling value the post-buckling slope regardless of the Poisson's ratio structure becomes greater. The noteworthy point in this diagram is that when the dimensions of the cell unit becomes greater, the post-buckling slope of the structure changes its sign and will be positive. As a result the structure becomes more stable in post-buckling regime.

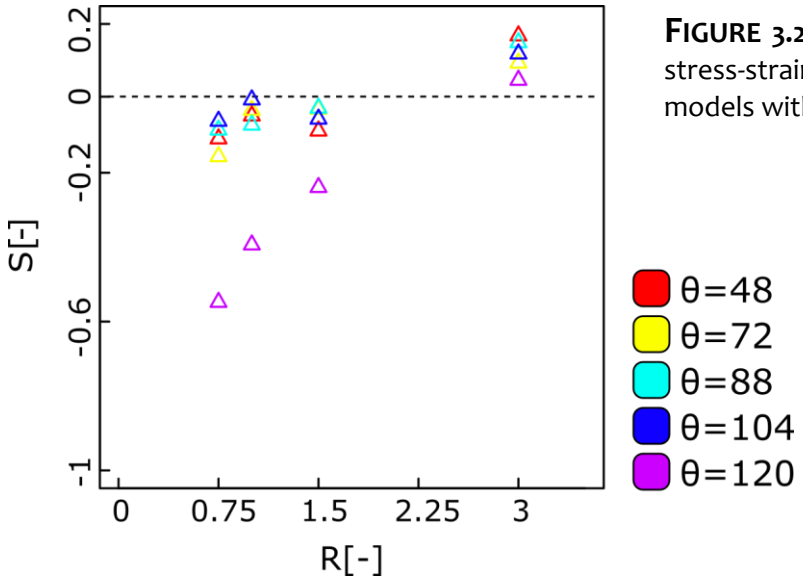

FIGURE 3.2.8 Post-buckling slopes driven from stress-strain curves for cellular cylindrical models with different scaling parameter

3.2.5 Results corresponding to change of the ratio a/b

The values of the critical load, weight parameter Φ and structural parameters for two reference models $\nu = -1.35, -0.05, 0.87$ and other six models made by variation of the ratio a/b are given in the table 3.2.7. The last column of the table states that by increasing the ratio, critical load also tends to be greater. Reference models are highlighted by the green color.

TABLE 3.2.7 Values of the critical load, weight parameter Φ and geometrical parameters for cellular cylindrical models created by variation of the ratio a/b.

a/b	θ^o	υ	h (mm)	R	r (mm)	L (mm)	Φ	F_{cr} (N)
1	88	-0.05	5	1	28.65	112.5	0.19	0.89
1	120	0.87	5	1	28.65	112.5	0.17	2.35
1.5	48	-1.35	5	1	28.65	112.5	0.31	0.84
1.5	88	-0.05	5	1	28.65	112.5	0.22	2.16
1.5	120	0.87	5	1	28.65	112.5	0.20	3.54
2	48	-1.35	5	1	28.65	112.5	0.34	1.80
2	88	-0.05	5	1	28.65	112.5	0.25	2.66
2	120	0.87	5	1	28.65	112.5	0.23	4.49

The stiffness and weight-normalized stress strain curves extracted from models with different ratio a/b shown in Figure 3.2.9 states that by increasing the ratio a/b in all cellular models, the normalized critical stress becomes greater. The normalized strain stress curves of the models presented in the table 3.2.7 are depicted in Figure 3.2.9. The green curves are related to the reference models.

Here again a closer look at the results driven from the normalized strain stress curves of models with different ratio a/b demonstrated in Figure 3.2.9 reveals that the post-buckling slope of the cellular cylinder varies by alteration the ratio a/b of the reference rectangle. This variation in post-buckling slope is depicted in Figure 3.2.10. As can be seen, by increasing the ratio a/b the post-buckling slope of the models with negative and zero Poisson's ratio slightly decreases. However post-buckling slope trend for the model with positive Poisson's ratio is in reverse and tends to increase by increasing the ratio a/b.

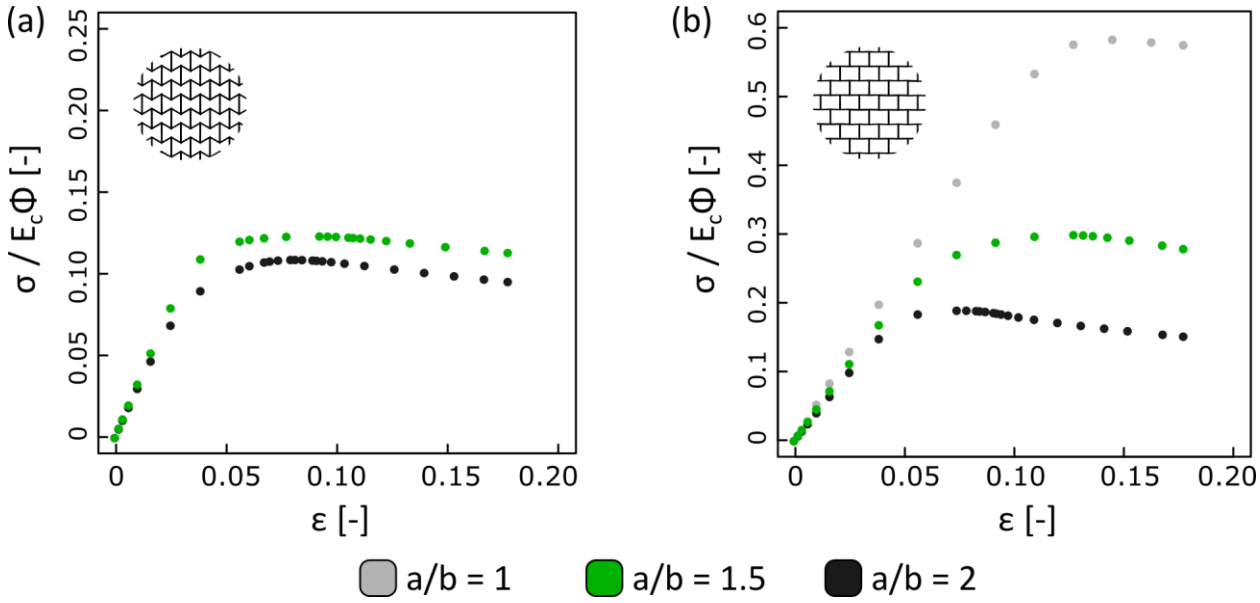

FIGURE 3.2.9 Normalized stress-strain curves for cellular cylindrical models with different ratio a/b:**(a)** cellular cylinder with $\upsilon = -1.35$, **(b)** cellular cylinder with $\upsilon = -0.05$

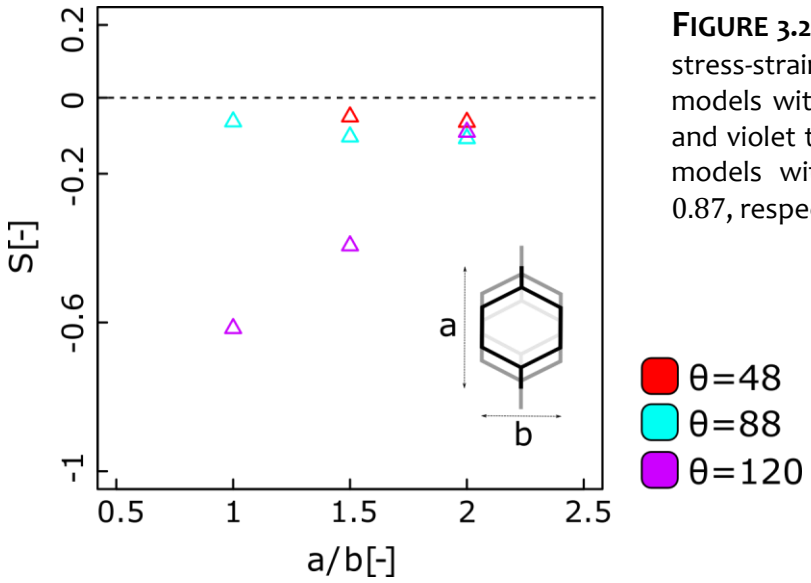

FIGURE 3.2.10 Post-buckling slopes driven from stress-strain curves for cellular cylindrical models with different ratio a/b: the red, cyan and violet triangles in the graph correspond to models with $\upsilon = -1.35$, $\upsilon = -0.05$ and $\upsilon = 0.87$, respectively

Chapter 4

Conclusions & Recommendations

4.1 Conclusions

The purpose of this study is to investigate the buckling and post-buckling behavior of cellular structures under the influence of changing their geometric parameters. The models studied in this research were designed and analyzed in two plate and cylindrical geometries. The primary reference models first were analyzed by numerical finite element method and then fabricated by additive manufacturing technology and subjected to mechanical buckling test. The results of numerical simulation and experimental approach for all 5 reference models have a very good agreement, which is evidence that the numerical method used in this research has a high accuracy. The results show that in the cellular plate structure, Poisson's ratio has a small effect on the stiffness-weight-normalized critical stress of the structure. However the normalized critical stress in cellular plates with different Poisson's ratio gains its maximum value generally in the auxetic region and close to Poisson's ratio equals to zero. On the other side, in a cylindrical structure, the normalized critical stress increases with increasing Poisson's ratio. This is due to the fact that conventional cylindrical structures become thicker when compressed due to their positive Poisson's ratio, which in turn increases their buckling resistance. A close look on the results of sufficient slender cellular plates has shown that the post-buckling behavior of the cellular plate with a Poisson's ratio close to zero has the least dependence on the out-of-plane thickness of the plate. Moreover, the post-buckling slope of the strain stress diagram reaches its minimum value for the zero Poisson's ratio. However, as the Poisson's ratio of the plate moves away from zero, the dependency of its post-buckling stability to the out-of-plane thickness increases. On the other side, the results of the data of the cylindrical structure show that the post-buckling behavior of this structure for the maximum Poisson's ratio is the most affected by the change in membrane thickness. The structure also has a larger negative slope for the maximum Poisson's ratio. As a result, although the cellular cylinder with maximum Poisson's ratio has a higher buckling resistance, it is more unstable in the post-buckling regime. Moreover it seems that for plate models when the ratio of the in-plane thickness of the struts to the scaling parameter, ie. th/R increases, the auxeticity has practically less effect on the post-buckling behavior of the structure. The results have also reveals the superiority of using a cellular plate with zero Poisson's ratio over a bulk plate with the same Poisson's ratio especially in smaller thicknesses. The scaling parameter has a greater effect on the post-buckling behavior of the cylindrical cellular structure, so that with increasing the scaling parameter of the structure, the slope value increases and changes from negative to positive.

In general, all structural parameters including the Poisson's ratio (for both plate and cylindrical models), the out-of-plane thickness (for plate models), the membrane thickness (for cylindrical models), the in-plan thickness of the struts (for plate models), the width (for plate models), the scaling parameter of the unit cells (for both plate and cylinder models) and the height-to-width ratio of the unit cells (for both plate and cylinder models) have undeniable effects on the critical buckling load and post-buckling behavior of structures. In fact, by changing the geometric parameters, a wide range of post-buckling slopes of the structure can

be achieved in both plate and cylindrical geometry and the post-buckling behavior of the structure can be tuned by designing geometric parameters.

4.2 Recommendations for future works

As mentioned in chapter two, Gibson's re-entratn honeycomb model was used as a basis unit cell of cellular structures. one can also use other models of unit cells that provides auxetic properties. Also, as mentioned before, in this study structures were under action of the uniaxial compressive buckling load. While for the cylindrical cellular structure, other types of buckling can be studied, such as buckling under internal pressure (to simulate blood flow inside the vessel) or under bending moment.

REFERENCES

1. *Lim, T. C. (2015). Auxetic materials and structures (pp. 55-56). Singapore: Springer.*
2. *Young T (1807) On passive strength and friction. Course of lectures on natural philosophy and the mechanical arts: lecture, vol 13. Taylor and Walton, London, pp 109–113*
3. *Voigt W (1910) Lehrbuch der Kristallphysik. Teubner, Berlin*
4. *Love AEH (1927) A treatise on the mathematical theory of elasticity, 4th edn. Cambridge University Press, Cambridge*
5. *Hearmon RFS (1946) The elastic constants of anisotropic materials. Rev Mod Phys 18(3):409 440*
6. *Veronda DR, Westmann RA (1970) Mechanical characterization of skin-finite deformations. J Biomech 3(1):111–124*
7. *Kittinger E, Tichy J, Bertagnolli E (1981) Example of a negative effective Poisson's ratio. Phys Rev Lett 47(10):712–713*
8. *Gibson LJ, Ashby MF, Schajer GS, Roberson CI (1982) The mechanics of two-dimensional cellular materials. Proc R Soc Lond A 382(1782):25–42*
9. *Almgren RF (1985) An isotropic three-dimensional structure with Poisson's ratio = –1. J Elast 15 (4):427–430*
10. *Lakes R (1987) Negative Poisson's ratio materials. Science 238(4826):551*
11. *Evans KE (1991) Auxetic polymers: a new range of materials. Endeavour 15(4):170–174*
12. *Yeganeh-Haeri A, Weidner DJ, Parise JB (1992) Elasticity of α-cristobalite: a silicon dioxide with a negative Poisson's ratio. Science 257(5070):650–652*
13. *Williams J L and Lewis J L (1982) Properties and an anisotropic model of cancellous bone from the proximal*
14. *Veronda D R and Westmann R A (1970) Mechanical characterization of skin—finite deformations J. Biomech. 3 111–24*

15. *Lees C, Vincent J V and Hillerton J E (1991) Poisson's ratio in skin Bio-Med. Mater. Eng. 1 19 23*

16. *Ren, X., Das, R., Tran, P., Ngo, T. D., & Xie, Y. M. (2018). Auxetic metamaterials and structures: a review. Smart materials and structures, 27(2), 023001.*

17. *Baughman R H (2003) Auxetic materials: avoiding the shrink Nature 425 667*

18. *Wang N (2014) Stem cell mechanics: auxetic nuclei Nat. Mater. 13 540–2*

19. *Lakes R (1987) Foam structures with negative Poisson's ratio. Science 235(4792):1038–1040*

20. *He CB, Liu PW, Griffin AC (1998) Toward negative Poisson ratio polymers through molecular design. Macromolecules 31(9):3145–3147*

21. *Sloan MR, Wright JR, Evans KE (2011) The helical auxetic yarn—a novel structure for composites and textiles; geometry, manufacture and mechanical properties. Mech Mater 43 (9):476–486*

22. *Gibson LJ (2005) Biomechanics of cellular solids. J Biomech. https://doi.org/10.1016/j.jbiomech.2004.09.027*

23. *Deshpande VS, Fleck NA, Ashby MF (2001) Effective properties of the octet-truss lattice material. J Mech Phys Solids 49:1747–1769. https://doi.org/10.1016/S0022-5096(01)00010-2*

24. *AshbyMF (2006) The properties of foams and lattices. Philos Trans R Soc A Math Phys Eng Sci 364:15–30. https://doi.org/10.1098/ rsta.2005.1678*

25. *Abate, K. M., Nazir, A., Yeh, Y. P., Chen, J. E., & Jeng, J. Y. (2020). Design, optimization, and validation of mechanical properties of different cellular structures for biomedical application. The International Journal of Advanced Manufacturing Technology, 106(3), 1253-1265.*

26. *C. Chu, G. Graf, D.W. Rosen, Design for additive manufacturing of cellular structures, Comput. Aided. Des. Appl. 5 (2008) 686–696, https://doi.org/10.3722/cadaps.2008. 686-696.*

27. *R. Lakes, Materials with structural hierarchy, Nature 361 (1993) 511–515, https:// doi.org/10.1038/361511a0.*

28. *A.G. Leach, The thermal conductivity of foams. I.Models for heat conduction, J. Phys. D. Appl. Phys. 26 (1993) 733–739, https://doi.org/10.1088/0022-3727/26/5/003.*

29. *D. Almonti, N. Ucciardello, Design and thermal comparison of random structures realized by indirect additive manufacturing,Materials (Basel) 12 (2019) 2261, https:// doi.org/10.3390/ma12142261.*

30. *K. Ushijima, D.-H. Chen, H. Nisitani, Energy absorption efficiency in cellular solids, Int. J. Mod. Phys. B. 22 (2008) 1730–1735, https://doi.org/10.1142/ S021797920804733X.*

31. *Rohacell, High-performance structural foam cores, https://www.rohacell.com/product/ rohacell/en/about/ 2018, Accessed date: 2 March 2019.*

32. *Shinko Wire Company, Ltd, http://www.shinko-wire.co.jp/english/ 2018, Accessed date: 20 February 2019.*

33. *Jetté B, Brailovski V, Dumas M, Simoneau C, Terriault P (2018) Femoral stem incorporating a diamond cubic lattice structure: design, manufacture and testing. J Mech Behav BiomedMater 77:58–72. https://doi.org/10.1016/j.jmbbm.2017.08.034*

34. *Yan C, Hao L, Hussein A et al (2015) Microstructure and mechanical properties of aluminium alloy cellular lattice structures manufactured by direct metal laser sintering. Mater Sci Eng A 628:238–246. https://doi.org/10.1016/j.msea.2015.01.063*

35. *Kang H, Lin CY, Hollister SJ (2010) Topology optimization of three dimensional tissue engineering scaffold architectures for prescribed bulk modulus and diffusivity. Struct Multidiscip Optim 42: 633–644. https://doi.org/10.1007/s00158-010-0508-8*

36. *Hollister S (2006) Porous scaffold design for tissue engineering. Nat Mater 5:590. https://doi.org/10.1038/nmat1683*

37. *Alderson A and Alderson K L (2007) Auxetic materials proceedings of the institution of mechanical engineers J. Aerosp. Eng. G 221 565–75*

38. *Masters I G and Evans K E (1996) Models for the elastic deformation of honeycombs Compos. Struct. 35 403–22*

39. *Grima J N and Evans K E (2000) Auxetic behavior from rotating squares J. Mater. Sci. Lett. 19 1563–5*

40. *Grima J N, Alderson A and Evans K E (2004) Negative Poisson's ratios from rotating rectangles Comput. Methods Sci. Technol. 10 137–45*

41. *Grima J N, Zammit V, Gatt R, Alderson A and Evans K E (2007) Auxetic behaviour from rotating semi-rigid units Phys. Status Solidi b 244 866–82*

42. *Rafsanjani A and Damiano P (2016) Bistable auxetic mechanical metamaterials inspired by ancient geometric motifs Extreme Mech. Lett. 9 291–6*

43. *Caddock, B. & Evans, K., (1995). Negative Poisson ratios and strain-dependent mechanical properties in arterial prostheses. Biomaterials, Volume 16, pp. 1109.*

44. *Evans, K. E. & Alderson, K. L., (2000). Auxetic materials: the positive side of being negative. Engineering Science and Education, pp. 148-154.*

45. *Alderson, A. & Alderson, K., (2005). Expanding materials and applications: exploiting auxetic textiles. Technical Textiles Int, Volume 14, pp. 29-34.*

46. *Moyers, R., (1992). Dilator for Opening the Lumen of a Tubular Organ. United State of America, Patent No. 5108413.*

47. *Hengelmolen, R., (2002). Auxetic tubular liners. Great Britain, Patent No. 2393657.*

48. *Simkins, V., Alderson, A., Davies, P. & Alderson, K., (2005). Single fibre pullout tests on auxetic polymeric fibres. J Mat Sci, Volume 40, pp. 4355-4364.*

49. *Ali M N and Rehman I U (2011) An auxetic structure conFigured as oesophageal stent with potential to be used for palliative treatment of oesophageal cancer; development and in vitro mechanical analysis J. Mater. Sci., Mater. Med. 22 2573–81*

50. *Kuribayashi K, Tsuchiya K, You Z, Tomus D, Umemoto M, Ito T and Sasaki M 2006 Self-deployable origami stent grafts as a biomedical application of Ni-rich TiNi shape memory alloy foil Mater. Sci. Eng. A 419 131–7*

51. *Burriesci G and Bergamasco G 2011 Annuloplasty prosthesis with an auxetic structure US Patent 8034103B2*

52. *Amin, F., Ali, M. N., Ansari, U., Mir, M., Minhas, M. A., & Shahid, W. (2015). Auxetic coronary stent endoprosthesis: Fabrication and structural analysis. Journal of applied biomaterials & functional materials, 13(2), 127-135.*

53. *Zadpoor, A. A. (2020). Meta-biomaterials. Biomaterials science, 8(1), 18-38.*

54. *Kolken, H. M., Janbaz, S., Leeflang, S. M., Lietaert, K., Weinans, H. H., & Zadpoor, A. A. (2018). Rationally designed meta-implants: a combination of auxetic and conventional meta biomaterials. Materials Horizons, 5(1), 28-35.*

55. *Scarpa, F. (2008). Auxetic materials for bioprostheses [In the Spotlight]. IEEE Signal Processing Magazine, 25(5), 128-126.*

56. *Nazir, A., Arshad, A. B., & Jeng, J. Y. (2019). Buckling and post-buckling behavior of uniform and variable-density lattice columns fabricated using additive manufacturing. Materials, 12(21), 3539.*

57. *Sui, Q., Fan, H., & Lai, C. (2015). Failure analysis of 1D lattice truss composite structure in uniaxial compression. Composites Science and Technology, 118, 207-216.*

58. *Magnucka-Blandzi, E. (2008). Axi-symmetrical deflection and buckling of circular porous cellular plate. Thin-walled structures, 46(3), 333-337.*

59. *Overvelde, J. T. B., Shan, S., & Bertoldi, K. (2012). Compaction through buckling in 2D periodic, soft and porous structures: effect of pore shape. Advanced Materials, 24(17), 2337 2342.*

60. *Jabbari, M., Mojahedin, A., Khorshidvand, A. R., & Eslami, M. R. (2014). Buckling analysis of a functionally graded thin circular plate made of saturated porous materials. Journal of Engineering Mechanics, 140(2), 287-295.*

61. *Tang, H., Li, L., & Hu, Y. (2018). Buckling analysis of two-directionally porous beam. Aerospace Science and Technology, 78, 471-479.*

62. *Pihler-Puzović, D., Hazel, A. L., & Mullin, T. (2016). Buckling of a holey column. Soft Matter, 12(34), 7112-7118.*

63. *Nazir, A., & Jeng, J. Y. (2020). Buckling behavior of additively manufactured cellular columns: Experimental and simulation validation. Materials & Design, 186, 108349.*

64. *Timoshenko SP, Gere JM (1961) Theory of elastic stability, 2nd edn. McGraw-Hill, New York*

65. *Obrecht, H., Rosenthal, B., Fuchs, P., Lange, S., & Marusczyk, C. (2006). Buckling, postbuckling and imperfection-sensitivity: Old questions and some new answers. Computational Mechanics, 37(6), 498-506.*